Introduction

Focused ultrasound surgery

W. Jeffrey Elias, M.D., and Neal F. Kassell, M.D.

Department of Neurological Surgery, University of Virginia Health System, Charlottesville, Virginia

We are pleased to present this month's issue of *Neurosurgical Focus*, which is dedicated to MR-guided focused ultrasound (FUS) surgery, an entirely new technology that may well revolutionize the field of neurosurgery. Since the first human clinical trials were conducted using transcranial FUS treatments only a few years ago, there has been a surge in interest worldwide for the application of MR-guided, high-intensity FUS for the treatment of various disorders such as neurooncological disease, stroke, functional neurosurgical disorders, and many others to come.[1] Diseases that were once thought to require treatment with invasive, neurosurgical operations may now be amenable to this noninvasive and precise intervention.

In this issue, we present a wide overview of potential applications for FUS surgery. Dr. Daniel Jeanmonod, who pioneered the first stereotactic FUS central lateral thalamotomies, presents his vast experience in the treatment of chronic neuropathic pain. His group also presents its approach to measuring the accuracy of FUS lesioning, which will be very important in years to come as other subcortical nuclei are targeted for functional lesioning. We are also very pleased to present a very novel concept of FUS technology to open the blood-brain barrier for the delivery of therapeutic agents in the treatment of brain tumors. There are many potential applications of FUS intervention in vascular disorders, and a very complete overview of sonothrombolysis for acute ischemic stroke is included as well as a review of the use of intravascular ultrasonography for diagnostic purposes.

In the few years that transcranial FUS has been available, the door has opened for treatment of a variety of neurological conditions. Patients may soon be faced with the option of choosing this precise noninvasive technology for the treatment of their neurological condition. We hope you enjoy this issue.
(http://thejns.org/doi/abs/10.3171/2011.11.FOCUS11317)

Disclosure

Dr. Elias declares no conflict of interest. Dr. Kassell declares direct stock ownership with Insightec and a personal relationship with the FUS Foundation.

Reference

1. McDannold N, Clement GT, Black P, Jolesz F, Hynynen K: Transcranial magnetic resonance imaging-guided focused ultrasound surgery of brain tumors: initial findings in 3 patients. **Neurosurgery 66:**323–332, 2010

Please include this information when citing this paper: DOI: 10.3171/2011.11.FOCUS11317.

Neurosurg Focus 32 (1):E1, 2012

Transcranial magnetic resonance imaging–guided focused ultrasound: noninvasive central lateral thalamotomy for chronic neuropathic pain

Daniel Jeanmonod, M.D.,[1,2] Beat Werner, M.Sc.,[3] Anne Morel, Ph.D.,[1,4] Lars Michels, Ph.D.,[1,3] Eyal Zadicario, M.Sc.,[5] Gilat Schiff, B.Sc.,[5] and Ernst Martin, M.D.[3]

[1]Department of Functional Neurosurgery and [4]Center for Clinical Research, University Hospital Zürich; [2]Center of Ultrasound Functional Neurosurgery, Solothurn; [3]MR-Center, University Children's Hospital, Zürich, Switzerland; and [5]InSightec, Ltd., Tirat Carmel, Israel

Object. Recent technological developments open the field of therapeutic application of focused ultrasound to the brain through the intact cranium. The goal of this study was to apply the new transcranial magnetic resonance imaging–guided focused ultrasound (tcMRgFUS) technology to perform noninvasive central lateral thalamotomies (CLTs) as a treatment for chronic neuropathic pain.

Methods. In 12 patients suffering from chronic therapy-resistant neuropathic pain, tcMRgFUS CLT was proposed. In 11 patients, precisely localized thermal ablations of 3–4 mm in diameter were produced in the posterior part of the central lateral thalamic nucleus at peak temperatures between 51°C and 64°C with the aid of real-time patient monitoring and MR imaging and MR thermometry guidance. The treated neuropathic pain syndromes had peripheral (5 patients) or central (6 patients) origins and covered all body parts (face, arm, leg, trunk, and hemibody).

Results. Patients experienced mean pain relief of 49% at the 3-month follow-up (9 patients) and 57% at the 1-year follow-up (8 patients). Mean improvement according to the visual analog scale amounted to 42% at 3 months and 41% at 1 year. Six patients experienced immediate and persisting somatosensory improvements. Somatosensory and vestibular clinical manifestations were always observed during sonication time because of ultrasound-based neuronal activation and/or initial therapeutic effects. Quantitative electroencephalography (EEG) showed a significant reduction in EEG spectral overactivities. Thermal ablation sites showed sharply delineated ellipsoidal thermolesions surrounded by short-lived vasogenic edema. Lesion reconstructions (18 lesions in 9 patients) demonstrated targeting precision within a millimeter for all 3 coordinates. There was 1 complication, a bleed in the target with ischemia in the motor thalamus, which led to the introduction of 2 safety measures, that is, the detection of a potential cavitation by a cavitation detector and the maintenance of sonication temperatures below 60°C.

Conclusions. The authors assert that tcMRgFUS represents a noninvasive, precise, and radiation-free neurosurgical technique for the treatment of neuropathic pain. The procedure avoids mechanical brain tissue shift and eliminates the risk of infection. The possibility of applying sonication thermal spots free from trajectory restrictions should allow one to optimize target coverage. The real-time continuous MR imaging and MR thermometry monitoring of targeting accuracy and thermal effects are major factors in optimizing precision, safety, and efficacy in an outpatient context.

(http://thejns.org/doi/abs/10.3171/2011.10.FOCUS11248)

Key Words • central lateral thalamotomy • neuropathic or neurogenic pain • transcranial magnetic resonance imaging–guided focused ultrasound

Considering the inherent risks related to neurosurgical procedures, such as infections and hemorrhages, there is an obvious demand for less invasive alternative procedures. Following extensive preclinical investigations,[4–8,10,11,13,15,24,25,31,32] a clinically relevant prototype of a tcMRgFUS device for thermal ablation was developed.[9,12,14] Because of its noninvasiveness, focused ultrasound technology eliminates the risk of infection, reduces the risk of bleeding, and limits collateral damage to nontargeted tissue. Magnetic resonance imaging allows precise intraprocedural localization of the ablation target, definition and verification of safety margins for the ultrasound treatment, real-time monitoring of thermal ablation dynamics, and intra- and posttreatment assessment of intervention results.[2,3,21] The tcMRgFUS technique involves the transformation of sonic into thermal energy and the production of a thermolesion. The possibility of

Abbreviations used in this paper: CLp = posterior part of the thalamic central lateral nucleus; CLT = central lateral thalamotomy; DT = diffusion tensor; EEG = electroencephalography; tcMRgFUS = transcranial magnetic resonance imaging–guided focused ultrasound; VAS = visual analog scale; VLp = posterior part of the thalamic motor ventral lateral nucleus.

applying this technique transcranially (that is, without injury to skin and skull) has great potential in the field of neurosurgery.[16,22]

A recent landmark clinical study[23] examined the feasibility and initial technical results of tcMRgFUS and showed for the first time in 3 patients that it is possible to focus the ultrasound beam through the intact skull into the brain and to visualize internal heating at the focal point and on the brain surface by using MR imaging temperature mapping. These findings constitute a significant step forward in establishing an entirely noninvasive alternative therapy to surgery for brain disorders.

Based on our long-term clinical experience in functional neurosurgery for neuropathic (or neurogenic) pain with radiofrequency stereotactic interventions in the medial thalamus,[17,19,20] and after preclinical studies with phantoms, biological tissues, and ex vivo human head preparations, we adapted our interventional procedure to perform CLTs in patients suffering from chronic neuropathic pain using the tcMRgFUS technology. The study was approved by the ethics committee of Zurich University and the state of Zurich (Kantonale Ethikkommission des Kantons Zürich). An initial report about the short-term results for 9 patients has already been published.[26] The present report provides clinical and neurophysiological results over 1 year as well as analyses of the targeting precision and the postoperative MR imaging visualization of the produced thermolesions.

Methods

Patient Population

Twelve patients with chronic therapy-resistant neuropathic pain were enrolled for tcMRgFUS CLT and provided their written informed consent. For the sake of safety, a thermal spot of only 42°C was placed in the first patient. This intervention did not result in a thermolesion and this patient was excluded from further analysis. Therapy resistance was established based on the lack of efficacy and/or the side effects of antiepileptic and antidepressant drugs. Patients were 45–75 years old and suffered from facial pain (3 patients), thoracic pain (1 patient), lower-extremity pain (3 patients), upper-extremity pain (4 patients), and hemibody pain (1 patient), of central (6 patients) or peripheral (5 patients) origin (Table 1). The causal lesions at the origin of the different neuropathic pain syndromes were amputation (phantom limb pain, 1 patient), root compression in failed–back surgery syndrome (1 patient), root compression by neurinoma (1 patient), herpes zoster infection (1 patient), nerve trauma (1 patient), spinal cord lesion (2 patients), putaminal lesion (1 patient), brachial plexus avulsion (2 patients), and thalamic infarct (1 patient). The duration of pain before treatment was between 1.5 and 21 years (mean 8.5 years). A pre- and postoperative pain assessment was performed using a detailed questionnaire, including the items of the McGill Pain Questionnaire. The VAS rating of pain intensity was noted for the least and worst pain intensities on a scale between 1 and 100. In addition, patients provided a global percentage value of postoperative pain relief as compared with the preoperative state. In patients with chronic therapy-resistant neuropathic pain, a pain relief scale and VAS value comparisons for pain intensity reduction after treatment are the most adapted and commonly recognized assessment indicators to serve as primary outcome measures for success. Patients were clinically examined as follows: repetitive assessments during the treatment (see below); clinical examination on the evening of the treatment day and 24 and 48 hours afterward; telephone consultation at 1 month after treatment; and full reassessment at 3 months and 1 year after treatment.

Prior to treatment, the patients underwent CT scanning (512 × 512 matrix, 1-mm slice thickness) that covered the entire cranium as well as an MR imaging examination with T1- and T2-weighted images and DT imag-

TABLE 1: Summary of clinical and treatment data in 11 patients who underwent tcMRgFUS*

Case No.	Duration of Pain (yrs)	Location of Pain	Cause of Pain	CLT Side	Max Temp at Target (°C)	Sensory Improvements	Activation Effects
1	6	leg	root compression (disc herniation)	lt/rt	53	+	paresthesias in leg
2	8.5	hemibody	thalamic infarct	lt	51	+	vestibular, pain in head
3	2.5	face	traumatic trigeminal nerve injury	rt†	57	+	vestibular, pain in face
4	1.5	face	striatal	rt	59	−	vestibular, nausea, paresthesias in face, pain in face
5	4	face	postherpetic neuralgia	lt/rt	55	+	absent
6	9	arm	root compression (neurinoma)	lt/rt†	58	+	vestibular, vomiting, pain in head
7	17	arm	avulsion of brachial plexus	lt/rt†	57	−	vestibular, pain in head, paresthesias in arm
8	8	leg	phantom leg pain	rt†	55	−	pain in head
9	16	arms & legs	paraplegia	lt/rt	60	−	vestibular, pain in leg
10	7	thorax	syringomyelia	lt/rt	64	+	vestibular, pain in head, nausea
11	21	arm	avulsion of brachial plexus	lt	64	−	vestibular, paresthesias, pain in head

* The mean duration of pain among the patients was 8.5 years. Neurological deficits occurred in only one patient (Case 11): neglect and dysmetria because of bleeding and ischemia. Abbreviation: Temp = temperature ; + = improvement; − = no change.

† Complement to radiofrequency CLT.

ing. Identical MR imaging series were obtained at 2 days, 3 months, and 1 year postsonication.

Surgical Procedure

The treatment was performed in a 3-T MR imaging system (Signa HDx, GE) using the ExAblate 4000 device (InSightec), which features a 30-cm-diameter hemispherical 1024 element phased-array transducer operating at 650 kHz and held by a mechanical positioner. Magnetic resonance imaging was performed using an 8-channel torso phased-array coil.

The patient's scalp was fully and closely shaved, and the head was immobilized by fixation in an MR imaging–compatible frame (Radionics; Fig. 1). A circular flexible silicone membrane with a central hole was stretched around the patient's head and sealed to the outer face of the transducer to contain the degassed and chilled (15°–20°C) water that was circulated in the area between the head and the transducer. This membrane is tight enough to prevent water leakage without preventing blood circulation to the scalp.

Axial and sagittal T1- and T2-weighted fast spin echo images were obtained and coregistered to the previously acquired MR and CT images and to the current MR imaging/transducer coordinates. These images allowed us to calibrate the system and to produce precise stereotactic planes for target determination. The target area, the CLp, was localized on 3D T1-weighted MR images using the stereotactic multiarchitectonic Morel atlas of the human thalamus and basal ganglia.[27] The coordinates of the targets were then entered into the planning software of the tcMRgFUS system.

Several low-power sonications of 10–20 seconds duration were applied to induce peak temperatures of 39°–42°C, known to be below the ablation threshold. They allowed us to assess the exact position and size of the thermal spot and the overall safety profile of the applied sonication parameters.[15] Several high-power sonications were then applied in an iterative process guided by MR imaging and MR thermometry, with stepwise increases in the acoustic power and energy to finally achieve a peak temperature at the target between 51°C and 64°C (Fig. 2). The final peak temperature in each treatment is an outcome of various factors. Thermocoagulation effects on tissue can be produced and visualized from 50°C and up, with a 100% necrosis considered to arise at 55°–57°C. Optimal coverage of the target and the clinical feedback from patients both play a role in determining the final peak temperatures. These factors explain their range between 55°C and 64°C for the 9 patients with complete lesioning (see C*linical Results*). Typically, we applied sonications of 10 to 20 seconds in duration with up to a maximum acoustic power of 1200 and 800 W, respectively, corresponding to 12,000 J per sonication. The mean peak focal temperature achieved in the treatments was 53 ± 3.3°C (range 48°–61°C).

Fig. 1. Photograph of a patient ready for the sonication. The head is immobilized in a stereotactic frame. The transducer is held and positioned by a mechanical positioning system. The silicone membrane seals the space between the patient's head and the transducer, which is filled by degassed, cooled, and circulated water.

Patients were fully awake and responsive during all stages of the intervention. The only medication administered before the procedure consisted of lorazepam 2.5 mg orally. In 2 patients, a subcutaneous opiate injection was necessary because of back pain due to a motionless supine position on the MR imaging table for an extended period of time. During the entire series of sonications, patients were examined and questioned repeatedly to ensure their neurological integrity and to assess 1) changes in pain qualities, extension, and intensity; 2) potential somatosensory improvements; 3) the appearance of somatosensory, vestibular, and vegetative manifestations experienced during the treatment; and 4) the absence of any motor or somatosensory deficit.

The CLT was performed unilaterally (contralateral to the pain location) in 5 patients and bilaterally in 6 patients. A bilateral CLT is, in general, necessary, and it is as sparing of brain functions as a unilateral one.[19] In 4 patients, the tcMRgFUS treatment complemented a previously performed radiofrequency treatment. The CLT was performed unilaterally for the following reasons: complement to radiofrequency treatment (2 patients), appearance of bleeding (1 patient; see *Clinical Results*), immediate 100% pain relief after treatment of the first side (1 patient), and intolerance of a longer intervention time (1 patient).

Target Reconstruction Method

To evaluate the accuracy of tcMRgFUS targeting, the 3D coordinates of the centers of the sonication lesions, outlined on T2-weighted MR images obtained 48 hours after sonication, were measured and compared with presurgical stereotactic coordinates of the ablation targets. The dorsoventral coordinates were determined by the distance from the anterior commissure–posterior commissure plane passing through the center of the anterior and posterior commissures (on sagittal and/or coronal MR imaging); the anteroposterior coordinates, by the distance from the posterior commissure (on axial and sagittal MR imaging); and the mediolateral coordinates, by the distance from the thalamoventricular border (on coronal and axial MR imaging).

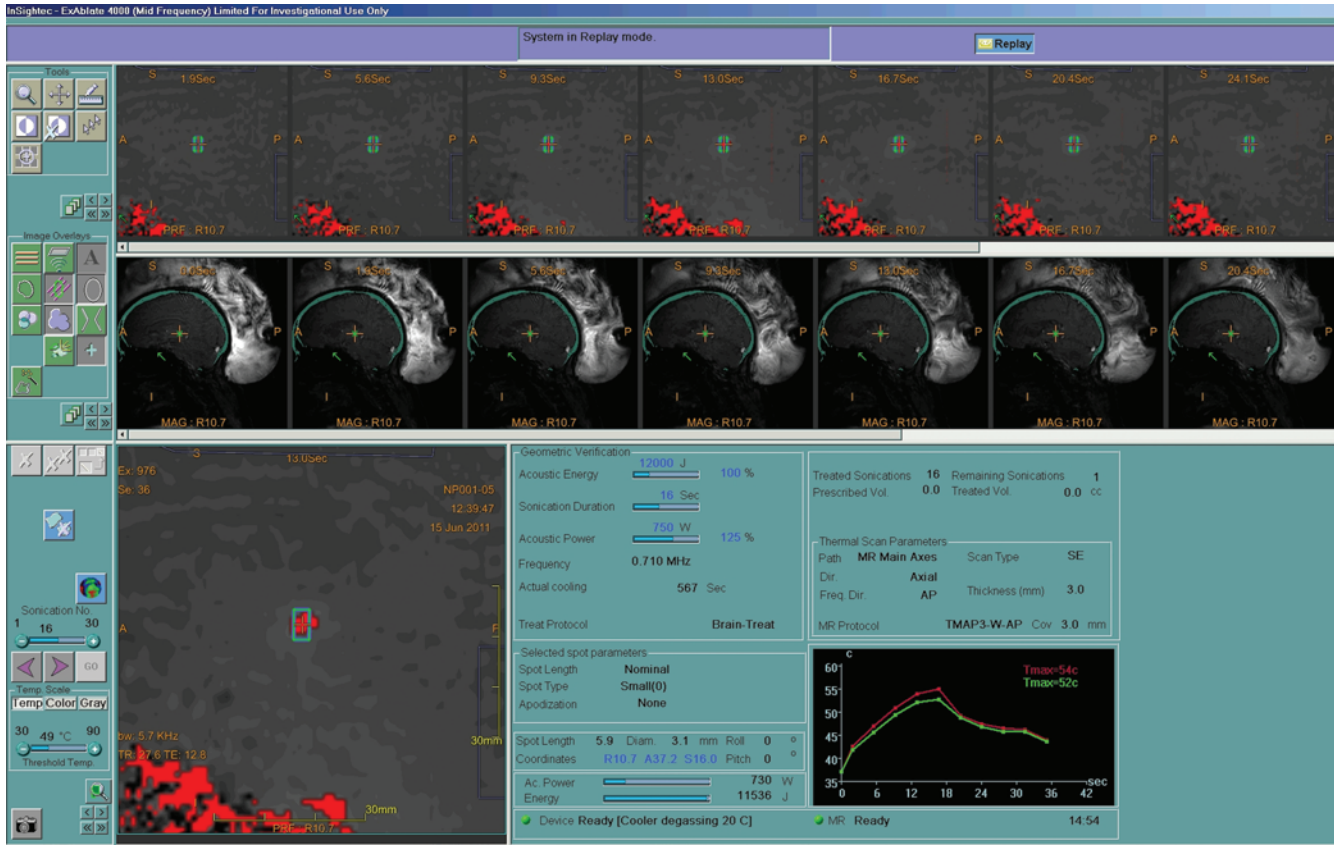

Fig. 2. Screenshot of the ExAblate 4000 display showing a series of proton resonance frequency MR images (obtained every 3.7 seconds, **upper**) and a series of magnitude images **(center)**. Magnification of a proton resonance frequency picture **(lower left)** showing in the center a thermal spot centered in the calculated target display *(blue rectangle)*. Display **(lower right)** showing the applied acoustic energy, sonication duration, acoustic power, target coordinates, thermal scan parameters, and temperature curve.

Quantitative EEG Procedure

Electroencephalography recording was performed at the time of clinical assessment, before entry into the study. The clinical states of the patients, reassessed at the time of enrollment in the month before treatment, remained unchanged, requiring no repetition of EEG recordings. A 10-minute EEG recording was monitored during alternating eyes-open and eyes-closed states (2 blocks with eyes open and 2 blocks with eyes closed). The EEG activity was recorded from a cap with 60 scalp channels (Easycap) using a 500-Hz sampling rate, 32-mV input range, and 0.1- to 250-Hz bandpass filters. The impedance was kept below 20 kΩ. Electrodes were mounted according to the 10–20 system plus the following 10–10 system sites: FPz, AFz, FCz, CPz, POz, Oz, Iz, F5/6, FC1/2/3/4/5/6, FT7/8/9/10, C1/2/5/6, CP1/2/3/4/5/6, TP7/8/9/10, P5/6, PO1/2/9/10, OI1/2. Both O1/2 and FP1/2 were placed 2 cm laterally from the standard positions for more even coverage. Note that F1 served as the recording reference and F2 was the ground electrode. Two additional electrodes were placed below the outer canthus of each eye to measure for electrooculography.

BrainVision Analyzer software (version 1.05, Brain Products) served for offline processing of the EEG. Subsequently, electrooculography channels were discarded from further analysis. Data were digitally bandpass filtered (0.5–70 Hz, 24 dB/oct, and 50-Hz notch) and downsampled to 250 Hz. An infomax independent component analysis was calculated to remove artifacts related to eye movements, eye blinks, and muscle contractions. Movement-related artifacts, which may not be suitable for independent component analysis correction, were excluded from the unmixing procedure. Components were profiled by their topography, activation time course, and spectrogram. After artifact removal, the components were first back-projected to the EEG and then transformed to the average reference. Segments with remaining artifacts were marked and excluded from successive analysis (mean length of the EEG was about 4 minutes for each resting state condition). Next, the data were parsed into 2-second epochs. Absolute spectral power was estimated for each epoch using fast Fourier transform (Hanning window: 10%, zero-padded, resolution 0.5 Hz). The mean spectral band power was calculated from 1–48 Hz. Spectral bands were defined as follows: delta (2–4 Hz), theta (4–8 Hz), alpha1 (8–13 Hz), and beta (13–30 Hz). (Note that the superior spectral band limit is included only in the next higher band.) The EEG was analyzed in terms of absolute spectral power as well as electrode-wise comparisons to preserve topographic information (topoplots). For each separate condition, spectral power values were averaged across fast Fourier transform epochs and aver-

aged within the above frequency bands. Group means were compared using t-statistics ($p < 0.05$ indicated significance).

Results

Clinical Results

In the first 2 patients of this series, the therapeutic lesions placed in the CLp, as seen 48 hours after treatment on T2-weighted and DT images, were too small to cover it in any sufficient manner. The tcMRgFUS treatment could thus be considered complete in only 9 of the 11 patients. An analysis of global pain relief percentages as reported by the patients and of VAS values was performed for these 9 patients only; results are listed in Table 2. The preoperative mean VAS score was 59.5/100. Significant pain relief (mean group value 55%) was already reported during and at the end of the procedure. More reliable pain relief percentages were collected at 2 days (mean group value 71.1%, 9 patients), 3 months (mean group value 49.4%, 9 patients), and 1 year (mean group value 56.9%, 8 patients) after treatment. The postoperative mean VAS score was 34.3/100 at 3 months and 35.3/100 at 1 year, representing a 42.3% and 40.7% postoperative improvement, respectively.

At the 1-year follow-up, among 8 patients, 5 took no drugs against pain, but 3 maintained a globally unchanged regimen. Drug intake is, for many reasons, not a good marker of the postoperative evolution of patients who have suffered from long-standing, therapy-resistant neuropathic pain. On the one hand, some patients may have stopped their drug intake before the intervention because of insufficient or absent efficacy or because of side effects. On the other hand, some patients have habituated to their drugs for years and are afraid to reduce or stop them, making a consequent and predetermined drug reduction program practically and ethically impossible.

Six patients experienced significant intraoperative somatosensory improvements in and around the pain area, which they spontaneously mentioned during the treatment. These improvements were confirmed after the intervention and remained at the 3-month and 1-year follow-ups.

Patients reported clinical effects during sonication, such as pain relief (9 patients), vestibular with or without vegetative manifestations (8 patients), paresthesias (4 patients), or dysesthesias/pain (9 patients). These symptoms could already be observed at focal temperatures below 50°C.

In 1 patient, displacement of the headframe occurred, but it was repositioned without negative consequences. In the last minutes of the procedure after all planned sonications had been completed, the last patient in this series experienced the acute appearance of right-sided motor hemineglect with dysmetria of the arm and leg and dysarthria. Magnetic resonance imaging examinations immediately and 48 hours thereafter revealed the presence of a bleed 8–10 mm in maximal diameter centered in the targeted CLp, as well as ischemic changes in the VLp. These were causal for the motor symptoms presented by the patient. Subsequent control MR images showed a good progressive resorption of the bleeding. Clinically, there was a 70%–80% reduction in the motor symptoms over the next 24 hours. With time, all dysmetric manifestations disappeared except during activation of the finer functions of speaking and writing, which at 1 year posttreatment remained impeded during demanding and stressful personal and professional interactions.

Lesion Coordinate Reconstruction for Assessment of Targeting Precision

The sonication lesions were at best visible 48 hours after the intervention (Fig. 3 upper) and consisted of a mostly hyperintense ellipsoid lesion with a diameter of 3–4 mm and a length of 4–5 mm. It was surrounded by a

TABLE 2: Summary of postoperative data in 11 patients who underwent tcMRgFUS*

	Pain Relief (%)				VAS Score (lowest–highest, mean)			
Case No.	Acute	2 Days	3 Mos	1 Yr	Before Sonication	3 Mos After Sonication	1 Yr After Sonication	1 Yr Postop Drug Intake
1	100	70	0	lost to FU	70–80	16–79	UN	reduced†
2	30	30	0–30	lost to FU	72–100	40–70	UN	unchanged
3	10	100	80	80	52–73, 62.5	5–20, 12.5	9–16, 12.5	stopped
4	70	50	50	95	40–80, 60	0–72, 36	9–36, 22.5	stopped
5	100	80	0	deceased‡	12–78, 45	0–50, 25	UN	UN
6	30	100	90	100	39–62, 50.5	0–11, 5.5	0	stopped
7	30	50	50	40	22–85, 53.5	15–84, 49.5	21–86, 53.5	unchanged
8	100	100	70	50	56–85, 70.5	13–80, 46.5	77	unchanged
9	0	10	0	0	67–90, 78.5	54–89, 71.5	11–84, 47.5	unchanged
10	100	75	90	80	44–91, 67.5	0–14, 7	0–28, 14	stopped
11		75	15	10	25–70, 47.5	30–80, 55	30–80, 55	stopped
overall mean§	55	71.1	49.4	56.9	59.5	34.3	35.3	UN

* FU = follow-up; UN = unavailable.
† Includes opiates.
‡ Unrelated medical cause.
§ The mean values for global pain relief and VAS were calculated for Cases 3–11 only.

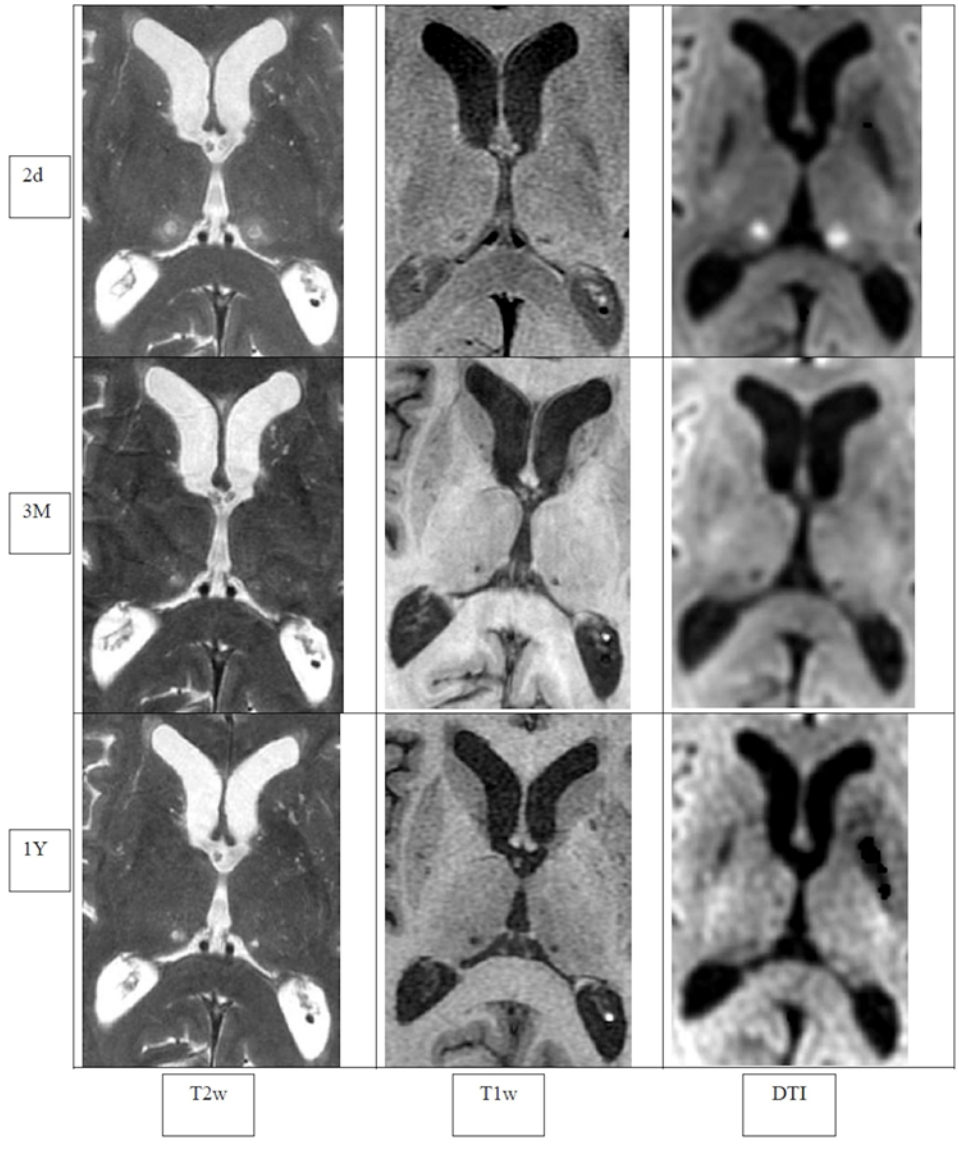

Fig. 3. Magnetic resonance images showing the therapeutic lesions 2 days (2d), 3 months (3M), and 1 year (1Y) after the sonication. DTI = diffusion tensor images, isotropic diffusion mode; T1w = T1-weighted images; T2w = T2-weighted images.

fuzzy and irregularly shaped area of perifocal vasogenic edema, which completely receded over a month. Lesions were significantly smaller at 3 and 12 months after treatment (Fig. 3 center and lower). A detailed neuroradiological description of the sonication lesions was previously published.[26]

The median and mean (± standard deviation) of the targeting accuracy are given in millimeters in Table 3 for the patients in Cases 1–9 and separately for the first and second groups treated sequentially. The deviations for the first group (5 patients, 9 lesions) are larger in all axes than for the second group (4 patients, 9 lesions) treated after the implementation of procedural improvements, that is, better accuracy in the thermal spot realignment during the verification phase at low temperatures, and an optimization of the determination of the center frequency of the MR acquisition for proper thermal imaging projection. The increased accuracy between the 2 subgroups was most marked in the anteroposterior direction (from 1.17 ± 0.58 to 0.39 ± 0.46 mm). The mean values for the whole group are < 1 mm in all axes, but larger in the mediolateral axis than in the other axes.

Localization of the tcMRgFUS lesions in the thalamus is illustrated in Fig. 4. Projections of the lesions onto horizontal sections of the Morel atlas[27] showed the following: of 18 lesions, 7 enclosed most, if not the whole, anteroposterior extent of the CLp (targeted in CLT); 5 enclosed half of it; and 6 enclosed up to one-third. Most partial CLT lesions encroached onto the pulvinar, and only 2 encroached on the posteriormost part of the mediodorsal nucleus. The first series of lesions (Cases 1–5, Subgroup 1) tended to be more posterior and overlapped less with the CLp than the rest of the lesions (Cases 6–9, Subgroup 2). This result corresponds to the measurements shown in Table 3. Note that in the patients in Cases 3, 6, and 7, a part of the excentering of the focused ultrasound lesions

TABLE 3: Precision of tcMRgFUS targeting*

Parameter	Total Patients		Subgroup 1		Subgroup 2	
	Mean ± SD	Median	Mean ± SD	Median	Mean ± SD	Median
no. of patients	9		5		4	
dorsoventral	0.58 ± 0.63	0.5	0.61 ± 0.57	0.5	0.56 ± 0.68	0
anteroposterior	0.78 ± 0.65	1.0	1.17 ± 0.58	1.5	0.39 ± 0.46	0
mediolateral	0.83 ± 0.78	0.5	1.01 ± 0.85	0.7	0.82 ± 0.79	0.5

* Values of dorsoventral, anteroposterior, and mediolateral differences between centers of the sonication lesions and presurgical target coordinates are expressed in mm.

is related to target adaptations due to previously made radiofrequency CLT lesions and not only to suboptimal procedural factors.

Quantitative EEG Assessment

The spectral comparison of the 8 patients who underwent a 3- and 12-month follow-up EEG recording revealed 2 major findings. First, spectral power was elevated in all frequency bands (delta–beta) before the sonication (Fig. 5 upper). Second, frequency band–specific spectral power amplitudes were reduced 3 and 12 months after the sonication, and thus were approaching the spectral curve of healthy volunteers. An electrode-wise comparison of frequency band–specific spectral power showed that several scalp locations displayed significantly elevated power before as compared with 12 months after sonication (Fig. 5 lower). On the topoplots featured in Fig. 5, black dots indicate the electrodes, which show significantly ($p < 0.05$, $t > 2$) higher spectral power before as compared with 12 months after sonication, in delta (2–4 Hz) and theta (4–8 Hz) bands at frontal, centrotemporal, and parietal electrodes; and in alpha (8–13 Hz) and beta (13–30 Hz) bands at centroparietal electrodes.

Discussion

This report on the clinical, neurophysiological, and neuroanatomical results of tcMRgFUS CLT for neuropathic pain demonstrates the precision and efficacy of this surgical approach and confirms the short-term results reported previously.[26]

The clinical results presented here support our long experience with radiofrequency CLT treatment for chronic therapy-resistant neuropathic pain.[19,20] The patients in this series showed a typical mean group pain relief profile across time, from 71% at 2 days after treatment to 49% at 3 months and 57% at 1 year after treatment. The VAS improvement was similar at 3 months (42%) and at 1 year (41%). This profile can be explained as follows: the immediate reduction of low-frequency overactivity using CLT provides the patient with acute relief. However, complex nonlinear systems, like the thalamocortical system, display typically protracted dynamics when they change from one activity level to another and search for a new resting state. This explains why the EEG spectral improvements, in parallel with clinical relief, develop over at least 1 year.[28,30] After the initial pain relief and as the thalamocortical network just begins its retuning (reorganization) toward normal activity, emotional, cognitive, and social factors intervene and influence the patient's evolution as he or she revisits specific personal goals put aside because of chronic pain and progressively adapts to new individual goals and concepts. This endeavor becomes less and less demanding as time goes by and the thalamocortical network comes closer to normality.

Previous studies[28–30] have related the clinical phenomenon of chronic neuropathic pain to an increase in low- and high-frequency spectral EEG and magnetoencephalography activities. This correlation is further supported by the evidence of reduced theta overactivity in the EEG recordings of patients treated with CLT.[28,30] Electroencephalography spectral analysis can thus be used as an additional tool to diagnose chronic neuropathic pain states and monitor their postoperative evolution. The EEG spectral data presented here are fully compatible with these studies and demonstrate 1) EEG overactivities in all frequency domains and 2) their reduction, particularly strong in the beta range, after the tcMRgFUS treatment. They serve as additional evidence in favor of thalamocortical mechanisms being at the source of neuropathic pain.

The absence of postoperative clinical deficits, known for years about medial thalamotomies, has been confirmed for CLT, a medial thalamotomy centered on the CLp where an abnormal low-threshold calcium spike burst activity was recorded.[17] Results in the present study confirm the sparing mode of action of CLT, which selectively targets dysfunctional thalamocortical regulators, initiating a resumption of normal thalamocortical dynamics while sparing all functions supported by unaffected thalamocortical regulators and executors. The absence of postoperative kindling of new neuropathic pain mechanisms has been shown years after CLT and can be related to the selective reduction of the thalamocortical pathophysiology at the source of neuropathic pain phenomena.[19,20] Six patients experienced immediate and significant somatosensory improvements, which persisted at the 3-month and 1-year follow-ups. This result corresponds with observations after radiofrequency lesions[18] and can also be related to the reduction of thalamocortical overactivity by CLT.

Effects during sonication, whether somatosensory, vestibular, or vegetative, were observed in all patients. They may have 2 origins: 1) an activation of neurons during the few seconds before the thermal ablation effect and 2) initial manifestations of the resumption of a more normal thalamocortical dynamics, as is routinely seen in our experience with radiofrequency CLT, thereby indicat-

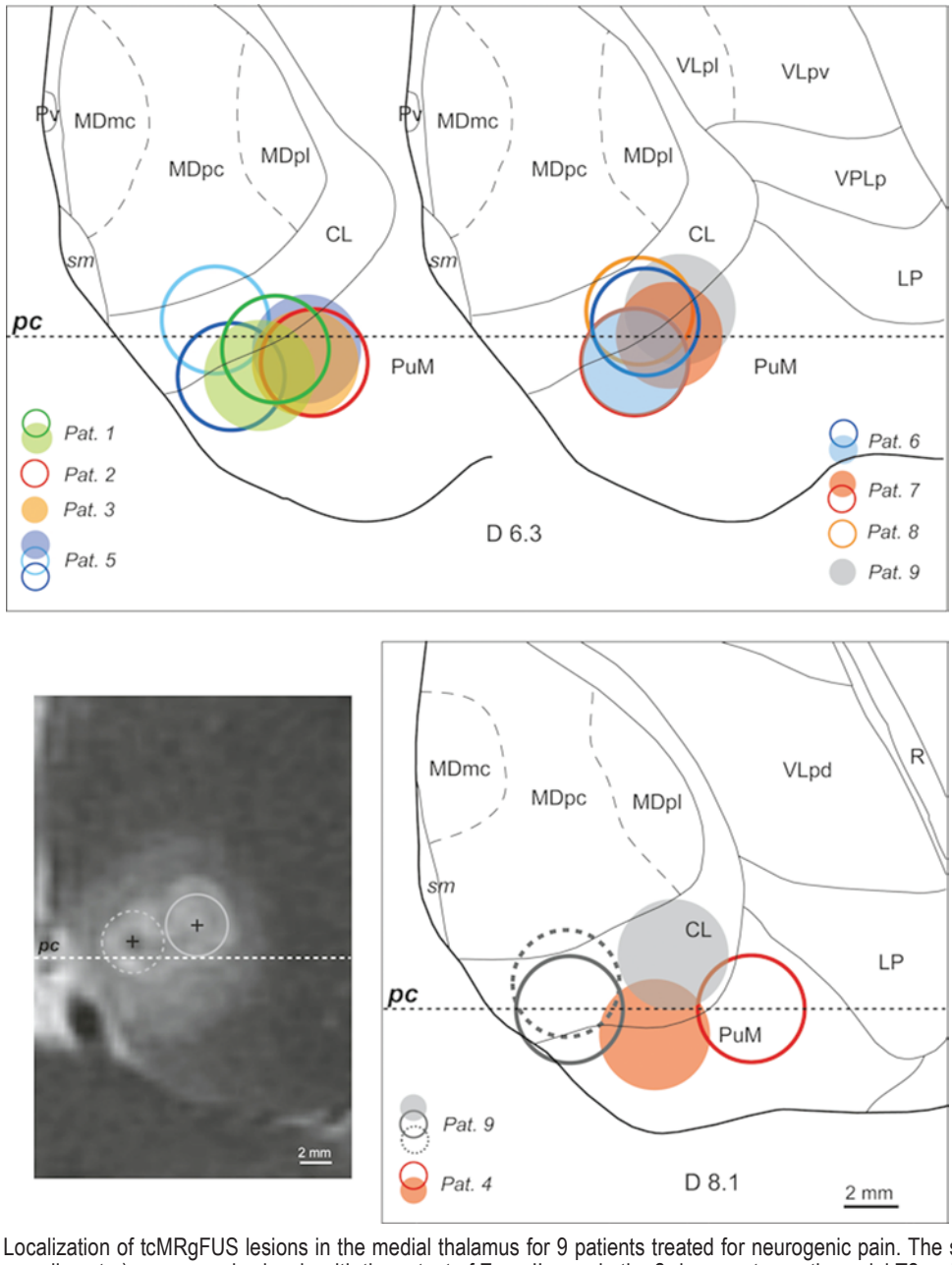

Fig. 4. Localization of tcMRgFUS lesions in the medial thalamus for 9 patients treated for neurogenic pain. The size of the lesions (4-mm diameter) corresponds closely with the extent of Zone II seen in the 2-days postoperative axial T2-weighted MR image **(lower left)**. The location of the lesion in relation to the CLp is determined by projection of the corresponding atlas maps (6.3 **[upper]** and 8.1 **[lower right]** mm dorsal to the intercommissural plane) onto the MR image by using the position of the posterior commissure (pc, *dotted line*) for alignment. The 2 lesions projected on the MR image are the 2 anteriormost lesions in the patient in Case 9 **(lower right)**. CL = central lateral; LP = lateral posterior; MDmc = mediodorsal magnocellular division; MDpc = mediodorsal parvocellular division; MDpl = mediodorsal paralamellar division; PuM = medial pulvinar; Pv = paraventricular; R = reticular thalamic nucleus; sm = stria medullaris; VLpd = ventral lateral posterior, dorsal division; VLpl = ventral lateral posterior, paralamellar division; VLpv = ventral lateral posterior, ventral division; VPLp = ventral posterior lateral, posterior part..

ing appropriate target placement. To monitor safety and acquire real-time feedback and information, the presence of a clinician by the patient's side throughout the treatment phase is required. This practice ensures that the sonication effects, including changes in neurological parameters, as well as patient safety and comfort during the extended period of time in the MR imaging unit are closely monitored.

The tcMRgFUS CLT thermolesions as seen on MR imaging 2 days after sonication were surrounded by a vasogenic edema, which was no longer visible after 1 month. Visualization of the thermolesion itself receded between 1 and 3 months. These observations are indicative of a selective neuronal coagulation with few hemorrhagic components, which are often seen with radiofrequency thermolesions and correlate with a much longer

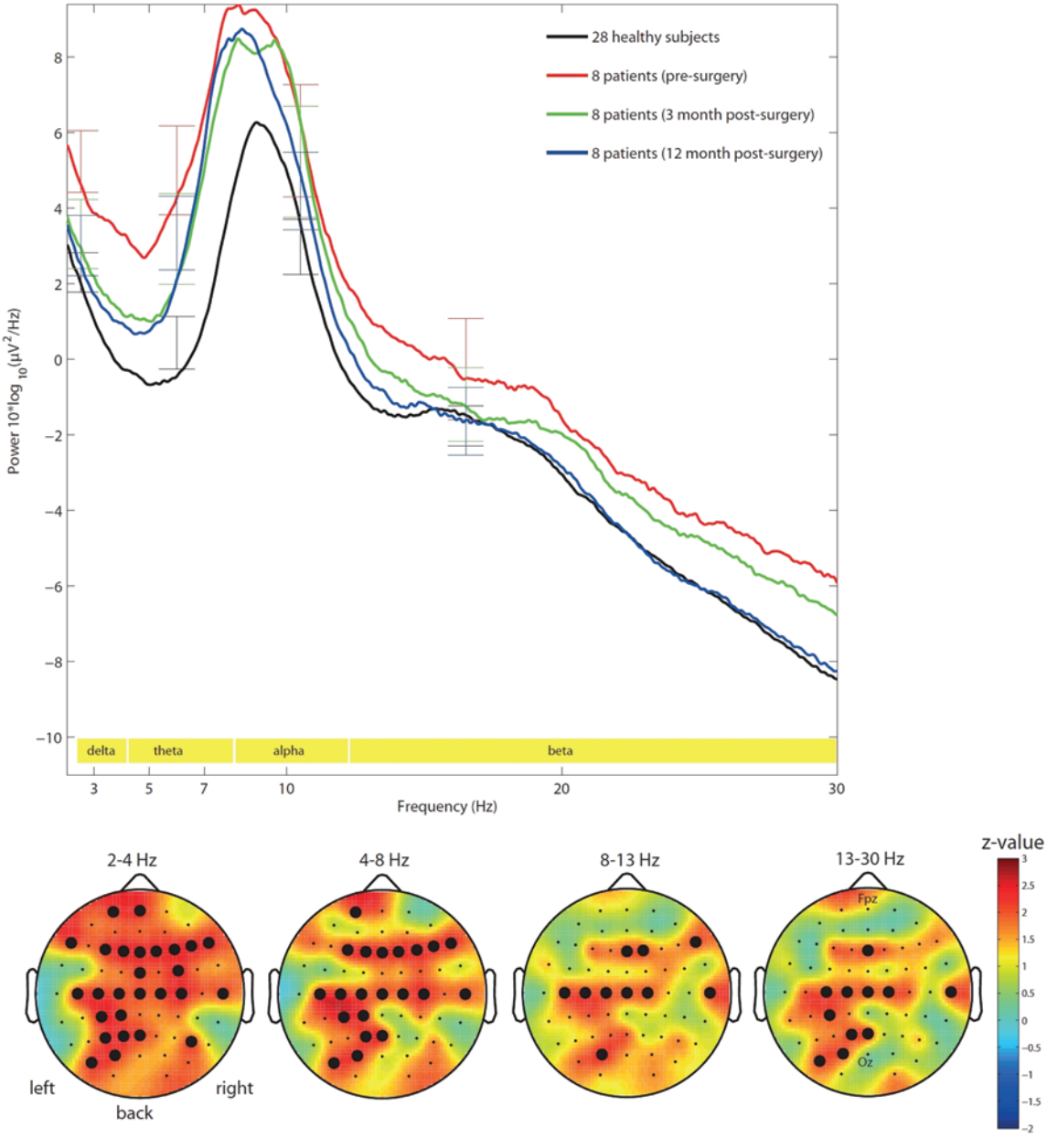

Fig. 5. Upper: Graph showing power spectral curves of the patients before and after surgery with standard deviations of the means *(vertical bars)*. *Black curve* is for controls. Frequency bands are shown in *yellow* at the bottom of the graph. **Lower:** Topoplots showing electrode-wise comparisons. *Black dots* indicate the electrodes, which showed significantly higher spectral power before surgery as compared with 12 months after surgery.

maintenance of edema. With tcMRgFUS, there is no mechanical trauma of the target tissue, and the temperature at the center of the hotspot is not as high as with radiofrequency ablation. With radiofrequency ablation, the temperature, depending on the electrode geometry, must be much higher than 60°C at the electrode tip to achieve the necessary heating over the desired target volume. At 48 hours postsonication, the blood-brain barrier was seen to be closed.[26] All of these observations are compatible with a clean thermolesion displaying a fast healing process and speak against the possibility of unexpected deleterious long-term tissue phenomena. In this context, the bleeding that occurred in our last patient demands an explanation, particularly since he presented no increased risk factors (he had normal blood pressure and coagulation). A detailed case study was performed to analyze the factors that might have facilitated this event. Two factors were considered: first, the possibility of the development of a cavitation effect, although a detailed analysis provided no direct evidence in its favor. Nevertheless, this possibility requires the installation of a cavitation detector to detect and stop this phenomenon as soon as it appears. Second, a temperature-related factor must be considered, supported by published evidence[32] and confirmed by recent experimental data collected in the context of this case study. Accordingly, we recommend maintaining the sonication

temperatures below 60°C. Note that the bleeding itself, centered in the adequately targeted CLp, did not produce deficits. It is the ischemia, extending anteriorly and laterally into the VLp, that caused the typical motor symptomatology. We hypothesize a blood-induced vasospasm in the VLp as a causal link between the 2 events.

Our target reconstructions demonstrate precision within a millimeter for all 3 target coordinates. The classic stereotactic techniques involving penetration of an electrode into the brain cannot, despite adequate technological accuracy, reach such final precision because of the unforeseeable mechanical shift of brain tissue by the electrode.[1] In addition, the tcMRgFUS CLT should allow for optimal target volume coverage thanks to the absence of electrode trajectory restrictions. Such optimization should develop with increased procedural experience and further technological developments, both decreasing the time devoted to optimal target coverage during treatment. This should correlate with higher long-term pain relief scores as compared with our previous results with CLT.[19] The patient group in the present study is too small to be conclusive on this question, and further long-term studies on larger patient groups will have to verify whether this is indeed the case. Sonication also proved to be particularly helpful for 4 patients who had previously been treated with radiofrequency CLT, facilitating the complementary treatment by avoiding potential shifts of penetrations through gliotic tissue.

Conclusions

Results of the current study highlight the precision and efficiency of tcMRgFUS for treating chronic neuropathic pain. The noninvasiveness of the procedure and specifically the continuous MR imaging and MR thermometry monitoring of the intervention represent major factors toward an optimization of safety conditions. This radiation-free technology can be applied to other functional brain disorders as well as to numerous other neurosurgical indications and is an important option because of the elimination of brain tissue shift or trauma during therapy. Besides, tcMRgFUS has a probably reduced bleeding risk, no risk of intracranial infection, and is not limited in target coverage by trajectory constraints.

Disclosure

This work was supported by the University of Zürich, the Swiss Federal Institute of Technology Zürich, the University Children's Hospital Zürich, the Swiss National Center of Competence in Research (NCCR) "Computer Aided and Image Guided Medical Interventions", the Focused Ultrasound Surgery Foundation (Charlottesville, VA), and the Sanitas Hospital in Kirchberg. Mr. Zadicario is an employee of InSightec, Ltd.

Author contributions to the study and manuscript preparation include the following. Conception and design: Jeanmonod, Werner, Morel, Michels, Zadicario, Martin. Acquisition of data: Jeanmonod, Werner, Morel, Michels, Schiff, Martin. Analysis and interpretation of data: Jeanmonod, Morel, Michels, Schiff, Martin. Drafting the article: Jeanmonod, Morel, Michels. Critically revising the article: all authors. Reviewed submitted version of manuscript: Jeanmonod, Werner, Morel, Zadicario, Schiff, Martin. Approved the final version of the manuscript on behalf of all authors: Jeanmonod. Statistical analysis: Morel, Michels. Administrative/technical/material support: Jeanmonod, Zadicario, Schiff, Martin. Study supervision: Jeanmonod, Martin.

Acknowledgments

The authors are most grateful for the technical support of InSightec, Ltd. They thank M. Gallay and A. Poveda-Ramos for intraoperative patient monitoring and support.

References

1. Bourgeois G, Magnin M, Morel A, Sartoretti S, Huisman T, Tuncdogan E, et al: Accuracy of MRI-guided stereotactic thalamic functional neurosurgery. **Neuroradiology 41:**636–645, 1999
2. Chen L, Bouley D, Yuh E, D'Arceuil H, Butts K: Study of focused ultrasound tissue damage using MRI and histology. **J Magn Reson Imaging 10:**146–153, 1999
3. Chung AH, Jolesz FA, Hynynen K: Thermal dosimetry of a focused ultrasound beam in vivo by magnetic resonance imaging. **Med Phys 26:**2017–2026, 1999
4. Clement GT, Hynynen K: Correlation of ultrasound phase with physical skull properties. **Ultrasound Med Biol 28:**617–624, 2002
5. Clement GT, Hynynen K: Micro-receiver guided transcranial beam steering. **IEEE Trans Ultrason Ferroelectr Freq Control 49:**447–453, 2002
6. Clement GT, Hynynen K: A non-invasive method for focusing ultrasound through the human skull. **Phys Med Biol 47:**1219–1236, 2002
7. Clement GT, Sun J, Giesecke T, Hynynen K: A hemisphere array for non-invasive ultrasound brain therapy and surgery. **Phys Med Biol 45:**3707–3719, 2000
8. Clement GT, White J, Hynynen K: Investigation of a large-area phased array for focused ultrasound surgery through the skull. **Phys Med Biol 45:**1071–1083, 2000
9. Clement GT, White PJ, King RL, McDannold N, Hynynen K: A magnetic resonance imaging-compatible, large-scale array for trans-skull ultrasound surgery and therapy. **J Ultrasound Med 24:**1117–1125, 2005
10. Cohen ZR, Zaubermann J, Harnof S, Mardor Y, Nass D, Zadicario E, et al: Magnetic resonance imaging-guided focused ultrasound for thermal ablation in the brain: a feasibility study in a swine model. **Neurosurgery 60:**593–600, 2007
11. Connor CW, Clement GT, Hynynen K: A unified model for the speed of sound in cranial bone based on genetic algorithm optimization. **Phys Med Biol 47:**3925–3944, 2002
12. Hynynen K, Clement GT, McDannold N, Vykhodtseva N, King R, White PJ, et al: 500-element ultrasound phased array system for noninvasive focal surgery of the brain: a preliminary rabbit study with ex vivo human skulls. **Magn Reson Med 52:**100–107, 2004
13. Hynynen K, Jolesz FA: Demonstration of potential noninvasive ultrasound brain therapy through an intact skull. **Ultrasound Med Biol 24:**275–283, 1998
14. Hynynen K, McDannold N, Clement G, Jolesz FA, Zadicario E, Killiany R, et al: Pre-clinical testing of a phased array ultrasound system for MRI-guided noninvasive surgery of the brain—a primate study. **Eur J Radiol 59:**149–156, 2006
15. Hynynen K, Vykhodtseva NI, Chung AH, Sorrentino V, Colucci V, Jolesz FA: Thermal effects of focused ultrasound on the brain: determination with MR imaging. **Radiology 204:** 247–253, 1997
16. Jagannathan J, Sanghvi NT, Crum LA, Yen CP, Medel R, Dumont AS, et al: High-intensity focused ultrasound surgery of the brain: part 1—A historical perspective with modern applications. **Neurosurgery 64:**201–211, 2009
17. Jeanmonod D, Magnin M, Morel A: Low-threshold calcium

spike bursts in the human thalamus. Common physiopathology for sensory, motor and limbic positive symptoms. **Brain 119:**363–375, 1996
18. Jeanmonod D, Magnin M, Morel A: A thalamic concept of neurogenic pain, in Gebhart GF, Hammond DL, Jensen TS (eds): **Proceedings of the 7th World Congress on Pain. Progress in Pain Research and Management, Vol 2.** Seattle: International Association for the Study of Pain, 1994, pp 767–787
19. Jeanmonod D, Magnin M, Morel A, Siegemund M: Surgical control of the human thalamocortical dysrhythmia: I. Central lateral thalamotomy in neurogenic pain. **Thalamus Relat Syst 1:**71–79, 2001
20. Jeanmonod D, Morel A: The central lateral thalamotomy for neuropathic pain, in Lozano AM, Gildenberg Pl, Tasker RR (eds): **Textbook of Stereotactic and Functional Neurosurgery, ed 2.** Berlin: Springer-Verlag, 2009, pp 2081–2096
21. Jolesz FA, Hynynen K, McDannold N, Tempany C: MR imaging-controlled focused ultrasound ablation: a noninvasive image-guided surgery. **Magn Reson Imaging Clin N Am 13:** 545–560, 2005
22. Jolesz FA, McDannold N: Current status and future potential of MRI-guided focused ultrasound surgery. **J Magn Reson Imaging 27:**391–399, 2008
23. McDannold N, Clement GT, Black P, Jolesz F, Hynynen K: Transcranial magnetic resonance imaging-guided focused ultrasound surgery of brain tumors: initial findings in 3 patients. **Neurosurgery 66:**323–332, 2010
24. McDannold N, King RL, Hynynen K: MRI monitoring of heating produced by ultrasound absorption in the skull: in vivo study in pigs. **Magn Reson Med 51:**1061–1065, 2004
25. McDannold N, Vykhodtseva N, Jolesz FA, Hynynen K: MRI investigation of the threshold for thermally induced blood-brain barrier disruption and brain tissue damage in the rabbit brain. **Magn Reson Med 51:**913–923, 2004
26. Martin E, Jeanmonod D, Morel A, Zadicario E, Werner B: High-intensity focused ultrasound for noninvasive functional neurosurgery. **Ann Neurol 66:**858–861, 2009
27. Morel A: **Stereotactic Atlas of the Human Thalamus and Basal Ganglia.** New York: Informa Healthcare, 2007
28. Sarnthein J, Stern J, Aufenberg C, Rousson V, Jeanmonod D: Increased EEG power and slowed dominant frequency in patients with neurogenic pain. **Brain 129:**55–64, 2006
29. Schulman JJ, Ramirez RR, Zonenshayn M, Ribary URS, Llinas R: Thalamocortical dysrhythmia syndrome: MEG imaging of neuropathic pain. **Thalamus Relat Syst 3:**33–39, 2005
30. Stern J, Jeanmonod D, Sarnthein J: Persistent EEG overactivation in the cortical pain matrix of neurogenic pain patients. **Neuroimage 31:**721–731, 2006
31. Sun J, Hynynen K: The potential of transskull ultrasound therapy and surgery using the maximum available skull surface area. **J Acoust Soc Am 105:**2519–2527, 1999
32. Vykhodtseva NI, Sorrentino V, Jolesz FA, Bronson RT, Hynynen K: MRI detection of the thermal effects of focused ultrasound on the brain. **Ultrasound Med Biol 26:**871–880, 2000

Manuscript submitted September 15, 2011.
Accepted October 27, 2011.
Please include this information when citing this paper: DOI: 10.3171/2011.10.FOCUS11248.

Address correspondence to: Daniel Jeanmonod, M.D., Center of Ultrasound Functional Neurosurgery, Leopoldstrasse 1, 4500 Solothurn, Switzerland. email: daniel.jeanmonod@gmail.com.

Neurosurg Focus 32 (1):E2, 2012

Measurement of targeting accuracy in focused ultrasound functional neurosurgery

Technical note

David Moser, B.Sc.,[1] Eyal Zadicario, M.Sc.,[2] Gilat Schiff, B.Sc.,[2] and Daniel Jeanmonod, M.D.[1]

[1]Center of Ultrasound Functional Neurosurgery, Solothurn, Switzerland; and [2]InSightec, Ltd., Tirat Carmel, Israel

The object of this study was to describe a method of measuring targeting accuracy in functional neurosurgery using MR imaging and the *Stereotactic Atlas of the Human Thalamus and Basal Ganglia*. This method should be useful for any functional procedure using these tools or similar ones, and is described here in the specific context of focused ultrasound surgery. The authors describe the atlas coordinate system used, the different relevant targeting and accuracy definitions, the tools used, the intraoperative target determination, the postoperative target reconstructions, and the calculation of the therapeutic lesion volume. The proposed method has been applied to the specific situation of measuring targeting accuracy in focused ultrasound functional neurosurgery. The authors found mean absolute global targeting accuracies between 0.54 and 0.72 mm (SDs between 0.34 and 0.42 mm), with 85% of measured coordinates within 1 mm. The proposed method may be particularly useful in the context of functional neurosurgical procedures implying therapeutic ablations, be they through radiofrequency, focused ultrasound, or any other technique. This method allows an ongoing control of the targeting precision, a basic requirement in any functional neurosurgical procedure.
(http://thejns.org/doi/abs/10.3171/2011.10.FOCUS11246)

Key Words • **anterior commissure** • **posterior commissure** • **stereotactic atlas** • **targeting accuracy** • **thalamoventricular border** • **transcranial magnetic resonance–guided focused ultrasound**

The therapeutic application of focused ultrasound in functional neurosurgery requires refined target reconstructions and precise targeting accuracy measurements within the millimeter domain. Because targets are in normal tissue, coordinates have to be established for each target on the basis of a stereotactic atlas of the human brain. Such an atlas uses internal landmarks to position a coordinate system onto the brain, allowing the placement of any desired target inside the brain. We use the *Stereotactic Atlas of the Human Thalamus and Basal Ganglia*,[1,2] which provides the following essential qualities better than other atlases (such as the Schaltenbrand-Wahren): 1) guaranteed proper cutting angles, due to use of a special guillotine; 2) maps drawn every 0.9 mm; 3) use of several histological staining techniques (multiarchitectonic atlas); and 4) an atlas based on a histological experience from 7 human autopsy brains, and consecutive atlas maps drawn from 4 hemispheres.

In functional neurosurgery, 2 steps of the treatment procedure need to be performed with a precision to within 1 mm: 1) the projection, based on the atlas, of the 3 coordinates of a chosen target onto the intraoperative MR imaging; and 2) the determination of the 3D position of the realized therapeutic lesion on postoperative MR imaging. This second step allows the establishment of the targeting accuracy of the entire therapeutic procedure.

Abbreviations used in this paper: AC = anterior commissure; FRFSE = fast recovery fast-spin echo; ICL = intercommissural line; PC = posterior commissure; RAS = Right-left, Anterior-posterior, Superior-inferior.

The targeting accuracy measurement procedure presented here can be used in any functional neurosurgical setup. It has been developed in the context of a clinical study that has as its goal to provide relief to patients suffering from chronic therapy-resistant functional brain disorders (neuropathic pain, Parkinson disease, and essential tremor) by performing a small therapeutic ablation in or around the thalamus using the ExAblate 4000 Neuro (InSightec, Ltd.). This device allows the transcranial and MR-guided application of focused ultrasound energy into brain tissue. As stated above, this application must be performed with a precision to within 1 mm; that is, the center of the therapeutic lesion must lay a maximum of 1 mm away from the center of the desired target. In the following sections, we will present our targeting accuracy measurement method and then apply it as an example to the analysis of the precision of our first 9 focused ultrasound procedures.

Methods

Atlas Coordinate System

The use of a brain atlas provides a coordinate system independent from the coordinate matrices of the MR and ultrasound systems. The atlas is based on specific chosen neuroanatomical structures serving as landmarks. The neuroanatomical landmarks used in the *Stereotactic Atlas of the Human Thalamus and Basal Ganglia*[1,2] are the AC and PC. On a midsagittal scan (Fig. 1 upper), a line passing through the center of these commissures (the ICL) is used to create the axial dorsoventral "zero" plane. The dorsal direction is above this plane and the ventral is below. The PC is used as the "zero" reference for the anteroposterior axis: positive values are anterior to the PC while negative values are posterior to it. On an axial scan (Fig. 1 lower), the ICL is drawn passing through the middle of the third ventricle. The mediolateral axes (right and left) are parallel to the lines passing through the centers of the 2 commissures, themselves perpendicular to the ICL. On the atlas maps, the reference grid starts laterally in the zero position in the middle of the ventricle. However, the width of the ventricle can vary significantly from patient to patient. The thalamoventricular border has thus been chosen as the zero (reference) point for the determination of the mediolateral target coordinate (Fig. 1 lower).

Targets and Accuracies

There are 3 different kinds of targets for each accuracy measurement: the chosen target, based on surgical experience and established in terms of atlas coordinates; the target prescribed in the ExAblate software; and the realized target visible on postoperative MR images. We qualify all targets by the coordinates of their center. We shall call the atlas target the chosen target. Following the atlas-based determination of the position of the target on the intraoperative MR images, we enter its position coordinates in the "Advanced Options" section of the ExAblate software. These MR (RAS) coordinates define the prescribed target. Lastly, the realized target is measured on the MR postoperative examination.

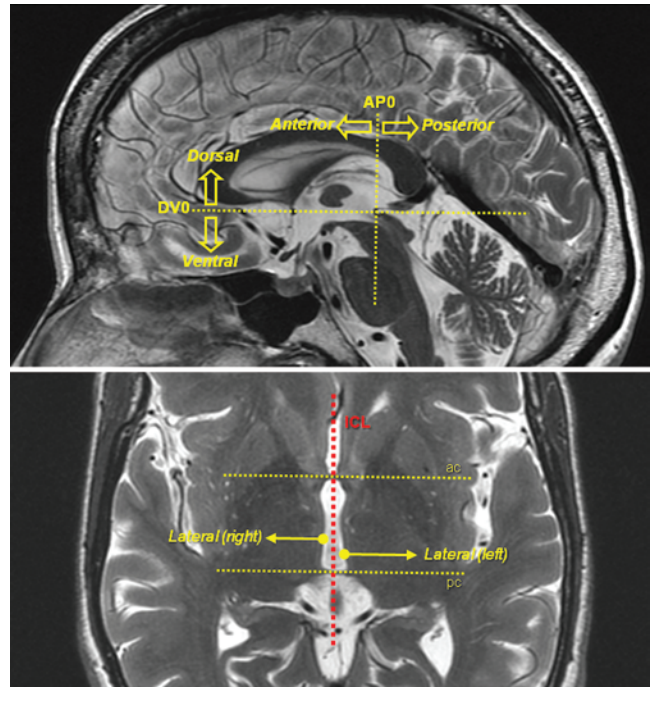

Fig. 1. Magnetic resonance images demonstrating the atlas coordinate system. **Upper:** Midsagittal scan showing the main axes of the relative coordinates system: the dorsoventral (DV) and anteroposterior (AP) axes. The DV axis corresponds to the superior-inferior coordinate system axis in MR systems when the patient's head is not tilted and the patient lays head-first on the MR imaging cradle. **Lower:** Axial scan showing the DV0 plane with the AC and PC. The lateral axes begin at the thalamoventricular borders. The zero of theses axes will then vary depending on the AP position of the target.

On this basis, we may compute 2 accuracies: the global accuracy, which is defined as the difference between the realized and the atlas target center coordinates; and the device accuracy, which is the difference between the prescribed and the realized target center coordinates, given in millimeters. For the 3 directions (mediolateral, anteroposterior, and dorsoventral), the global accuracy can be computed as the difference between the atlas target and the realized target:

global accuracy = realized target – atlas target.

This global accuracy depends on the precision of many steps during the treatment process. The first relevant step is defined as the planning accuracy, which depends on the reconstruction of the atlas target on the intraoperative MR images. This reconstruction provides the prescribed target center coordinates. The planning accuracy can therefore be obtained as follows:

planning accuracy = prescribed target – atlas target.

This planning accuracy, subtracted from the global accuracy, then gives a device accuracy:

device accuracy = global accuracy – planning accuracy.

From the technical point of view, the device accuracy is the most relevant to define the precision of the targeting of the device itself. It should be noted that this accuracy contains the manual correction (with its own accuracy) that can be applied during the treatment and a

purely technical accuracy (such as electronic steering of the transducer):

device accuracy = manual correction + manual correction accuracy + technical accuracy.

If no manual correction is applied during the treatment, it means that:

manual correction = manual correction accuracy = 0,

the device accuracy is then equal to the technical accuracy.

In the best case, this manual correction should fully compensate for the technical deviation of the device:

manual correction + manual correction accuracy = technical accuracy

which implies a device accuracy being equal to 0.

This best case strongly depends on the skills of the user to visually estimate the technical deviation of the machine and correct it. Therefore, the device accuracy may be considered as man- as well as machine-based. However, the manual correction (and its accuracy) depends mainly on the quality of the MR thermal maps and is therefore technically related.

Summarizing and simplifying, the 3 accuracies we want to obtain are the global accuracy, the planning accuracy, and the device accuracy:

global accuracy = device accuracy + planning accuracy.

These accuracies can be considered as 3D vectors with their sign (+ or –) for each direction. But the device and planning accuracies should not compensate each other; for example, if a +1 mm difference on a direction is measured for 1 targeting accuracy and a –1 mm difference for the other targeting accuracy in the same direction, the mean will be zero. The mean should, however, be 1 mm, and this is obtained by using the absolute value of the device and planning accuracies.

Measurement Tools

A brief description of the tools used to determine and reconstruct targets is shown in Table 1. One thing to be noted is that the intraoperative target determination is performed on the MR workstation during the operation while postoperative target reconstructions are conducted on a normal desktop computer (not mentioned in the table).

Magnetic Resonance Imaging

The precision of all target determinations and reconstructions rely on MR imaging. If the 3 orientations are not orthogonal and precisely prescribed, a very significant error in target determination and measurements may happen. All MR series must be performed in the same way as the *Stereotactic Atlas*[1,2] maps, that is, with the zero axial plane passing through the centers of the AC and PC. A minimum of 2 out of the 3 orientations (axial, sagittal, and coronal) is required to prescribe a target or to perform a target reconstruction. We work mainly with the sagittal and the axial series.

The sagittal scans have to be prescribed on the "3-plane localizer" images, using axial and coronal orientations. Care must be taken to prescribe a precisely midsagittal slice, thus allowing the detailed visualization of the AC and PC. This is performed mainly on a transthalamic 3-plane localizer axial image, and the prescription of the midsagittal slice must pass in the middle of the third ventricle with the proper angle (Fig. 2 right). The tilt of this plane has to be checked on the coronal 3-plane localizer image (Fig. 2 left), also adjusting the angle here so that the plane will be strictly midsagittal. The prescription of the axial series then needs to be performed using this midsagittal image and the same coronal 3-plane localizer image. Summing up, the central axial slice has to pass through the centers of the AC and PC (Fig. 3 right), while its tilt has to follow the patient's head tilt as noted on the coronal images (Fig. 3 left).

Target Determination

For each operation, the atlas target center coordinates are determined using intraoperative MR T2-weighted FRFSE sagittal and axial series in the following manner: 1) choose 2-mm slice thickness, 0-mm gap MR images using the procedure described above; 2) locate the slice containing the 2 commissures (AC and PC) on the axial series using the GE viewer software; 3) draw the ICL; 4) perpendicularly to this line (angle tool) draw 2 parallel lines in the middle of each commissure and a third one through the midcommissural point; 5) copy these lines on all slices of the series; 6) browse the MR axial slices

TABLE 1: Tools for targeting accuracy measurement*

Tool	Use
hardware	
InSightec ExAblate 4000 Neuro	focused ultrasound op
GE Discovery MR750 3.0T	
body coil	intraop setup
32-channel head coil	postop setup
software	
InSightec ExAblate Focused Ultrasound Brain software	op & postop prescribed target center measurement
GE Viewer software (on MR console)	intraop target determination
Carestream PACS version 11.0 (DICOM viewer)	realized target measurement on postop MR images
Mathworks Matlab R2009b	data processing

* DICOM = digital imaging and communications in medicine; PACS = picture archiving and communication system.

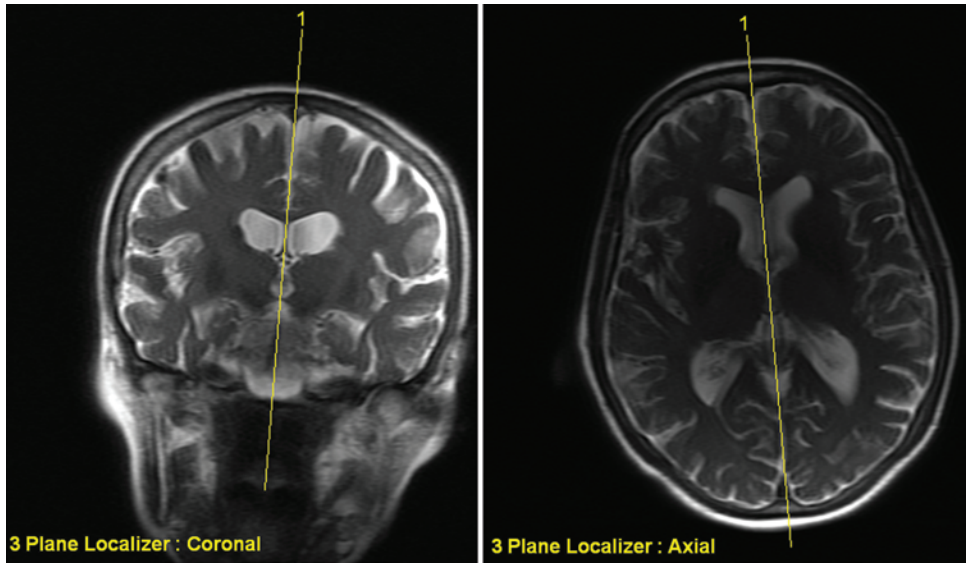

Fig. 2. Magnetic resonance prescription of the T2-weighted FRFSE midsagittal scan on 3-plane localizer images. The angles of rotation **(right)** and tilt **(left)** of the head have to be taken into account and the prescription lines positioned accordingly, passing through the center of the third ventricle.

dorsal or ventral depending on the dorsoventral position of the target; 7) determine the anteroposterior position of the target on the ICL and draw a line through this position and parallel to the ones passing through the centers of the AC and PC (the anteroposterior target coordinate is positioned in relation to 1 of the 3 landmarks—AC, PC, or midcommissural point—that is closest to the target, with the goal of reducing the effect of interindividual variability); 8) from the thalamoventricular border, go laterally on this line to the target position; and 9) note the RAS coordinates of this point, representing the atlas target now translated into RAS coordinates. In our setup, these coordinates are entered into the "Advanced Options" section of the ExAblate software.

Target Reconstructions

The position of the center of the realized target is determined on postoperative MR T2-weighted FRFSE sagittal and axial series in essentially the same manner as for the target determination: 1) choose 2-mm thickness, 0-mm gap MR slices of the thalamus, produce a strict midsagittal slice and then an axial dorsoventral zero slice passing precisely through the center of the AC and PC, as described in the imaging procedure above; 2) on the dorsoventral zero slice, draw the ICL; 3) perpendicularly to this line ("angle tool") draw 2 parallel lines in the middle of each commissure and a third one through the midcommissural point; 4) copy these lines on all slices of the series; 5) locate the axial slice where the realized target is the most

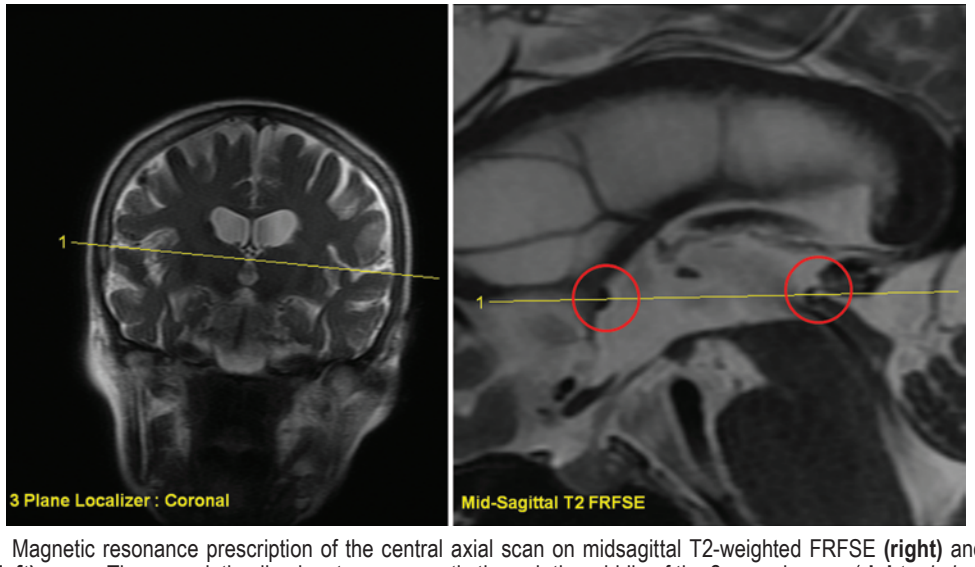

Fig. 3. Magnetic resonance prescription of the central axial scan on midsagittal T2-weighted FRFSE **(right)** and 3-plane localizer **(left)** scans. The prescription line has to pass exactly through the middle of the 2 commissures (**right,** *circles*) while its tilt has to be set according to the tilt of the patient's head **(left)**.

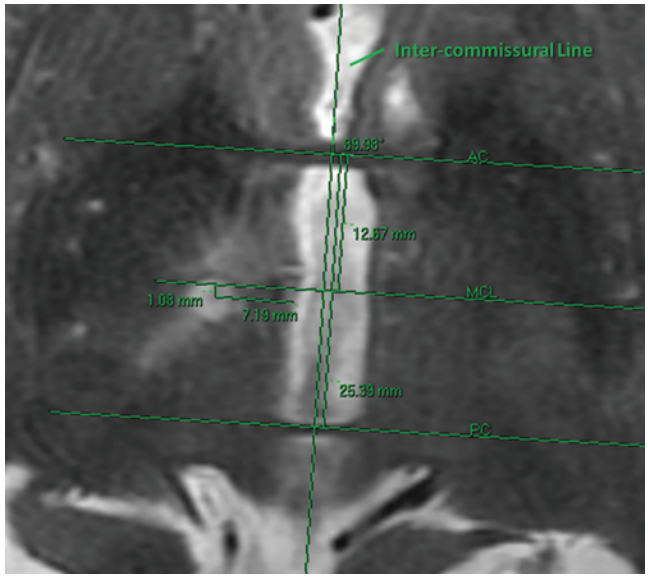

Fig. 4. Realized target reconstruction (AP and mediolateral coordinates of the center) on MR T2-weighted FRFSE axial images obtained 2 days postoperatively. The AP direction is parallel to the ICL while the mediolateral direction is perpendicular to this line. MCL = midcommissural line.

visible and the largest; 6) draw a line that is parallel to the ones passing through the centers of the 2 commissures and that passes through the center of the realized target, and measure the distance between the thalamoventricular border and the center of the realized target, thus obtaining the mediolateral target position (Fig. 4); 7) on the ICL, measure the distance between 1 of the 3 landmarks—AC, PC, or midcommissural point—that is closest to the realized target and the line passing through its center, thus obtaining the anteroposterior target position (Fig. 4); 8) draw the ICL on the midsagittal slice, passing through the center of the 2 commissures; 9) copy this line on all slices of the series; 10) locate the sagittal slice where the realized target is the most visible and the largest; and 11) perpendicularly to the ICL (angle tool), measure the distance between the ICL and the estimated center of the realized target, thus obtaining the dorsoventral target position.

To check the accuracy of the placement of the target into the ExAblate software (blue circle on Fig. 5), we proceed in our setup to the "Replay Mode" of the ExAblate workstation. This process is nearly the same as for the reconstruction of the center of the realized target: 1) on the "Replay Mode," select the "planning" images; 2) locate the axial slice containing the dorsoventral zero plane; 3) draw the ICL; 4) perpendicularly to this line draw 2 parallel lines through the middle of each commissure (AC and PC) and a third one through the midcommissural point; 5) copy these lines on the image where the blue circle representing the prescribed target is best seen; 6) draw a line that is parallel to those passing through the centers of the 2 commissures and that passes through the center of the prescribed target, and measure the distance between the thalamoventricular border and the center of

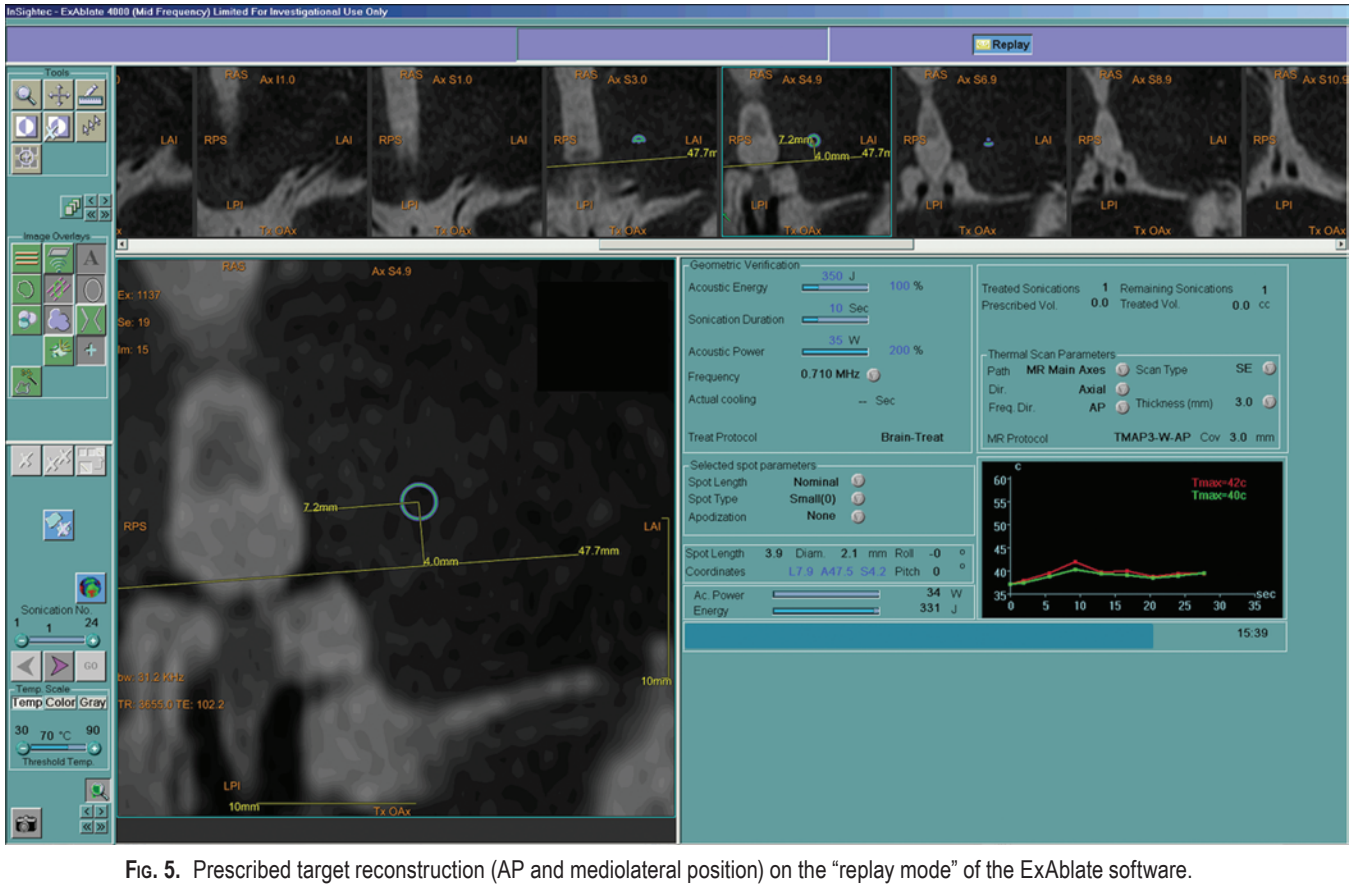

Fig. 5. Prescribed target reconstruction (AP and mediolateral position) on the "replay mode" of the ExAblate software.

the prescribed target, thus obtaining the mediolateral target position (Fig. 5); 7) on the ICL, measure the distance between 1 of the 3 landmarks—AC, PC, or midcommissural point—that is closest to the prescribed target and the line passing through its center, obtaining thus the anteroposterior target position (Fig. 5); 8) draw the ICL on the midsagittal slice, passing through the center of the 2 commissures; 9) copy this line on the image where the blue rectangle representing the prescribed target is best seen; and 10) perpendicularly to the ICL, measure the distance between the ICL and the center of the prescribed target, thus obtaining the dorsoventral target position.

Estimated Volume of the Lesion

On all axial scans (in general 3) in which the realized target is visible, determine its diameters (measure 2 perpendicular diameters and take the mean; Fig. 6A–C). On T2-weighted images, the lesion with its center and crown can be relatively easily differentiated from the surrounding vasogenic edema, which is less hyperdense.

On the sagittal scan in which the realized target is the largest, measure its height (Fig. 6D). The volume of the realized target can then be computed as the sum of the volume of 2 truncated cones:

$$V_1 = 1/6*\pi*h*(r_1^2 + r_1*r_2 + r_2^2)$$

$$V_2 = 1/6*\pi*h*(r_2^2 + r_2*r_3 + r_3^2)$$

$$V_{tot} = V_1 + V_2$$

in which h is the height of the realized target and r_1, r_2, and r_3 are the mean radii of the realized target.

Results

As an illustration of the described procedure, Figures 7 and 8 display the targeting accuracy measurements for our first 9 focused ultrasound treatments, comprising 11 reconstructed realized targets. Figure 7 shows the obtained absolute global accuracies, including means and SDs. In more than 33 measured coordinates, 5 (15.2%) exceed 1 mm (maximum 1.7 mm). The mean value for each of the 3 directions is comprised inside 1 mm: 0.54 ± 0.34 mm for the anteroposterior direction and 0.72 mm for both the mediolateral and dorsoventral directions (± 0.42 and 0.39 mm, respectively). Figure 8 shows the computed planning and device accuracies.

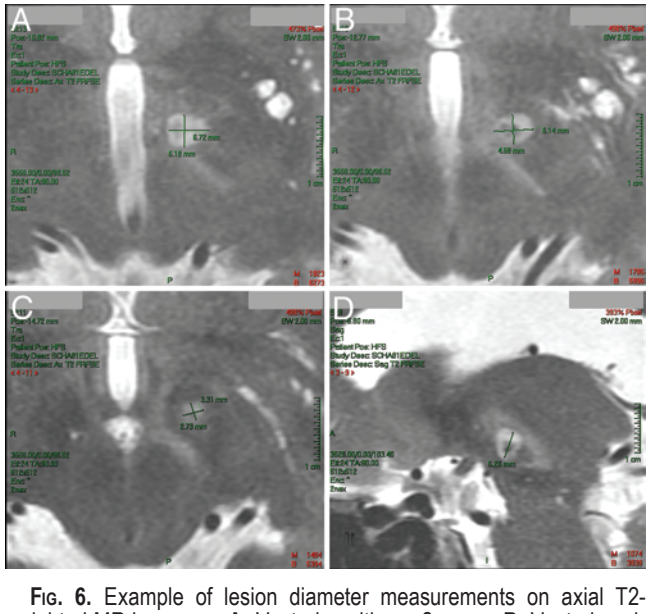

Fig. 6. Example of lesion diameter measurements on axial T2-weighted MR images. **A:** Ventral position = 2 mm. **B:** Ventral position = 4 mm. **C:** Ventral position = 6 mm. **D:** Measurement of the height of the lesion on a sagittal T2-weighted image. These values are used to compute an estimated volume of the lesion.

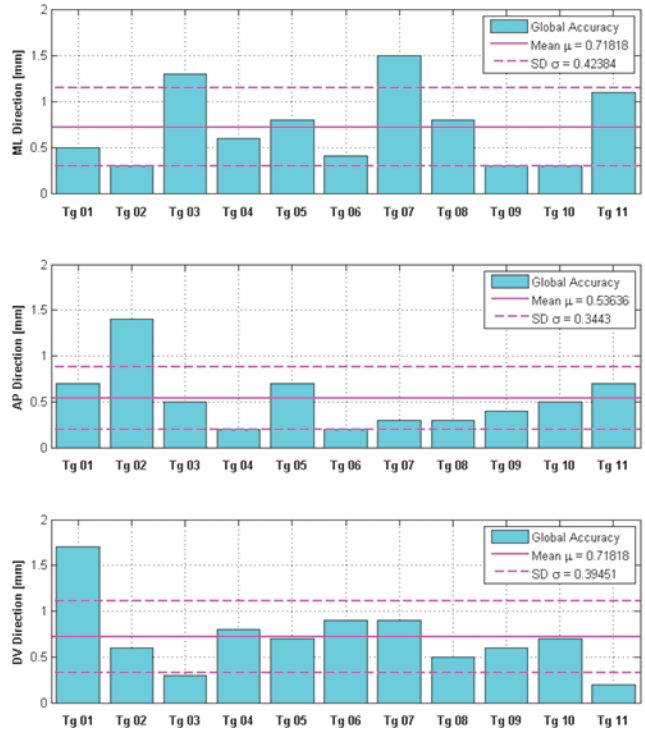

Fig. 7. Graph of absolute value of the global accuracy for the first 11 targets in the 3 directions, with the mean and SDs for each. ML = mediolateral; Tg = target.

Discussion

In the last 22 years our group has, as a routine, developed and applied target accuracy controls based on the *Stereotactic Atlas of the Human Thalamus and Basal Ganglia*.[1,2] This was warranted by our choice to perform selective small ablations based on pathophysiological evidence. We hope that the procedure presented here will be considered useful by colleagues and groups initiating their experience with therapeutic ablations using focused ultrasound.

We would like to stress here the importance of 2 factors contributing to an adequate measurement of targeting accuracy: 1) the proper alignment of the collection of MR imaging slices used with correction of tilts and rotations, particularly relevant for lateral targets; and 2) the necessity of a high-resolution visualization of the 2 commissures, allowing a refined determination of their centers under a high magnification. In our experience, the described T2-weighted imaging without 3D reformatting

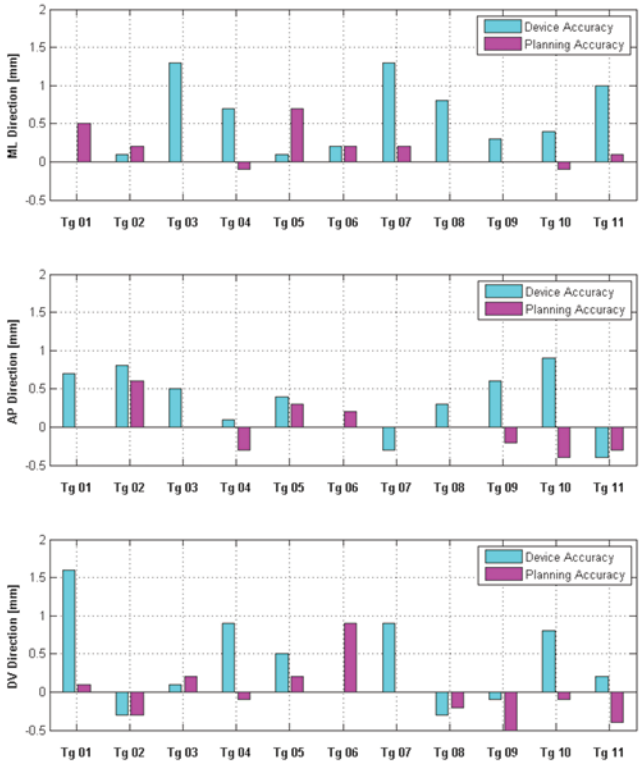

Fig. 8. Device and planning accuracy for the first 11 targets of the study. The sum of the absolute values of those 2 accuracies gives the global accuracy.

has been the best option, for both postoperative imaging using a 32-channel head coil, but also for intraoperative imaging using the body coil of the GE Discovery MR 750 system.

Although our experience is relatively small, using the described procedure in this paper we demonstrated that 84.8% of our targeted coordinates lie within 1 mm, providing a mean targeting accuracy of the focused ultrasound treatment of 0.72 mm maximum, thus fulfilling the basic criterion of an accuracy inside 1 mm. Such an accuracy requirement obeys clinical efficiency and safety criteria, and is globally compatible with the limitations of the target reconstruction procedure, primarily manual measurements on MR images, thickness of the MR slices (2 mm), lesion size (4 × 4 × 6 mm), and determination of the lesion center. Future technological developments can be expected to contribute to an even more precise targeting, but also increased experience, considering the particular importance of human decision-making for an optimized treatment process.

Disclosure

Eyal Zadicario and Gilat Schiff are employees of InSightec, Ltd.

Author contributions to the study and manuscript preparation include the following. Conception and design: Moser, Jeanmonod. Acquisition of data: Moser. Analysis and interpretation of data: all authors. Drafting the article: Moser. Critically revising the article: Zadicario, Jeanmonod. Reviewed submitted version of manuscript: Moser. Approved the final version of the manuscript on behalf of all authors: Moser. Statistical analysis: Moser. Administrative/technical/material support: Moser, Schiff, Jeanmonod. Study supervision: Jeanmonod.

Acknowledgment

The authors thank Mrs. Franziska Rossi for support in text and table formatting and Dr. A. Morel for her review of the manuscript and useful comments.

References

1. Morel A: **Stereotactic Atlas of the Human Thalamus and Basal Ganglia.** New York: Informa Healthcare, 2007
2. Morel A, Magnin M, Jeanmonod D: Multiarchitectonic and stereotactic atlas of the human thalamus. **J Comp Neurol 387:** 588–630, 1997

Manuscript submitted September 15, 2011.
Accepted October 27, 2011.
Please include this information when citing this paper: DOI: 10.3171/2011.10.FOCUS11246.
Address correspondence to: David Moser, B.Sc., Center of Ultrasound Functional Neurosurgery, Leopoldstrasse 1, CH-4500 Solothurn, Switzerland. email: david.moser@sonimodul.ch.

Neurosurg Focus 32 (1):E3, 2012

Focused ultrasound disruption of the blood-brain barrier: a new frontier for therapeutic delivery in molecular neurooncology

Arnold B. Etame, M.D.,[1] Roberto J. Diaz, M.D.,[1] Christian A. Smith, Ph.D.,[1] Todd G. Mainprize, M.D.,[1] Kullervo Hynynen, Ph.D.,[2] and James T. Rutka, M.D., Ph.D.[1]

[1]Division of Neurosurgery, Department of Surgery, The Hospital for Sick Children; and [2]Department of Imaging Research, Sunnybrook Research Institute, University of Toronto, Canada

Recent advances in molecular neurooncology provide unique opportunities for targeted molecular-based therapies. However, the blood-brain barrier (BBB) remains a major limitation to the delivery of tumor-specific therapies directed against aberrant signaling pathways in brain tumors. Given the dismal prognosis of patients with malignant brain tumors, novel strategies that overcome the intrinsic limitations of the BBB are therefore highly desirable. Focused ultrasound BBB disruption is emerging as a novel strategy for enhanced delivery of therapeutic agents into the brain via focal, reversible, and safe BBB disruption. This review examines the potential role and implications of focused ultrasound in molecular neurooncology.
(http://thejns.org/doi/abs/10.3171/2011.10.FOCUS11252)

Key Words • **brain tumor** • **blood-brain barrier** • **focused ultrasound** • **chemotherapy**

Malignant glioma is the most common primary brain tumor in adults.[25] It exhibits extensive invasion into the brain parenchyma, thereby evading the current multimodal therapeutic paradigms of conventional chemotherapy, radiotherapy, and surgery. Despite tremendous advances in this multimodal treatment scheme, the prognosis for patients with malignant glioma remains dismal.[68–70] The mean survival after symptom onset remains 12–16 months, with over 70%–80% of patients dead within 2 years.[69] The highly invasive nature and the complex molecular underpinnings of the disease both account for its intransigence to current conventional therapies. Hence, molecularly directed therapeutic targets are essential to improve clinical outcome. As a result, there is an impetus to deciphering critical signaling pathways in hopes of identifying putative molecular targets.

However, a major challenge to the delivery of molecular pathway–targeting therapeutics is the transport across the BBB, which creates both structural and physiological impediments to delivery.[53] The BBB limits the effectiveness of many conventional chemotherapeutic drugs, making systemic administration an ineffective option for the vast majority of chemotherapy agents.[17] For instance, doxorubicin is a chemotherapy agent that does not appreciably cross the BBB yet has been very effective against malignant gliomas in vitro.[79] Similar delivery challenges plague molecular-based targeted glioma therapy given the various transport mechanisms that govern BBB delivery.

Generally, for therapeutic agents to cross the BBB, they must employ either passive or active transport mechanisms.[51] Small (< 400 D) nonpolar lipophilic agents are easily transported passively,[52] whereas polar or water-based compounds generally require active transport mechanisms.[38,39] Furthermore, the BBB expresses drug-efflux transporter proteins that physiologically exclude therapeutic agents from the brain. A well-known efflux transporter is the P-glycoprotein, which is a substrate for most chemotherapy agents.[2,33] Another confounding factor that could significantly affect delivery of therapeutic agents into brain tumors is the potential variability in vascular permeability among tumors, as well as between tumors and normal brain.[3,5,6,16,34,46,47,55] Potential solutions require either structural modifications of therapeutic agents or transient, safe, and reversible modifications of the BBB to enable delivery into the brain. The latter strategy of BBB modification appears practically more appealing given the complexities of redesigning and modifying molecular therapeutic agents. Ideally, strategies that transiently increase BBB permeability should be focal, safe, reversible, and noninvasive.

Abbreviations used in this paper: BBB = blood-brain barrier; FUS = focused ultrasound; HSV = herpes simplex virus; MNP = magnetic nanoparticle.

Focused ultrasound disruption of the BBB is emerging as a very promising novel noninvasive technology that can circumvent some of the anatomical limitations of the BBB, thereby enhancing delivery of therapeutic agents into the brain.[21,42] Low-frequency ultrasound waves are delivered transcranially and result in BBB disruptions in focal areas of the brain. Given the potential for focal and selective delivery in conjunction with the inherent advantage of enhanced therapeutic delivery, this review will examine the potential applications and implications of FUS in molecular neurooncology.

Conventional Nonfocal BBB Disruption Strategies

Since most therapeutic agents do not readily cross the BBB, several strategies to temporally disrupt the BBB have been embarked upon previously (Table 1). Transient disruption of the BBB can be obtained using an osmotic agent such as mannitol, which is delivered intraarterially via carotid arteries.[1] The feasibility of such an approach has been demonstrated in brain tumors.[45,57] Furthermore, alkylated alcohols such as alkyl-glycerol open the BBB in a similar fashion when delivered intraarterially.[32] Besides osmotic agents, there are receptor-mediated mechanisms that can enhance permeability of the BBB. A notable example is the bradykinin system where analogs such as *RMP-7* have been employed for enhanced permeability of the BBB.[12,59] Preclinical application of bradykinin analogs with intraarterial carboplatin appeared promising with increased drug levels in the brain.[13] However, when a similar strategy was applied in Phase II trials for childhood brain tumors[76] and recurrent gliomas,[56] the clinical results were not as promising. A major pitfall was failure to obtain reasonable therapeutic concentrations within the brain.

Enhanced permeability of the BBB can have both beneficial and deleterious effects. Although the BBB limits delivery of therapeutics into the brain, it also protects the brain from systemic toxins. Blood-brain barrier disruption strategies that employ osmotic agents such as mannitol or bradykinin analogs can result in widespread BBB disruption and the potential for deleterious consequences. Therefore, an obvious shortcoming of the aforementioned BBB disruption strategies is the lack of targeted delivery applications.

Focused Ultrasound Disruption of the BBB: Principles

A unique advantage of FUS disruption of the BBB over other conventional BBB disruption schemes is the selective and regional permeability increases that result in enhanced local delivery within the brain (Table 2).[20–22,41,44] The technique entails transcranial delivery of low-frequency ultrasound waves that ultimately result in disruption of the BBB (Fig. 1).[23] Typically, ultrasonic exposure burst at 10 msec with pressure amplitudes less than 1 MPa are conventionally used for durations of 20–30 seconds repeated at the frequency of 1 Hz.[19] By employing low frequencies, the chances of permanent tissue damage are minimized. The technique can be used in conjunction with MR imaging for targeting purposes and documentation of focal BBB disruption, which is manifest by regional contrast extravasation (Fig. 2). Incorporation of intravenously administered lipid-encased perfluorocarbon gas microbubbles (1–5 μm in diameter) further lowers the frequency threshold for BBB disruptions, thereby allowing for much lower and safer frequencies to be used.[21,42,44] The feasibility of microbubble-assisted FUS disruption of the BBB was first successfully demonstrated a decade ago.[21] The FUS BBB disruption effects are not as apparent in the absence of microbubbles because acoustic powers are 2 orders of magnitude lower.[21] As the microbubbles traverse the capillaries, they can expand and collapse based on the ultrasonic input. It is hypothesized that FUS results in oscillation and concentration of microbubbles by the capillary walls, which in turn imparts mechanical forces that could result in BBB opening.[21,23,64] Furthermore, the microbubbles emit acoustic signals that have been highly correlated with BBB disruption in the absence of vascular damage, thus suggesting that acoustic signals could serve as a surrogate for safety.[40] The safety of FUS disruption of the BBB is well documented, and the overall effects are transient and reversible with no overt neuronal injury.[21,22,44] The ensuing BBB disruption lasts at most for approximately 4 hours.[63]

Focused Ultrasound Disruption of BBB: Design

The overall schematic for preclinical FUS systems for BBB disruption is illustrated in Fig. 3.[18] The animal is anesthetized and positioned supine with the scalp submerged in a chamber containing degassed water. Low-frequency ultrasound waves emitted from a focused transducer are transmitted through the degassed water into the cranium. Prior to BBB disruption, animals receive lipid microbubbles and the therapeutic agent of interest. Magnetic resonance imaging of the brain is often used to select a focal area of interest for disruption of the BBB. Disruption of the BBB is then accomplished using a burst of low-frequency ultrasound. Magnetic resonance imaging of the animal brain is performed prior to and after FUS BBB disruption. The region of BBB disruption

TABLE 1: Enhanced BBB delivery strategies

intraarterial via carotid arteries
intraventricular
osmotic agents such as mannitol
BBB permeation analogues such as bradykinin
convection-enhanced interstitial delivery

TABLE 2: Advantages of FUS-mediated therapeutic delivery

focal & targeted delivery minimizes problems seen w/ widespread BBB disruption
transient disruption of BBB, hence reversible
noninvasive transcranial technique
enhanced delivery of chemotherapy, gene therapy, & monoclonal antibodies across BBB

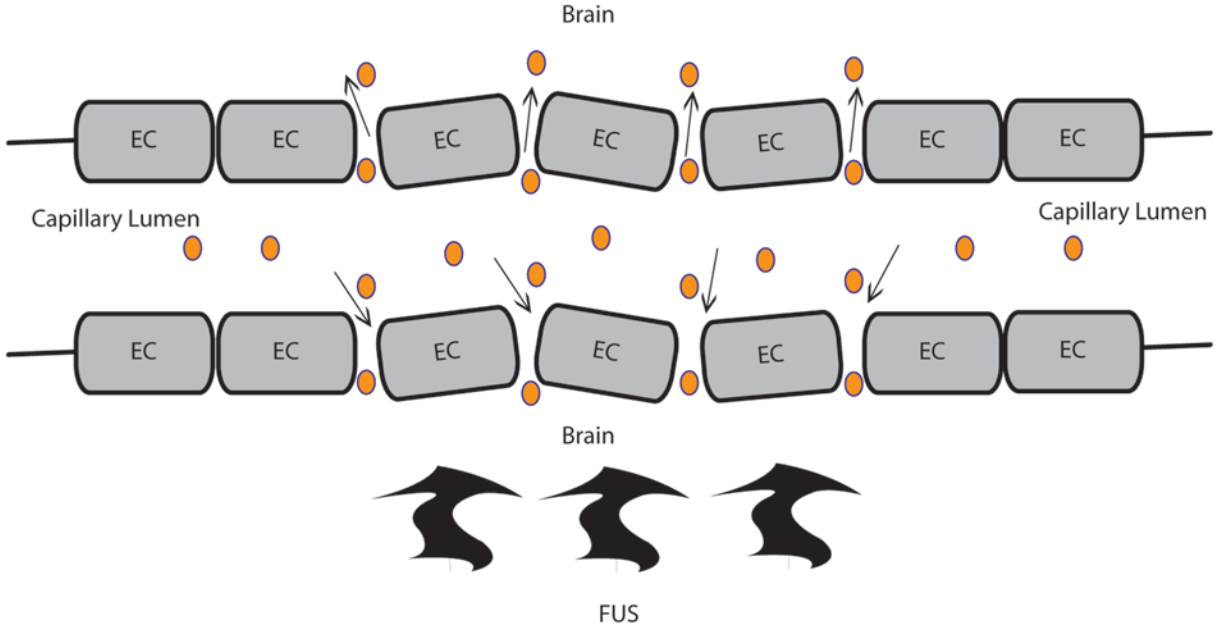

Fig. 1. Schematic of enhanced BBB delivery following FUS disruption of the BBB. Focused ultrasound delivers low-frequency ultrasound waves that cause mechanical oscillations in microbubbles, resulting in disruption of the tight junctions of endothelial cells (ECs) and in enhanced BBB permeability to agents.

is confirmed on T1-weighted contrast-enhanced MR images (Fig. 2).

Preclinical Applications of FUS

Table 3 provides a succinct summary of enhanced BBB delivery strategies.

Delivery of Antibodies Into the Brain

One of the most practical therapeutic attributes of FUS is the ability to deliver antibodies into the brain, which was demonstrated in a previous study. Kinoshita et al.[30] were able to demonstrate the BBB crossing of dopamine D(4) receptor–targeting antibody and subsequent antigen recognition within the brain via FUS mediation. Traditionally, a major hurdle in antibody therapeutics is the very limited ability of antibodies to cross the BBB in light of absent large water channels or active transport mechanisms for antibodies in cerebrovascular endothelium. However, there are several neurological disorders for which antibody-mediated therapy would be advantageous. For instance, in Alzheimer disease, there is accumulation of amyloid-β plaques, which form the basis for toxicity and cognitive impairment.[60] Interestingly, direct intracranial administration of anti–amyloid β antibodies in transgenic mice,[73] as well as in normal animals,[78] led to a substantial amount of plaque reduction. A hindrance of direct intracranial injections is its invasiveness. Most recently, using MR imaging–guided FUS, anti–amyloid β antibodies were intravenously delivered into transgenic mice, and this resulted in significant plaque reduction 4 days posttreatment.[26] The investigators also noted that with FUS, a much lower dose of antibodies was effective as well for plaque reduction.

Another potential area of interest pertaining to antibody therapy is cancer targeting. Antitumor monoclonal antibodies that have been successfully used to target systemic cancers could have potential applications for metastatic or primary cancers in the brain. For instance, Herceptin, which is an anti-HER2 monoclonal antibody and a therapeutic target of breast cancer, was successfully delivered across the BBB with MR imaging–guided FUS as a proof-of-concept.[29] This proof-of-concept is very encouraging in light of potential extrapolations to other antitumor antibody candidates.

Delivery of Conventional Chemotherapy Agents Into the Brain

Given that the BBB significantly compromises the bioavailability of conventional chemotherapy agents into the brain, several strategies have been previously employed. The preclinical results have been promising, but only minimal benefits have been documented in clinical trials. One approach of augmenting brain concentration of chemotherapy agents has been the use of biodegradable matrices.[27,77] Matrices laden with chemotherapy agent are implanted within the tumor resection cavity. Other approaches have included convection-enhanced delivery systems[35,54] and intraarterial chemotherapy.[61] However, even with these approaches, insufficient chemotherapy bioavailability renders their efficacy suboptimal.

As a result, preclinical studies have been undertaken with FUS to assess the feasibility of chemotherapy delivery into brain tumors. This strategy was first successfully applied using doxorubicin, which does not appreciably cross the BBB.[74] The investigators successfully demonstrated a substantial increase in the concentration of liposome-encapsulated doxorubicin within the FUS-treated hemispheres of normal rats compared with the nontreated hemisphere. In a subsequent follow-up study, the investigators demonstrated a substantial therapeutic benefit

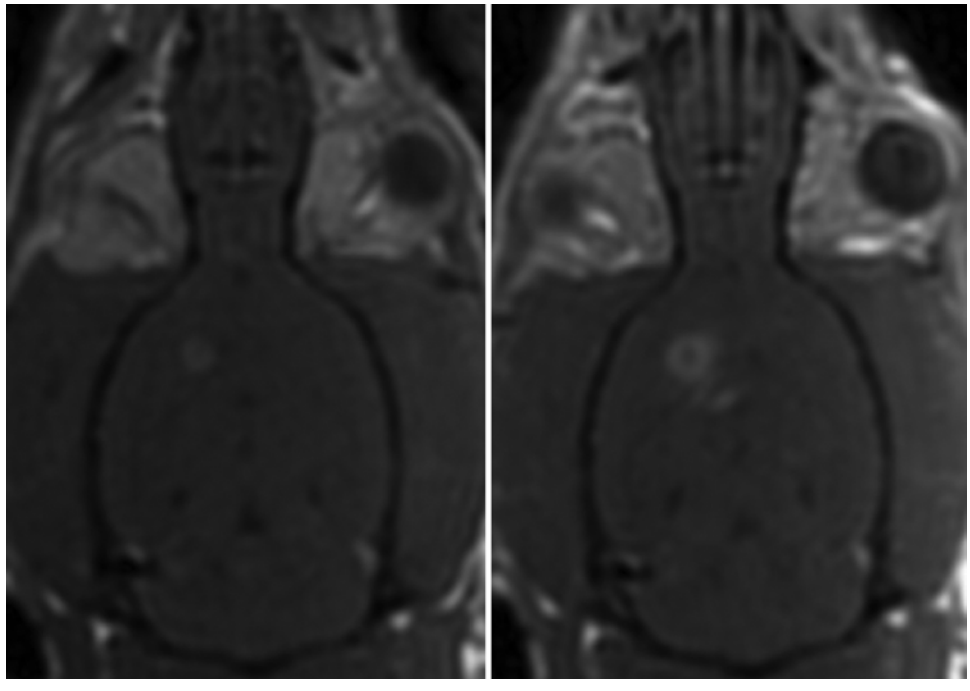

Fig. 2. Magnetic resonance imaging–guided FUS disruption of the BBB around a brain tumor graft. Coronal Gd-enhanced T1-weighted MR images of rat brain before **(left)** and after **(right)** sonication. Contrast enhancement around the sonicated right hemispheric tumor increases after sonication. The nonsonicated left hemisphere lacks contrast enhancement.

from FUS-mediated delivery of liposome-encapsulated doxorubicin in rats with intracranial gliomas.[75]

The delivery of methotrexate into the brain using FUS disruption of the BBB has been investigated as well. Mei and colleagues[43] assessed the FUS-assisted intracranial delivery of intravenous methotrexate into rabbit brains and compared this method with an intra–carotid artery injection. They noted targeted and enhanced delivery of intravenous methotrexate up to 10-fold with FUS. Furthermore, the FUS delivery strategy was noted to be more effective than intra–carotid artery delivery alone.

Most recently, Liu and colleagues[36] investigated FUS-mediated delivery of BCNU chemotherapy in animals with brain tumors. They reported substantial increases in tumor BCNU bioavailability in animals treated with FUS compared with nontreated animals. Accordingly, tumor progression was significantly compromised as evident by decreases in tumor size. The authors further demonstrated a significant survival benefit associated with FUS-mediated delivery of BCNU.

The preclinical data appear promising to date for FUS-mediated delivery of chemotherapy agents into the brain. Preliminary results demonstrate both feasibility and efficacy. Additional successful preclinical applications should pave the way for clinical studies.

Delivery of Therapeutic Nanoparticles Into the Brain

Nanotechnology-based delivery systems have generated substantial interest in light of demonstrated tumor-targeting applications.[28] Through such unique features, nanoparticle-delivery platforms could potentially circumvent some of the challenges associated with conventional chemotherapy for malignant brain tumors. However, the BBB remains a critical limitation for nanoplatforms. For instance, gold nanoparticles have gained prominence in nanotechnology-mediated cancer targeting for systemic cancers,[7,10,50] yet gold nanoparticles are significantly limited in their biodistribution to the brain following systemic delivery.[11,66,72] Therefore, strategies such as FUS that can increase BBB permeability to nanocarriers could enhance applicability of nanotechnology-based targeting in malignant brain tumors.

Liu and colleagues[37] recently assessed FUS-mediated delivery of an iron oxide MNPs conjugated to an antineoplastic agent, epirubicin. They used MNPs because of the favorable MR imaging characteristics, which could facilitate imaging. They demonstrated a substantial accumulation of MNPs, as well as epirubicin, up to 15 times the therapeutic range in the brain when delivered with FUS. They further showed decreased tumor progression in animals with brain tumors that received MNP with epirubicin via FUS. Similar to intracranial MNP targeted delivery, we have recently observed targeted enhanced parenchymal delivery of polyethylene glycol–coated gold nanoparticles into normal brain and to the periphery of parenchymal brain tumors in a rat model (AB Etame et al., unpublished data, 2011).

The prospects of combining FUS with nanoparticle-delivery platforms create a whole new avenue for targeting opportunities. The nanoplatforms are already very attractive for molecular targeting because nanoparticles can be easily functionalized with small molecule inhibitors, proteins, nucleic acid, ligands, and antibodies in any combination onto the surface of the nanoparticle.

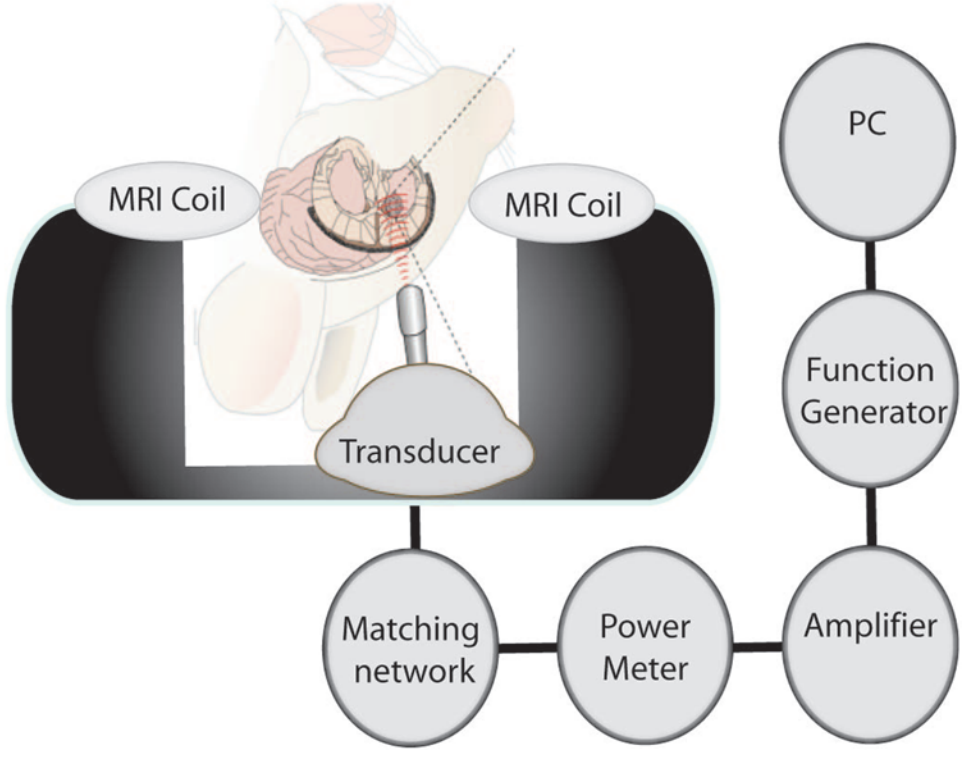

Fig. 3. Preclinical FUS BBB disruption system. The animal is positioned with the skull partially submerged in a degassed water tank, and microbubbles are intravenously administered. A focused transducer attached to a network power and personal computer (PC) system delivers low-frequency ultrasound, which disrupts the BBB. For targeting and for BBB disruption visualization, MR imaging is incorporated into the procedure.

Delivery of Gene-Based Therapies Into Brain Tumors

One of the major challenges with viral-based gene therapy for malignant brain tumors has been the inadequacy of therapeutic delivery.[15] Delivery strategies have included intratumoral injection,[24] convection-enhanced delivery systems,[8,58] and intraventricular delivery.[49] However, all 3 modalities are invasive. In addition, there are toxicity-related issues especially with intraventricular delivery.[49] On the other hand, intravascular delivery has been shown to be safe, but it is plagued by BBB limitations, which can be alleviated with BBB disrupting agents.[4,48] Because glioma gene therapy strategies are geared toward targeting invasive tumor cells that might have escaped local therapies of surgery and radiosurgery, focal and targeted delivery is very essential. Hence, FUS could play a major role in this endeavor. The main preclinical assessment of FUS-mediated delivery of viral vectors into the brain was performed using radiolabeled HSV vector.[62] Using a combination of autography and histological assessments, the investigators were able to demonstrate focal delivery of intravenously administered HSV within the hemisphere that was sonicated with FUS. While this study is encouraging, additional studies are warranted to assess the functional efficiency of this mode of viral vector delivery into the brain. Transgene expression via FUS

TABLE 3: Preclinical animal studies of FUS delivery across the BBB

Authors & Year	Study Finding
Kinoshita et al., 2006[30]	delivery of dopamine D(4) receptor–targeting antibody into brain
Sheikov et al., 2006	focal delivery of intravenously administered HSV-engineered vector across BBB of normal rats
Kinoshita et al., 2006[29]	delivery of Herceptin (anti-HER2 monoclonal antibody) into brain
Treat et al., 2007	successful enhanced delivery of doxorubicin across BBB of normal rats
Treat et al., 2009	successful enhanced delivery of doxorubicin across BBB of rat glioma models
Mei et al., 2009	successful enhanced delivery of doxorubicin across BBB of rabbit brain
Liu et al., 2010[36]	enhanced delivery of BCNU w/ FUS led to tumor remission & prolonged survival in rat glioma model
Jordão et al., 2010	delivery of anti–amyloid β antibodies via FUS led to Alzheimer plaque reduction in transgenic mouse model
Liu et al., 2010[37]	FUS delivery of iron oxide MNPs conjugated to epirubicin led to enhanced delivery, tumor remission, & prolonged survival in rat glioma models

delivery of DNA constructs could serve as an alternative to viral intracellular delivery methods.[31,67,71] Focused ultrasound has been previously employed for intrauterine gene delivery into fetal brain.[14] Furthermore, Shimamura and colleagues[65] have demonstrated enhanced delivery and expression of the *luciferase* gene in rat CNS using the microbubble-enhanced ultrasound method. The use of FUS-mediated targeted molecular therapy can thus be envisioned. For example, this technology could be used to deliver a gene that could complement a mutation in a tumor cell or, by delivery of a silencing gene, such as microRNA or short hairpin RNA gene, to downregulate the expression of an aberrantly expressed protein. Reduction in the expression of Survivin, an inhibitor of apoptosis, which is expressed in malignant glioma, has been achieved in a flank xenograft cervical cancer model using focused ultrasound delivery of a short hairpin RNA silencing vector targeting Survivin.[9] Further preclinical investigation to assess the potential of transcranial focused ultrasound for nonviral gene therapy in the CNS is warranted.

Future Directions

Preclinical studies thus far suggest that FUS with microbubbles can safely facilitate the focal delivery of a wide range of therapeutic agents into the brain. In this regard, FUS affords selective and targeted delivery. In addition, the potential to successfully combine FUS with other specialized targeted delivery systems such as nanoparticles and viral vectors carries tremendous promise in molecular neurooncology. Furthermore, FUS applications in animal brain tumor models demonstrate correlations between enhanced delivery and decreased tumor progression with a concomitant improved survival. Safety profiles have equally been established with FUS-mediated delivery strategies from a preclinical standpoint. If these preliminary preclinical results are sustainable, FUS-mediated delivery will play a pivotal role in the molecular therapeutics of malignant brain tumors.

Disclosure

The authors acknowledge the financial support of the following: CIHR MOP-74610, NIH grant no. EB003268, Canada Research Chair program, Congress of Neurosurgeons Penfield Award, Canadian Cancer Society Research Institute, Brain Tumour Foundation of Canada, and Brainchild Canada. Dr. Hynynen holds stock in FUS Instruments and is a patent holder in Brigham and Women's Hospital. He receives non–study related support from both FUS Instruments and Philips.

Author contributions to the study and manuscript preparation include the following. Conception and design: Rutka, Etame, Hynynen. Acquisition of data: Etame, Diaz, Smith. Analysis and interpretation of data: Rutka, Etame, Diaz, Hynynen. Drafting the article: Etame. Critically revising the article: Rutka, Diaz, Smith, Mainprize, Hynynen. Reviewed submitted version of manuscript: all authors.

References

1. Abbott NJ, Revest PA: Control of brain endothelial permeability. **Cerebrovasc Brain Metab Rev 3:**39–72, 1991
2. Alvarez M, Paull K, Monks A, Hose C, Lee JS, Weinstein J, et al: Generation of a drug resistance profile by quantitation of mdr-1/P-glycoprotein in the cell lines of the National Cancer Institute Anticancer Drug Screen. **J Clin Invest 95:**2205–2214, 1995
3. Arosarena O, Guerin C, Brem H, Laterra J: Endothelial differentiation in intracerebral and subcutaneous experimental gliomas. **Brain Res 640:**98–104, 1994
4. Barnett FH, Rainov NG, Ikeda K, Schuback DE, Elliott P, Kramm CM, et al: Selective delivery of herpes virus vectors to experimental brain tumors using RMP-7. **Cancer Gene Ther 6:**14–20, 1999
5. Blasberg RG, Kobayashi T, Horowitz M, Rice JM, Groothuis D, Molnar P, et al: Regional blood flow in ethylnitrosourea-induced brain tumors. **Ann Neurol 14:**189–201, 1983
6. Blasberg RG, Molnar P, Horowitz M, Kornblith P, Pleasants R, Fenstermacher J: Regional blood flow in RT-9 brain tumors. **J Neurosurg 58:**863–873, 1983
7. Brown SD, Nativo P, Smith JA, Stirling D, Edwards PR, Venugopal B, et al: Gold nanoparticles for the improved anticancer drug delivery of the active component of oxaliplatin. **J Am Chem Soc 132:**4678–4684, 2010
8. Chen MY, Hoffer A, Morrison PF, Hamilton JF, Hughes J, Schlageter KS, et al: Surface properties, more than size, limiting convective distribution of virus-sized particles and viruses in the central nervous system. **J Neurosurg 103:**311–319, 2005
9. Chen ZY, Liang K, Qiu RX: Targeted gene delivery in tumor xenografts by the combination of ultrasound-targeted microbubble destruction and polyethylenimine to inhibit survivin gene expression and induce apoptosis. **J Exp Clin Cancer Res 29:**152, 2010
10. Cheng Y, C Samia A, Meyers JD, Panagopoulos I, Fei B, Burda C: Highly efficient drug delivery with gold nanoparticle vectors for in vivo photodynamic therapy of cancer. **J Am Chem Soc 130:**10643–10647, 2008
11. De Jong WH, Hagens WI, Krystek P, Burger MC, Sips AJ, Geertsma RE: Particle size-dependent organ distribution of gold nanoparticles after intravenous administration. **Biomaterials 29:**1912–1919, 2008
12. Emerich DF, Dean RL, Osborn C, Bartus RT: The development of the bradykinin agonist labradimil as a means to increase the permeability of the blood-brain barrier: from concept to clinical evaluation. **Clin Pharmacokinet 40:**105–123, 2001
13. Emerich DF, Snodgrass P, Dean R, Agostino M, Hasler B, Pink M, et al: Enhanced delivery of carboplatin into brain tumours with intravenous Cereport (RMP-7): dramatic differences and insight gained from dosing parameters. **Br J Cancer 80:**964–970, 1999
14. Endoh M, Koibuchi N, Sato M, Morishita R, Kanzaki T, Murata Y, et al: Fetal gene transfer by intrauterine injection with microbubble-enhanced ultrasound. **Mol Ther 5:**501–508, 2002
15. Fulci G, Chiocca EA: The status of gene therapy for brain tumors. **Expert Opin Biol Ther 7:**197–208, 2007
16. Groothuis DR, Fischer JM, Lapin G, Bigner DD, Vick NA: Permeability of different experimental brain tumor models to horseradish peroxidase. **J Neuropathol Exp Neurol 41:**164–185, 1982
17. Haroun RI, Brem H: Local drug delivery. **Curr Opin Oncol 12:**187–193, 2000
18. Huang Y, Hynynen K: MR-guided focused ultrasound for brain ablation and blood-brain barrier disruption. **Methods Mol Biol 711:**579–593, 2011
19. Hynynen K: Ultrasound for drug and gene delivery to the brain. **Adv Drug Deliv Rev 60:**1209–1217, 2008
20. Hynynen K, McDannold N, Sheikov NA, Jolesz FA, Vykhodtseva N: Local and reversible blood-brain barrier disruption by noninvasive focused ultrasound at frequencies suitable for trans-skull sonications. **Neuroimage 24:**12–20, 2005
21. Hynynen K, McDannold N, Vykhodtseva N, Jolesz FA: Non-

invasive MR imaging-guided focal opening of the blood-brain barrier in rabbits. **Radiology 220:**640–646, 2001
22. Hynynen K, McDannold N, Vykhodtseva N, Jolesz FA: Noninvasive opening of BBB by focused ultrasound. **Acta Neurochir Suppl 86:**555–558, 2003
23. Hynynen K, McDannold N, Vykhodtseva N, Raymond S, Weissleder R, Jolesz FA, et al: Focal disruption of the blood-brain barrier due to 260-kHz ultrasound bursts: a method for molecular imaging and targeted drug delivery. **J Neurosurg 105:**445–454, 2006
24. Immonen A, Vapalahti M, Tyynelä K, Hurskainen H, Sandmair A, Vanninen R, et al: AdvHSV-tk gene therapy with intravenous ganciclovir improves survival in human malignant glioma: a randomised, controlled study. **Mol Ther 10:**967–972, 2004
25. Jemal A, Siegel R, Ward E, Murray T, Xu J, Smigal C, et al: Cancer statistics, 2006. **CA Cancer J Clin 56:**106–130, 2006
26. Jordão JF, Ayala-Grosso CA, Markham K, Huang Y, Chopra R, McLaurin J, et al: Antibodies targeted to the brain with image-guided focused ultrasound reduces amyloid-beta plaque load in the TgCRND8 mouse model of Alzheimer's disease. **PLoS One 5:**e10549, 2010
27. Judy KD, Olivi A, Buahin KG, Domb A, Epstein JI, Colvin OM, et al: Effectiveness of controlled release of a cyclophosphamide derivative with polymers against rat gliomas. **J Neurosurg 82:**481–486, 1995
28. Kim BY, Rutka JT, Chan WC: Nanomedicine. **N Engl J Med 363:**2434–2443, 2010
29. Kinoshita M, McDannold N, Jolesz FA, Hynynen K: Noninvasive localized delivery of Herceptin to the mouse brain by MRI-guided focused ultrasound-induced blood-brain barrier disruption. **Proc Natl Acad Sci U S A 103:**11719–11723, 2006
30. Kinoshita M, McDannold N, Jolesz FA, Hynynen K: Targeted delivery of antibodies through the blood-brain barrier by MRI-guided focused ultrasound. **Biochem Biophys Res Commun 340:**1085–1090, 2006
31. Kuliszewski MA, Kobulnik J, Lindner JR, Stewart DJ, Leong-Poi H: Vascular gene transfer of SDF-1 promotes endothelial progenitor cell engraftment and enhances angiogenesis in ischemic muscle. **Mol Ther 19:**895–902, 2011
32. Lee HJ, Zhang Y, Pardridge WM: Blood-brain barrier disruption following the internal carotid arterial perfusion of alkyl glycerols. **J Drug Target 10:**463–467, 2002
33. Lee JS, Paull K, Alvarez M, Hose C, Monks A, Grever M, et al: Rhodamine efflux patterns predict P-glycoprotein substrates in the National Cancer Institute drug screen. **Mol Pharmacol 46:**627–638, 1994
34. Lesniak MS, Brem H: Targeted therapy for brain tumours. **Nat Rev Drug Discov 3:**499–508, 2004
35. Lidar Z, Mardor Y, Jonas T, Pfeffer R, Faibel M, Nass D, et al: Convection-enhanced delivery of paclitaxel for the treatment of recurrent malignant glioma: a phase I/II clinical study. **J Neurosurg 100:**472–479, 2004
36. Liu HL, Hua MY, Chen PY, Chu PC, Pan CH, Yang HW, et al: Blood-brain barrier disruption with focused ultrasound enhances delivery of chemotherapeutic drugs for glioblastoma treatment. **Radiology 255:**415–425, 2010
37. Liu HL, Hua MY, Yang HW, Huang CY, Chu PC, Wu JS, et al: Magnetic resonance monitoring of focused ultrasound/magnetic nanoparticle targeting delivery of therapeutic agents to the brain. **Proc Natl Acad Sci U S A:**15205–15210, 2010
38. Löscher W, Potschka H: Drug resistance in brain diseases and the role of drug efflux transporters. **Nat Rev Neurosci 6:** 591–602, 2005
39. Löscher W, Potschka H: Role of drug efflux transporters in the brain for drug disposition and treatment of brain diseases. **Prog Neurobiol 76:**22–76, 2005
40. McDannold N, Vykhodtseva N, Hynynen K: Use of ultrasound pulses combined with Definity for targeted blood-brain barrier disruption: a feasibility study. **Ultrasound Med Biol 33:**584–590, 2007
41. McDannold N, Vykhodtseva N, Raymond S, Jolesz FA, Hynynen K: MRI-guided targeted blood-brain barrier disruption with focused ultrasound: histological findings in rabbits. **Ultrasound Med Biol 31:**1527–1537, 2005
42. McDannold NJ, Vykhodtseva NI, Hynynen K: Microbubble contrast agent with focused ultrasound to create brain lesions at low power levels: MR imaging and histologic study in rabbits. **Radiology 241:**95–106, 2006
43. Mei J, Cheng Y, Song Y, Yang Y, Wang F, Liu Y, et al: Experimental study on targeted methotrexate delivery to the rabbit brain via magnetic resonance imaging-guided focused ultrasound. **J Ultrasound Med 28:**871–880, 2009
44. Mesiwala AH, Farrell L, Wenzel HJ, Silbergeld DL, Crum LA, Winn HR, et al: High-intensity focused ultrasound selectively disrupts the blood-brain barrier in vivo. **Ultrasound Med Biol 28:**389–400, 2002
45. Neuwelt EA, Barnett PA, Bigner DD, Frenkel EP: Effects of adrenal cortical steroids and osmotic blood-brain barrier opening on methotrexate delivery to gliomas in the rodent: the factor of the blood-brain barrier. **Proc Natl Acad Sci U S A 79:**4420–4423, 1982
46. Neuwelt EA, Frenkel EP, D'Agostino AN, Carney DN, Minna JD, Barnett PA, et al: Growth of human lung tumor in the brain of the nude rat as a model to evaluate antitumor agent delivery across the blood-brain barrier. **Cancer Res 45:**2827–2833, 1985
47. Neuwelt EA, Frenkel EP, Gumerlock MK, Braziel R, Dana B, Hill SA: Developments in the diagnosis and treatment of primary CNS lymphoma. A prospective series. **Cancer 58:** 1609–1620, 1986
48. Nilaver G, Muldoon LL, Kroll RA, Pagel MA, Breakefield XO, Davidson BL, et al: Delivery of herpesvirus and adenovirus to nude rat intracerebral tumors after osmotic blood-brain barrier disruption. **Proc Natl Acad Sci U S A 92:**9829–9833, 1995
49. Oshiro EM, Viola JJ, Oldfield EH, Walbridge S, Bacher J, Frank JA, et al: Toxicity studies and distribution dynamics of retroviral vectors following intrathecal administration of retroviral vector-producer cells. **Cancer Gene Ther 2:**87–95, 1995
50. Paciotti GF, Myer L, Weinreich D, Goia D, Pavel N, McLaughlin RE, et al: Colloidal gold: a novel nanoparticle vector for tumor directed drug delivery. **Drug Deliv 11:**169–183, 2004
51. Pardridge WM: Blood-brain barrier biology and methodology. **J Neurovirol 5:**556–569, 1999
52. Pardridge WM: Blood-brain barrier drug targeting: the future of brain drug development. **Mol Interv 3:**90–105, 2003
53. Pardridge WM: Drug and gene targeting to the brain with molecular Trojan horses. **Nat Rev Drug Discov 1:**131–139, 2002
54. Parney IF, Kunwar S, McDermott M, Berger M, Prados M, Cha S, et al: Neuroradiographic changes following convection-enhanced delivery of the recombinant cytotoxin interleukin 13-PE38QQR for recurrent malignant glioma. **J Neurosurg 102:**267–275, 2005
55. Pathak AP, Schmainda KM, Ward BD, Linderman JR, Rebro KJ, Greene AS: MR-derived cerebral blood volume maps: issues regarding histological validation and assessment of tumor angiogenesis. **Magn Reson Med 46:**735–747, 2001
56. Prados MD, Schold SC JR SC, Fine HA, Jaeckle K, Hochberg F, Mechtler L, et al: A randomized, double-blind, placebo-controlled, phase 2 study of RMP-7 in combination with carboplatin administered intravenously for the treatment of recurrent malignant glioma. **Neuro Oncol 5:**96–103, 2003
57. Rapoport SI: Osmotic opening of the blood-brain barrier: principles, mechanism, and therapeutic applications. **Cell Mol Neurobiol 20:**217–230, 2000
58. Saito R, Krauze MT, Noble CO, Tamas M, Drummond DC, Kirpotin DB, et al: Tissue affinity of the infusate affects the distribution volume during convection-enhanced delivery into

rodent brains: implications for local drug delivery. **J Neurosci Methods 154:**225–232, 2006
59. Sanovich E, Bartus RT, Friden PM, Dean RL, Le HQ, Brightman MW: Pathway across blood-brain barrier opened by the bradykinin agonist, RMP-7. **Brain Res 705:**125–135, 1995
60. Shankar GM, Li S, Mehta TH, Garcia-Munoz A, Shepardson NE, Smith I, et al: Amyloid-beta protein dimers isolated directly from Alzheimer's brains impair synaptic plasticity and memory. **Nat Med 14:**837–842, 2008
61. Shapiro WR, Green SB, Burger PC, Selker RG, VanGilder JC, Robertson JT, et al: A randomized comparison of intra-arterial versus intravenous BCNU, with or without intravenous 5-fluorouracil, for newly diagnosed patients with malignant glioma. **J Neurosurg 76:**772–781, 1992
62. Sheikov N, McDannold N, Jolesz F, Zhang YZ, Tam K, Hynynen K: Brain arterioles show more active vesicular transport of blood-borne tracer molecules than capillaries and venules after focused ultrasound-evoked opening of the blood-brain barrier. **Ultrasound Med Biol 32:**1399–1409, 2006
63. Sheikov N, McDannold N, Sharma S, Hynynen K: Effect of focused ultrasound applied with an ultrasound contrast agent on the tight junctional integrity of the brain microvascular endothelium. **Ultrasound Med Biol 34:**1093–1104, 2008
64. Sheikov N, McDannold N, Vykhodtseva N, Jolesz F, Hynynen K: Cellular mechanisms of the blood-brain barrier opening induced by ultrasound in presence of microbubbles. **Ultrasound Med Biol 30:**979–989, 2004
65. Shimamura M, Sato N, Taniyama Y, Yamamoto S, Endoh M, Kurinami H, et al: Development of efficient plasmid DNA transfer into adult rat central nervous system using microbubble-enhanced ultrasound. **Gene Ther 11:**1532–1539, 2004
66. Sonavane G, Tomoda K, Makino K: Biodistribution of colloidal gold nanoparticles after intravenous administration: effect of particle size. **Colloids Surf B Biointerfaces 66:**274–280, 2008
67. Song S, Shen Z, Chen L, Brayman AA, Miao CH: Explorations of high-intensity therapeutic ultrasound and microbubble-mediated gene delivery in mouse liver. **Gene Ther 18:** 1006–1014, 2011
68. Stupp R, Hegi ME, Mason WP, van den Bent MJ, Taphoorn MJ, Janzer RC, et al: Effects of radiotherapy with concomitant and adjuvant temozolomide versus radiotherapy alone on survival in glioblastoma in a randomised phase III study: 5-year analysis of the EORTC-NCIC trial. **Lancet Oncol 10:**459–466, 2009
69. Stupp R, Mason WP, van den Bent MJ, Weller M, Fisher B, Taphoorn MJ, et al: Radiotherapy plus concomitant and adjuvant temozolomide for glioblastoma. **N Engl J Med 352:**987–996, 2005
70. Stupp R, Roila F: Malignant glioma: ESMO clinical recommendations for diagnosis, treatment and follow-up. **Ann Oncol 20 (Suppl 4):**126–128, 2009
71. Taniyama Y, Tachibana K, Hiraoka K, Aoki M, Yamamoto S, Matsumoto K, et al: Development of safe and efficient novel nonviral gene transfer using ultrasound: enhancement of transfection efficiency of naked plasmid DNA in skeletal muscle. **Gene Ther 9:**372–380, 2002
72. Terentyuk GS, Maslyakova GN, Suleymanova LV, Khlebtsov BN, Kogan BY, Akchurin GG, et al: Circulation and distribution of gold nanoparticles and induced alterations of tissue morphology at intravenous particle delivery. **J Biophotonics 2:**292–302, 2009
73. Thakker DR, Weatherspoon MR, Harrison J, Keene TE, Lane DS, Kaemmerer WF, et al: Intracerebroventricular amyloid-beta antibodies reduce cerebral amyloid angiopathy and associated micro-hemorrhages in aged Tg2576 mice. **Proc Natl Acad Sci U S A 106:**4501–4506, 2009
74. Treat LH, McDannold N, Vykhodtseva N, Zhang Y, Tam K, Hynynen K: Targeted delivery of doxorubicin to the rat brain at therapeutic levels using MRI-guided focused ultrasound. **Int J Cancer 121:**901–907, 2007
75. Treat LH, Zhang Y, McDannold N, Hynynen K: Impact of focused ultrasound-enhanced drug delivery on survival in rats with glioma. 8th International Symposium on Therapeutic Ultrasound. **AIP Conf Proc 1113:** 443–446, 2009
76. Warren K, Jakacki R, Widemann B, Aikin A, Libucha M, Packer R, et al: Phase II trial of intravenous lobradimil and carboplatin in childhood brain tumors: a report from the Children's Oncology Group. **Cancer Chemother Pharmacol 58:**343–347, 2006
77. Westphal M, Lamszus K, Hilt D: Intracavitary chemotherapy for glioblastoma: present status and future directions. **Acta Neurochir Suppl 88:**61–67, 2003
78. Wilcock DM, DiCarlo G, Henderson D, Jackson J, Clarke K, Ugen KE, et al: Intracranially administered anti-Abeta antibodies reduce beta-amyloid deposition by mechanisms both independent of and associated with microglial activation. **J Neurosci 23:**3745–3751, 2003
79. Wolff JE, Trilling T, Mölenkamp G, Egeler RM, Jürgens H: Chemosensitivity of glioma cells in vitro: a meta analysis. **J Cancer Res Clin Oncol 125:**481–486, 1999

Manuscript submitted September 16, 2011.
Accepted October 20, 2011.
Please include this information when citing this paper: DOI: 10.3171/2011.10.FOCUS11252.

Address correspondence to: James T. Rutka, M.D., Ph.D., The Arthur and Sonia Labatt Brain Tumor Research Centre, The Hospital for Sick Children, Division of Neurosurgery, Suite 1503, 555 University Avenue, Toronto, Ontario M5G 1X8, Canada. email: james.rutka@sickkids.ca.

Neurosurg Focus 32 (1):E4, 2012

Enhanced therapeutic agent delivery through magnetic resonance imaging–monitored focused ultrasound blood-brain barrier disruption for brain tumor treatment: an overview of the current preclinical status

Hao-Li Liu, Ph.D.,[1,2] Hung-Wei Yang, Ph.D.,[3] Mu-Yi Hua, Ph.D.,[3] and Kuo-Chen Wei, M.D.[4]

Departments of [1]Electrical Engineering and [3]Chemical and Material Engineering, Chang-Gung University; and [2]Molecular Imaging Center and [4]Department of Neurosurgery, Chang-Gung University and Memorial Hospital, Taoyuan, Taiwan

Malignant glioma is a severe primary CNS cancer with a high recurrence and mortality rate. The current strategy of surgical debulking combined with radiation therapy or chemotherapy does not provide good prognosis, tumor progression control, or improved patient survival. The blood-brain barrier (BBB) acts as a major obstacle to chemotherapeutic treatment of brain tumors by severely restricting drug delivery into the brain. Because of their high toxicity, chemotherapeutic drugs cannot be administered at sufficient concentrations by conventional delivery methods to significantly improve long-term survival of patients with brain tumors. Temporal disruption of the BBB by microbubble-enhanced focused ultrasound (FUS) exposure can increase CNS-blood permeability, providing a promising new direction to increase the concentration of therapeutic agents in the brain tumor and improve disease control. Under the guidance and monitoring of MR imaging, a brain drug-delivery platform can be developed to control and monitor therapeutic agent distribution and kinetics. The success of FUS BBB disruption in delivering a variety of therapeutic molecules into brain tumors has recently been demonstrated in an animal model. In this paper the authors review a number of critical studies that have demonstrated successful outcomes, including enhancement of the delivery of traditional clinically used chemotherapeutic agents or application of novel nanocarrier designs for actively transporting drugs or extending drug half-lives to significantly improve treatment efficacy in preclinical animal models.
(http://thejns.org/doi/abs/10.3171/2011.10.FOCUS11238)

Key Words • **focused ultrasound** • **brain tumor** • **blood-brain barrier** • **nanocarrier** • **magnetic resonance imaging**

Malignant glioma is a common and severe primary brain tumor with a high recurrence rate and an extremely high mortality rate within 2 years of diagnosis, even when surgical, radiological, and chemotherapeutic interventions are applied. Chemotherapy is currently an important adjuvant treatment that usually follows tumor debulking surgery. However, the efficacy of intravenously administered chemotherapeutic drugs is limited by their adverse systemic effects and poor penetration across the BBB, resulting in both insufficient local drug concentration in the tumor and extensive circulating body toxicity. Focused ultrasound is a recently discovered noninvasive technique that shows great promise for local and reversible enhancement of the permeability of the BBB to chemotherapeutic agents. The efficacy of brain tumor chemotherapy could potentially be significantly enhanced by FUS BBB disruption, as guided and monitored by MR imaging. In this paper we review the current status of brain tumor treatment, the role of the BBB, and current clinical and preclinical treatment modalities. We then describe the current status of MR imaging-monitored FUS BBB disruption, including a review of the technique itself and its application to chemotherapeutic agent delivery. Finally, we describe the novel use of MNPs to concurrently function as MR imaging contrast agents and active magnetic targeting agents for brain tumor treatment, which were developed by our research team.

Abbreviations used in this paper: BBB = blood-brain barrier; BCNU = 1,3-bis(2-chloroethyl)-1-nitrosourea; EPEG = *o*-(2-aminoethyl)polyethylene glycol; FUS = focused ultrasound; IC_{50} = half-maximal inhibitory concentration; MNP = magnetic nanoparticles.

Current Status of Brain Tumors and the BBB

At least 18,000 patients are diagnosed with malignant primary brain tumors in the US each year, and more than half of them have glioblastoma.[32] The median survival of patients with low-grade gliomas is 5–15 years, but it is only 9–12 months for patients with high-grade gliomas.[4,22]

Multicenter randomized trials suggest that the treatment of glioblastoma patients with debulking surgery and radiation therapy results in a median survival of only 12 months. Chemotherapy is also an important treatment modality for glioblastoma, but generally results in a limited and temporary response,[21] while producing side effects that further reduce the quality of the patient's remaining life.

In the US, the most common systemically administered adjuvant chemotherapeutic drugs are BCNU, procarbazine, vincristine and lomustine, or temozolomide. No particular drug or multidrug regimen with a proven superiority in glioblastoma treatment has emerged, and chemotherapeutic delivery has met with limited success. For example, BCNU has been used since the 1970s and remains a common and effective chemotherapeutic agent for brain tumors,[17] yet it provides only a small benefit in short-term survival.[13,60] Because of the substantial toxicity of chemotherapeutic agents like BCNU,[23] an important current question is how to deliver a sufficiently high therapeutic dose specifically to the target tumor area to improve performance.

The Blood-Brain Barrier

The BBB consists of the cerebral capillary endothelium, choroid plexus epithelium, and arachnoid membrane. Layered cells in these structures form "tight junctions"[47] containing several proteins.[53] Transcellular transport is further limited by low endocytic activity and the absence of fenestrations. The BBB prevents diffusion of toxic foreign substances into the brain parenchyma,[45] but also presents an almost impenetrable barrier to therapeutics such as cisplatin (molecular weight 299 D). The enhanced permeability and retention effect of therapeutic nanoparticles is also greatly restricted by the BBB.

The concentrations of anticancer drugs in the brain appear to be further limited by the pumping action of P-glycoprotein,[49,50] a large (140–170 kD) glycosylated transport protein[26] found in the luminal membrane of endothelial cell walls of the BBB.[12] Up to 50% of total glioma cells preserve P-glycoprotein function.[48,57] Despite the generally leaky nature of the vasculature of gliomas, these new vessels thus maintain some BBB properties that contribute to inefficient drug delivery. Moreover, BBB disruption in these tumors is highly heterogeneous, and the tumor core is often the most permeable compared with the impermeable proliferating brain tumor peripheral region.[15,20,42,43] Permeability does not necessarily correlate with tumor histology, size, or anatomical location, and glioblastoma cells have been found at great distances from the enhancing regions of the tumors.[7,27]

Current Chemotherapy Route for Brain Tumors

Chemotherapeutics currently delivered by intravenous injection need to reach the brain by penetrating through the BBB or blood-CSF barrier. Some chemotherapeutic agents such as temozolomide are used in both intravenous and oral form. Chemotherapeutic agents can also be delivered interstitially by local injection[51] or by direct implantation of drug-carrying biodegradable matrices into the debulked tumor cavity.[33,64] A 30-month trial in 240 patients found median survival times of 13.9 and 11.6 months for patients implanted with BCNU wafers or placebos, respectively.[64] However, Gliadel wafer (Eisai) implantation was found to cause adverse effects, including CSF leakage, intracranial hypertension, seizures, brain edema, healing abnormalities, and intracranial infection.[18]

In convection-enhanced delivery, chemotherapeutic agents are interstitially infused while maintaining a pressure gradient, thus generating bulk interstitial fluid flow through the brain after an open-skull procedure.[5] In small animal brains, convection-enhanced delivery has achieved much higher local levels of chemotherapy than intravenous administration. Local drug distribution depends on the volume and rate of the gradient of infusion and on the molecular weight, concentration, and polarity of the drug. Current obstacles to convection-enhanced delivery include low rates and volumes of infusion that can lead to heterogeneous distribution and high variable tumor interstitial fluid pressure that causes a fast efflux of chemotherapeutic drugs from the injection site.

Drug delivery across the BBB can also be enhanced by concurrent intraarterial administration of osmotic agents or hypertonic solutions.[14,24,42] Clinical trials of these agents showed an increased patient survival from 11.4 to 17.5 months. However, osmotic solutions cause systemic rather than localized alteration of the BBB and have been associated with complications such as stroke-like syndrome, transient (2–3 days) exacerbation of preexisting neurological deficits, temporary seizures, and potential tumor migration and formation of new tumor nodules at distant brain locations.[44]

Focused Ultrasound-Induced BBB Disruption

Concepts of FUS BBB Disruption

Recent studies have shown that in the presence of microbubbles and in the low-energy burst-tone mode, FUS can increase the local permeability of the BBB.[29–31] This BBB disruptive effect is temporary and reversible and does not damage neural cells. Compared with alternative approaches such as modified lipophilic chemicals or hypertonic solution infused through carotid arteries for enhancing chemotherapeutic agent delivery into the brain,[44] the advantages of MR imaging-guided or MR imaging-monitored FUS-mediated delivery of chemotherapeutic agents include its entirely noninvasive procedure, local BBB disruption that minimizes off-target effects, and reversible BBB disruption within several hours (representing a suitable time window for drug release; Fig. 1). These properties make FUS BBB disruption a very attractive method to consider for increasing the local concentrations of chemotherapeutic agents in glioblastoma.

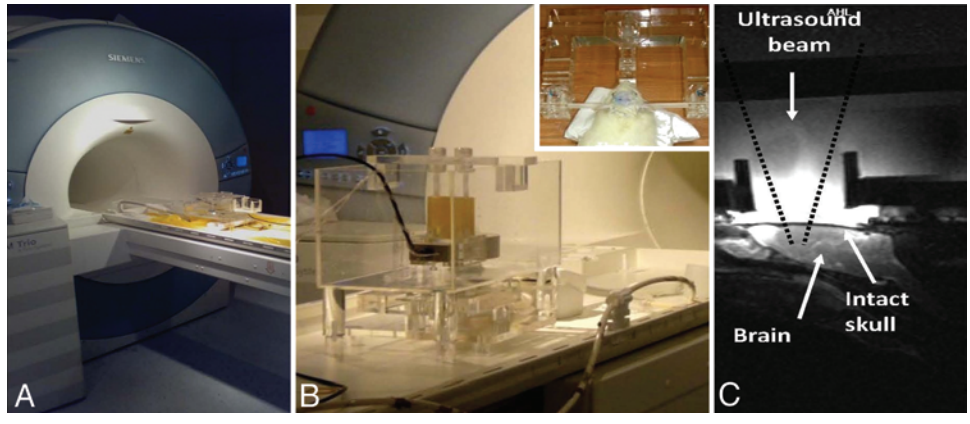

Fig. 1. Setup of the MR imaging system used to guide and monitor the FUS-induced BBB disruption. **A:** Magnetic resonance imaging machine. **B:** Animals with the stereotactic holder and the FUS transducers positioned on the MR imaging bed. **C:** Magnetic resonance imaging to provide a geometrical relationship between the animal and FUS transducer to guide and monitor the treatment procedure.

Focused Ultrasound BBB Disruption to Enhance Delivery of Liposomal Doxorubicin

The first promising outcome in FUS-enhanced brain drug delivery was the successful enhanced delivery of doxorubicin for preclinical brain tumor treatment.[58,59] Doxorubicin (Doxil, Ben Venue Laboratories) is a chemotherapeutic agent that can be encapsulated in long-circulating pegylated liposomes. In normal rat brain, Treat et al.[58] reported that at a microbubble concentration of 0.1 ml/kg, doxorubicin was delivered to the brain parenchyma at a concentration of 886 ± 327 ng/g tissue, thus reaching the therapeutic dose of doxorubicin treatment for breast carcinoma. With higher microbubble concentrations of 0.2 and 0.5 ml/kg, doxorubicin concentrations reached 2369 ± 946 and 5366 ± 659 ng/g tissue in the sonicated area, respectively, whereas doxorubicin concentrations in control tissue samples remained at or below 251 ± 119 ng/g tissue at all levels of the ultrasound contrast agent. The delivered doxorubicin concentration was highly correlated with the microbubble dose, which has since been shown to correlate with brain tissue damage mainly through microhemorrhages. The doxorubicin concentration also showed a strong correlation ($r = 0.87$) with MR imaging signal enhancement.

Later, Treat et al.[59] also reported the treatment efficacy of FUS-enhanced doxorubicin delivery in a small-animal glioma model. When tumor progression was monitored on a weekly basis by T2-weighted MR imaging of rats with implanted gliomas (9L glioma tumors), delayed tumor growth was observed in rats that received FUS-enhanced doxorubicin treatment, while tumors of the control and doxorubicin-only groups continued to grow exponentially after treatment. The median survival showed a modest FUS-dependent improvement from 29 days (doxorubicin-only) to 31 days (doxorubicin and FUS) compared with the 25 days of control or FUS-only treated rats. The percentage of long-term survival (> 40 days) in the FUS and doxorubicin group was 26.7%, whereas no rats in the other 3 groups survived longer than 34 days. There were no statistically significant differences in survival between the control, FUS-only, and doxorubicin-only groups.

Calculation of the exponential growth time constants for each rat by least-squares regression analysis confirmed that rats treated with FUS and doxorubicin had longer average tumor volume doubling times than any other group: whereas similar tumor growth rates were observed in the FUS-only or control groups (2.2 ± 0.3 and 2.3 ± 0.3 days, respectively), the FUS and doxorubicin group had a tumor growth rate of 3.7 ± 0.5 days compared with only 2.7 ± 0.4 days in the doxorubicin-only group. These results were consistent with an enhancement of chemotherapeutic efficacy by FUS.

Focused Ultrasound BBB Disruption to Enhance Delivery of BCNU

Following the successful delivery of doxorubicin, FUS-enhanced delivery of BCNU was also attempted.[37] The lipophilic BCNU (Fig. 2A) is a widely used, effective, and currently clinically approved chemotherapeutic agent for brain tumors.[17] It has been studied since 1970 and is one of the oldest drugs used to treat glioblastoma. Although BCNU contains lipophilic characteristics that allow its natural form to penetrate the BBB, its treatment efficacy is severely hampered by insufficient concentrations within the tumor due to its substantial body toxicity. Clinical trials demonstrated a modest (10%) benefit in survival over 1–2 years (10.1% at 1 year and 8.6% at 2 years compared with radiation therapy alone), but no significant difference in median patient survival (12 vs 9.4 months for radiation alone[16]). In contrast, a recent temozolomide Phase III trial showed a statistically significant benefit for patient survival rate (2-year survival rate of 26.5% compared with radiation alone[54]), with median survival extended to 15 months.[16]

In a test of enhanced delivery of BCNU in normal animal (rat) brain using an in-house–designed MR imaging-monitored FUS platform (Fig. 1), we reported that the BCNU concentration can be increased up to 340% (from 150 to 513 μg) compared with the contralateral unsonicated brain. When treating the tumor-bearing animal brain, there was a nearly 2-fold increase in BCNU (from 170 to 344 μg) at the tumor. Without presonication, the BCNU

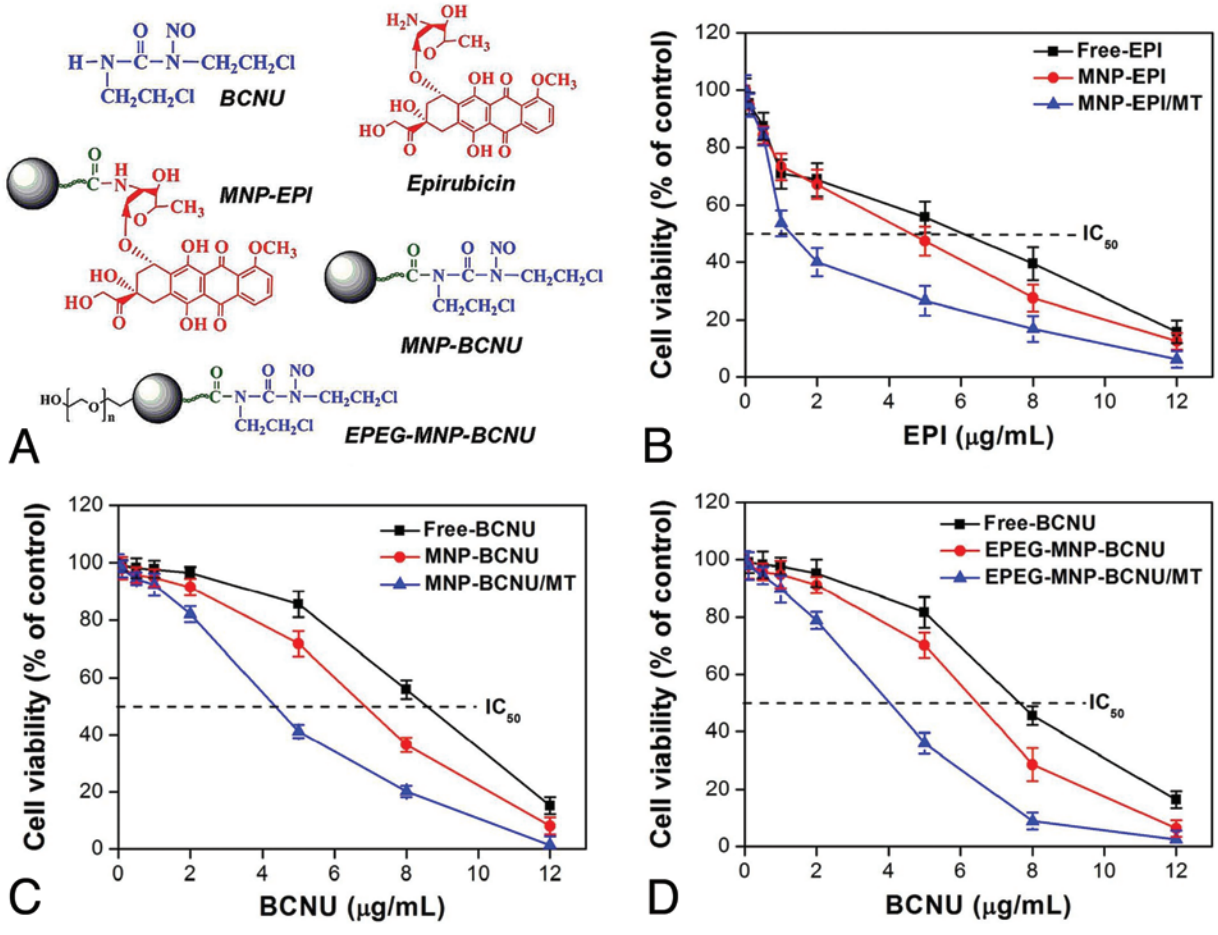

Fig. 2. Chemical structures **(A)** and cytotoxicities **(B–D)** of current chemotherapeutic agents and immobilization on MNPs. Graphs show cytotoxicity of free-epirubicin (EPI), MNP-EPI, and MNP-EPI/magnetic targeting (MT) on C6 cells for 48 hours of treatment **(B)**, cytotoxicity of free-BCNU, MNP-BCNU, and MNP-BCNU/MT on C6 cells for 48 hours of treatment **(C)**, and cytotoxicity of free-BCNU, EPEG-MNP-BCNU, and EPEG-MNP-BCNU/MT on U87 cells for 48 hours of treatment **(D)**.

concentrations at healthy and tumor-bearing brain sites were found to be similar (170 vs 150 μg, respectively).

Treatment efficacy was examined by observing tumor progression. Tumors in the control group grew from 0.13 ± 0.13 cm^3 (Day 10) to 0.28 ± 0.11 cm^3 (Day 31), and a similar trend was observed in the FUS-only group (from 0.11 ± 0.02 cm^3 at Day 10 to 0.32 ± 0.07 cm^3 at Day 31). The group treated with BCNU alone demonstrated a temporal decrease in tumor progression, but this effect was not sustainable, as tumors eventually grew to a similar level as in the control group (0.07 ± 0.03 cm^3 at Day 10 to 0.27 ± 0.17 cm^3 at Day 31). Combined FUS and BCNU provided the most significant suppression of tumor progression, with tumor size at 0.04 ± 0.08 cm^3 on Day 31.

When comparing survival, the median survival of control, FUS-only, and BCNU-only groups was 28.5, 25.5, and 33 days, respectively, confirming that BCNU prolonged animal survival. However, treatment with both FUS and BCNU produced the most significant benefit, increasing the median survival to 53 days (2 of 6 in the group survived for more than 60 days). Overall, the results suggest that the use of FUS to enhance BCNU delivery into brain tumors has a superior effect on suppressing tumor progression and improving animal survival than the use of either treatment alone.

Focused Ultrasound BBB Disruption to Enhance Delivery of Chemotherapeutic Agents for Brain Tumor Treatment

The successful delivery of clinically approved chemotherapeutic agents into the brain through FUS was reviewed in the previous section. Here we review the current literature of delivering nanoparticles into the brain, as well as our previous work on FUS-enhanced delivery of therapeutic nanocarriers (mainly MNPs), with the intention of improving the efficacy of brain tumor chemotherapy.

Characteristics of Delivered Substances for BBB Permeability

Central nervous system diseases such as brain gliomas and Alzheimer disease represent the largest and fastest-growing area of unmet medical needs. Their treatment is severely hampered by the restrictive tight junctions[65] of the capillary endothelial cells of the BBB that limit the pen-

etration of 98% of small molecules and almost all large molecules into the brain tissue.[45] Only drugs with low molecular weight and high lipid solubility are capable of crossing this specialized system.[1] Developing approaches such as nanobiotechnology to effectively, safely, and conveniently deliver therapeutic drugs to the CNS is therefore critically important.

The ability of nanomedicines to cross the BBB is affected by a number of factors including their size, charge, and surface properties. Nanoparticles must be large enough (30–100 nm) to avoid leakage into capillaries, but not so large (> 100 nm) that they are susceptible to macrophage-based clearance. Many studies have focused on the optimum size for nanocarriers used in brain disease treatment. There is general agreement that the volume of the distribution of nanocarriers in rat striatum is inversely proportional to the particle size. MacKay et al.[40] demonstrated that the ideal nanoparticle size for drug delivery in brain is less than 100 nm, because above this size, nanoparticles are retained near the site of injection and show restricted mobility. Studies on brain extracellular space yielded more precise information: the extracellular space is estimated to be between 35 and 64 nm in diameter in normal rat brain,[55] which means that many vectors larger than 100 nm will be too big to transit the normal neocortical extracellular space. Hydrophilic nanoparticles smaller than 100 nm have also been reported to avoid opsonization[2] and consequently show prolonged durations of action, as well as enhanced targeting to specific sites.[3] Sonavane et al.[52] evaluated the effect of increasing particle size on the biological distribution of nanoparticles following intravenous administration of the nanoparticle suspension prepared in sodium alginate solution in mice. Injection of different-sized gold nanoparticles (15, 50, 100, and 200 nm) clearly revealed that the distribution depends on the particle size in various tissues and organs. A higher amount of 15-nm nanoparticles was observed in all tissues including blood, liver, lung, spleen, kidney, brain, heart, and stomach. Nanoparticles larger than 200 nm were present at the lowest level in the brain compared with 15- and 50-nm particles, which could easily cross the BBB.[52]

The effect of surface charge on diffusivity of nanoparticles has also been studied in the rat brain. MacKay et al.[40] observed that the distribution nanoparticles with modest amounts of positive charge was significantly decreased compared with neutral nanoparticles ($p < 0.0005$). Cationic liposomes were found adjacent to the needle tract because of nonspecific binding to negatively charged structures in the brain parenchyma.[41] The low diffusivity of cationic liposomes presents a challenge because they are used as vectors for gene delivery.[19] Based on these results, a neutral or negative surface charge is required to obtain good diffusion. Most nanoparticles have been found to have increased permeability through brain capillary endothelial cells of the BBB (by transcytosis) when vectorized with cationic bovine serum albumin and poly(ethylene glycol)–poly(lactide).[39] Positive charges of the chitosan cationic compound may also electrostatically interact with the negatively charged brain endothelium to trigger adsorptive-mediated transport across the BBB.

Surface properties have a considerable impact on the diffusivity of colloidal vectors, especially because of the presence of steric coatings. Polyethylene glycol and dextran coatings significantly increase the distribution of nanoparticles.[46] Such biocompatible polymers are known to extend the systemic circulation of nanocarriers because they significantly reduce interactions with proteins.[35] Polyethylene glycol has also been shown to increase the BBB permeability of several conjugates.[6,45] Nevertheless, when nanoparticles were covered simply by albumin, the effect of size was reduced. The albumin coating masks hydrophobic structures of the polystyrene nanoparticles, thereby reducing the risk of eventual aggregation and binding to proteins in the extracellular space. Tosi et al.[56] conjugated poly(D,L-lactide-coglycolide) to a similopioid glycopeptide (g7) to produce nanoparticles (g7-nanoparticles) capable of crossing the BBB and delivering several kinds of molecules that are normally unable to cross the BBB to the CNS. In addition, solid lipid nanoparticles have been investigated as drug carriers to cross the BBB. Solid lipid nanoparticles improve the lipophilicity of the drug complex, thereby increasing the chance of transport of the incorporated drug.[61] Taken together, permeability of nanoparticles across the BBB requires either higher lipid solubility or surface conjugation of specific targeted ligands to polyethylene glycol derivatives.

Basic Concepts of MNPs for Biological Use

Magnetic nanoparticles are constitutes of magnetite (Fe_3O_4) that have received high attention for biomedical applications. Magnetic nanoparticles are also known as superparamagnetic iron oxide particles and have been used as contrast agents for MR imaging for more than 20 years.[62,63] At the same time, therapeutic applications of MNPs have also rapidly expanded. Magnetic nanoparticles can be conjugated to therapeutic agents such as drugs, proteins, enzymes, antibodies, or nucleotides and directed to specific organs, tissues, or tumors using an external magnetic field. This magnetic targeting is a promising strategy for achieving localized drug delivery to tumor tissue. The deposition, accumulation, and retention of drug-conjugated MNPs in tumors are enhanced by magnetic force. The feasibility of this application has recently been demonstrated in brain tumors.[9,11] Chertok et al.[9] showed that accumulation of nanoparticles was consistently enhanced with 9.6-fold selectivity for MNP accumulation in gliomas compared with the contralateral brain site. Magnetic nanoparticle distribution can be monitored in vivo by MR imaging in the brain. For example, MR spin-spin (R2) relaxivity measurement has been used to compare the R2 maps of animals that only received intravenously administered MNPs to those of animals that received intravenously administered MNPs combined with 0.4-T magnetic targeting. Image analysis confirmed that MNP distribution could be visualized in vivo in the brain and that magnetic targeting induced a 5-fold increase in MNP accumulation in the total glioma tumor mass.

Dose-Dependent Therapeutic MNPs: In Vitro Considerations

Traditional chemotherapeutic agents can be conjugat-

ed to MNPs to form therapeutic MNPs, for example MNP-epirubicin or MNP-BCNU (Fig. 2A). The concentrations of therapeutic MNPs that were required for 50% inhibition of cellular growth of glioma cells were initially determined in vitro. Pure MNPs without conjugated anticancer drugs have no apparent cytotoxic effect when cocultured in vitro with tumor cells. In contrast, abundant MNP-epirubicin that had presumably been taken up by endocytosis could be observed within cells by transmission electron microscopy. Furthermore, the particles passed into the nuclei and appeared to have induced apoptosis.

Conjugating epirubicin to MNPs did not affect its anticancer ability: the IC_{50} of free epirubicin and MNP-epirubicin was 6.1 and 4.6 μg/ml, respectively. The IC_{50} was reduced significantly to 1.3 μg/ml with magnetic targeting (Fig. 2B).[38] Free-BCNU and MNP-BCNU were also both toxic to C6 cells in a dose-dependent manner. The IC_{50} of MNP-BCNU was 6.9 μg/ml, which is lower than that of free-BCNU (8.6 μg/ml; Fig. 2C) due to greater thermal stability and a decreased rate of hydrolysis of conjugated BCNU, all leading to more efficient delivery of BCNU into the cells at 37°C. Magnetic targeting of MNP-BCNU led to a significant reduction in the IC_{50} to only 4.3 μg/ml (Fig. 2C),[28] suggesting that more of the MNP-BCNU was effectively guided to and concentrated at the target area.

To provide more effective MNPs, a self-protecting high-magnetic nanomedicine (EPEG-MNP-BCNU) was designed by grafting EPEG onto the surface of MNP-BCNU (Fig. 2A).[66] This nanomedicine (EPEG) acts to protect BCNU by slowing down its hydrolysis rate. The half-life of BCNU was thereby prolonged from 30 hours (MNP-BCNU) to 62 hours. Free-BCNU and EPEG-MNP-BCNU were both toxic to U87 cells in a concentration-dependent manner. However, the IC_{50} of the EPEG-MNP-BCNU was 6.4 μg/ml, which was lower than that of free-BCNU (8.5 μg/ml; Fig. 2D). Moreover, the IC_{50} was reduced significantly to only 4.0 μg/ml when an external magnetic field of 800 gauss was applied to the EPEG-MNP-BCNU (Fig. 2D).[66]

Focused Ultrasound BBB Disruption to Deliver MNPs Into Brain

Liu et al.[36] first demonstrated the application of FUS BBB disruption to enhance MNP delivery into the brain in small animals (Fig. 3). Their aim was to deliver MNPs into the brain and then use MR imaging monitoring of these MNPs to simultaneously detect BBB disruption and follow the status change of sonicated brain over time. An MNP contrast agent that was clinically approved for blood-pool MR imaging (Resovist, Schering AG Inc.; carboydextran-coated, 60-nm hydrodynamic size) was used. The local distribution of MNPs in the brain causes field inhomogeneity and concomitant signal loss on T2*-weighted images. The T2*-weighted images obtained before and after MNP administration and FUS delivery could therefore be used to detect the BBB disruption effect. This MR imaging-based method to detect BBB disruption was histologically confirmed.

Different levels of FUS pressure were tested, and the signal loss caused by intracranial hemorrhage or MNP leakage could be successfully distinguished by obtaining 2 T2*-weighted images before and after intravenous administration of MNPs.[36] The biodistribution of MNPs in the brain could also be followed over time by collection of T2*-weighted images. Over 70% of MNPs were cleared from the brain within 7 days. The deposition of MNPs in large animals (by changing the FUS to be low-frequency and planar) demonstrated clearance of MNPs over a similar period.[36] This study established a basis for the feasibility of using FUS to enhance MNPs in the brain and for modifying current commercially and clinically approved MNPs to be used as therapeutics with great potential for treatment of brain gliomas.

Therapeutic MNPs for FUS-Enhanced Delivery

Therapeutic MNPs have drawn considerable attention for their potential effect on CNS disease due to their superparamagnetic characteristics that can be guided by an external magnet and simultaneously provide contrast in MR imaging. In the previous section we described the development of MNP delivery into brain with the aid of FUS BBB disruption. Besides concurrent monitoring of the distributions of MNP by T2*-weighted MR imaging, R2 relaxometry MR imaging can be used to quantify the in vivo MNP concentration delivered into the animal brain.

The application of this method was first demonstrated in the normal animal brain to show a significant increase in therapeutic MNP deposition (Fig. 2A).[38] When applying FUS alone, the MNP concentration could be enhanced by up to 50% compared with the contralateral brain. However, with high-magnetization MNPs and the application of external magnetic targeting, the MNPs followed a time-dependent deposition in the sonicated brain, with up to a 20-fold increase compared with the contralateral brain. The calibrated epirubicin concentration in the sonicated/magnetic targeting site reached an upper limit of 21,738 ± 3477 μg/g, whereas FUS alone could only result in 1336 ± 1182 ng/g epirubicin deposition (Fig. 4). Hua et al.[28] similarly demonstrated the success of using magnetic targeting to deliver MNP-BCNU (Fig. 2A) into the brain tumor implant animal cells to confirm the effectiveness of the designed highly magnetized MNP. Tumors shrank markedly after 7 days of treatment with 5 mg/kg of MNP-BCNU with 24 hours of magnetic targeting. In contrast, tumor growth was not inhibited after 7 days by 13.5 mg/kg free-BCNU or 1.68 mg/kg MNP-BCNU with magnetic targeting.

This enhancement in therapeutic MNP delivery was also observed in tumor-bearing animals. Untreated animals showed no MNP accumulation after MNP-epirubicin administration. However, 11,982 ± 2105 ng of MNP-epirubicin was delivered when it was administered in combination with FUS/magnetic targeting, providing a 15-fold higher concentration than the therapeutic range in breast cancer (819 ± 482 ng/g tumor) previously reported for doxorubicin to reach a clinical response rate of 39%.

Control of tumor progression and survival were investigated next (Fig. 5). With a 7-day observation interval, the tumor volume in the FUS/magnetic targeting groups only increased by 106% ± 24% in treated animals com-

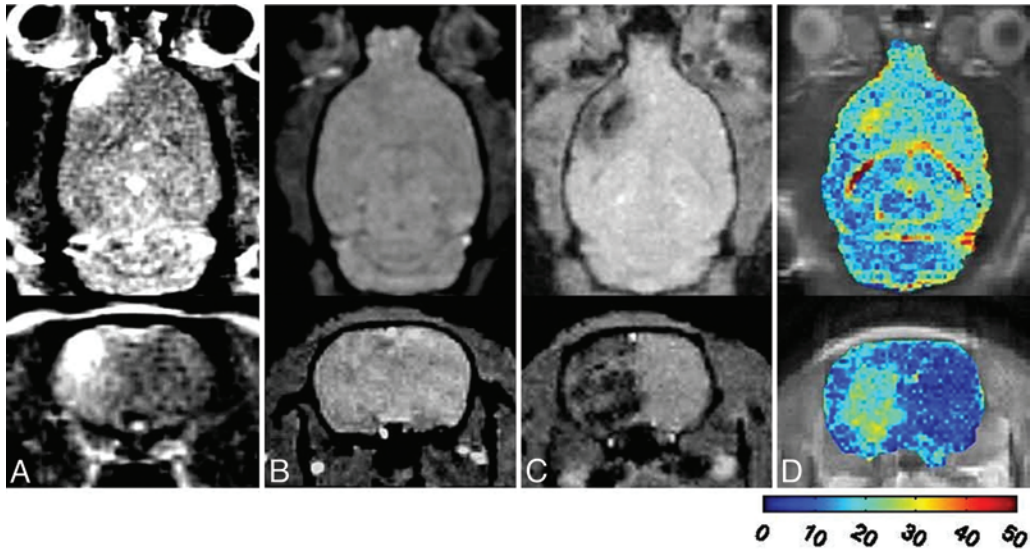

Fig. 3. Typical images (*upper*, coronal plane; *lower*, transverse plane) showing an animal undergoing FUS to induce BBB disruption, and monitoring the delivery of MNPs. **A:** Contrast-enhanced T1-weighted imaging after intravenously administered Gd-diethylenetriamine pentaacetic acid contrast agent. **B:** T2*-weighted imaging before administering MNP. **C:** T2*-weighted imaging after administering MNP and a 6-hour magnetic targeting procedure. **D:** R2 map to show the quantitative MNP distribution in the brain. Scale units are sec^{-1}.

pared with a 313% increase (± 103%) in controls, indicating that the combination of therapeutic MNPs with FUS/magnetic targeting provided the most effective means of controlling tumor progression. Moreover, in animal survival, the control and the FUS-enhancement-only treatment resulted in similar median animal survival times (23 and 20 days, respectively), whereas the median survival times were significantly improved by 66% in animals receiving MNP-epirubicin in conjunction with FUS/magnetic targeting treatment (30.5 vs 18.3 days, respectively).

Focused ultrasound combined with magnetic targeting to both passively and actively deliver MNPs thus represents a powerful technique to enhance the delivery of a wide range of macromolecule therapeutic substances into the CNS under the guidance and in vivo monitoring of drug quantification/distribution by MR imaging. Also, the synergistic drug delivery approach provided an improvement of approximately 3.4-fold in the drug's half-life (from 18 to 62 hours). Because of the longer circulation time of EPEG-MNP-BCNU, its accumulation was excellent (177.33 ± 23.13 μg of Fe ion) and approximately 1.65-fold higher than that of MNP-BCNU (107.72 ± 29.72 μg of Fe ion) after 24 hours of magnetic targeting. This observation supports the idea that EPEG-MNP-BCNU is more suitable than MNP-BCNU for in vivo antitumor studies. The survival rate in animals that received a low dose of BCNU (4.5 mg BCNU/kg in the form of EPEG-MNP-BCNU) was 63 days compared with 50 days in ani-

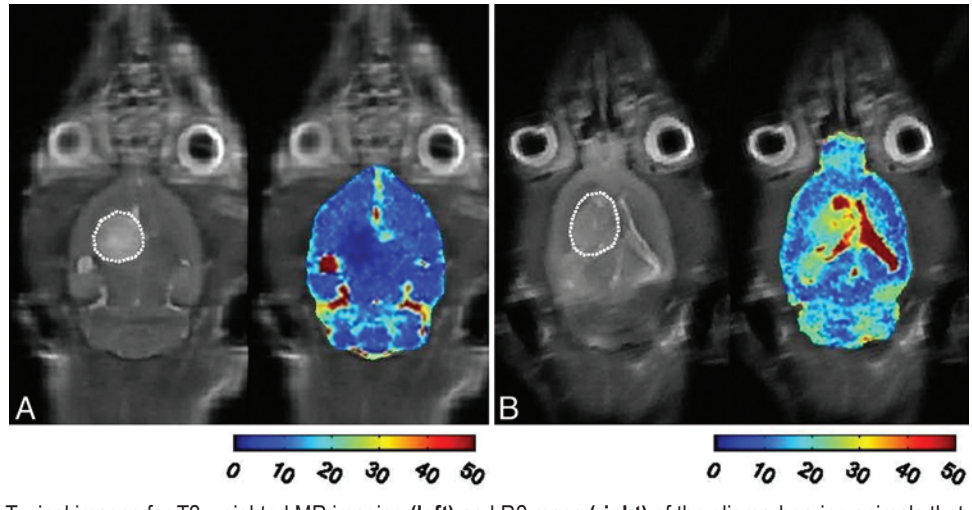

Fig. 4. Typical images for T2-weighted MR imaging **(left)** and R2 maps **(right)** of the glioma-bearing animals that did not **(A)** and did **(B)** undergo the FUS/magnetic targeting procedure. The FUS/magnetic targeting procedure demonstrates the enhancement of therapeutic MNP retention for at least 6 hours to improve the therapeutic efficacy of glioma treatment. Gliomas are outlined in white.

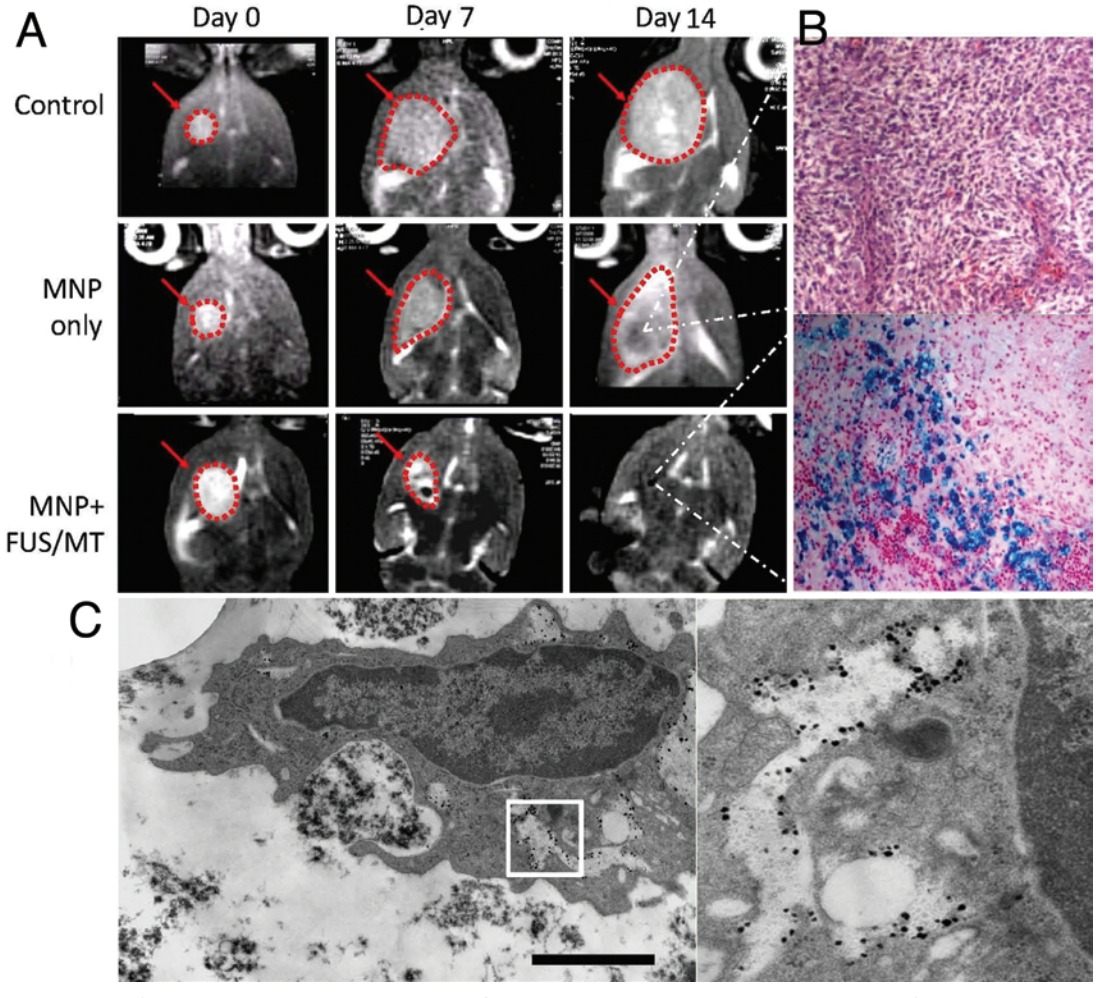

Fig. 5. Images from the authors' previous data. **A:** Glioma progression comparison monitored by T2-weighted MR imaging in 3 groups. control = control animal without receiving treatment; BCNU only = animal only receiving therapeutic MNP with immobilized BCNU; MNP+FUS/MT = animal receiving therapeutic MNP with FUS/magnetic targeting. Red dashed outlines contour the tumor border. **B:** Purl's Prussian blue staining of the tumor in animals without *(upper)* and with *(lower)* the FUS/magnetic targeting procedure that were killed on Day 14 to indicate therapeutic MNP deposition. **C:** Transmission electron microscopy images to show MNP uptake by the tumor cells; the enlarged region *(right)* shows MNP uptake and dispersal in the cell. Bar = 920 nm.

mals that received a high dose of free BCNU (13.5 mg BCNU/kg). This improvement could greatly enhance the potential of magnetic targeting therapy in clinical applications of cancer treatments.

Besides the above-mentioned highly magnetized MNP design to facilitate local drug delivery into the brain tumor, other attempts have been conducted to further improve the drug activity in the circulation. For example, injected MNPs act as foreign molecules to the body and are still limited by their insufficient stability in aqueous media and marked reticuloendothelial uptake in vivo.[34] In particular, the half-lives of MNPs are fairly short (in the range of minutes) due to their rapid capture and subsequent plasma clearance by macrophages of the reticuloendothelial system, especially in the liver.[10,25] However, self-protecting EPEG-MNP-BCNU[66] (Fig. 2A) is known to not only have a high capacity for BCNU drug loading and outstanding thermal stability, but long circulation times in vivo as well. The nanosize and excellent dispersion of EPEG-MNP-BCNU allow easier penetration of tissues and more efficient uptake by tumor cells with an enhanced permeability and retention effect.

Dose-Dependent Therapeutic MNPs: In Vivo Considerations

The dose dependency of therapeutic MNPs (Fig. 2A) for treatment of gliomas has also been investigated to determine the optimal enhancement conditions.[8] Normal/glioma rats were subjected to various treatments to compare their efficacy in delivering localized concentrations of nanoparticles to a specific region of the brain. Quantitative inductively coupled plasma optical emission spectrometry analysis of Fe content revealed that FUS alone or magnetic targeting alone only increased therapeutic MNP concentrations by 2-fold relative to the untreated brain. In contrast, the combination of magnetic targeting and FUS resulted in a 10-fold increase in MNP accumulation in the treated region relative to the untreated region.

During a 7-day MR imaging follow-up to track tumor progression, the control, BCNU-only, MNP-only,

and sham procedure (FUS/magnetic targeting but without MNP delivery) groups showed no tumor shrinkage (Fig. 6).[8] However, for groups receiving high-dose therapeutic MNPs (equivalent to 5 mg/kg of BCNU), tumor volumes were suppressed in the 1st week, both with and without applying FUS/magnetic targeting (–52% and –97%, respectively). The medium dose (equivalent to 1 mg/kg BCNU) appeared to represent the critical dose for suppression of tumor growth when FUS/magnetic targeting is applied (–79%), but tumors progressed in the sham group (296%). A low dose of therapeutic MNPs did not show repropression of tumor progression in either group (163% and 31%, respectively), although the magnetic targeting/FUS group had a relatively slow tumor progression rate. In evaluating animal survival, the median survival time also improved in animals receiving high and medium doses of BCNU-MNPs in conjunction with magnetic/ultrasound treatment; both reached 60 days or above, which was significantly longer that the other experimental groups (all < 33 days).

In the same study, CD68-positive cells were present in the tumor and constituted up to 30% of the tumor mass. The percentage of CD68-positive cells was unchanged in the control and MNP-delivered groups but increased in the MNP combined with FUS/magnetic targeting treatment groups; however, the presence of macrophages increased after sacrificing the treated animals. These findings suggested that MNPs alone do not cause severe immune activity, but the cytotoxic effect of the therapeutic MNPs causes tumor cell death and induces increased macrophage infiltration for the clearance of the necrotic tumor debris as well as the Fe particles.[8]

When summarizing the dosing comparison (Fig. 6), treatment with an effective BCNU dose of 5 mg/kg even without FUS/magnetic targeting was more effective at shrinking tumors than treatment with unbound BCNU at a dose of 13.5 mg/kg,[8] showing an enhanced permeability and retention effect for immobilized chemotherapy drugs on MNPs. The increased drug concentration in tumor cells may result not only from diffusion but also from phagocytosis of drug-bound particles by the cells. Overall, the magnetic/FUS system enhances drug delivery to tumors approximately 5-fold compared with BCNU alone, although the inductively coupled plasma optical emission spectrometry–measured drug amount can have up to a 26-fold enhancement in normal rat brains.[8]

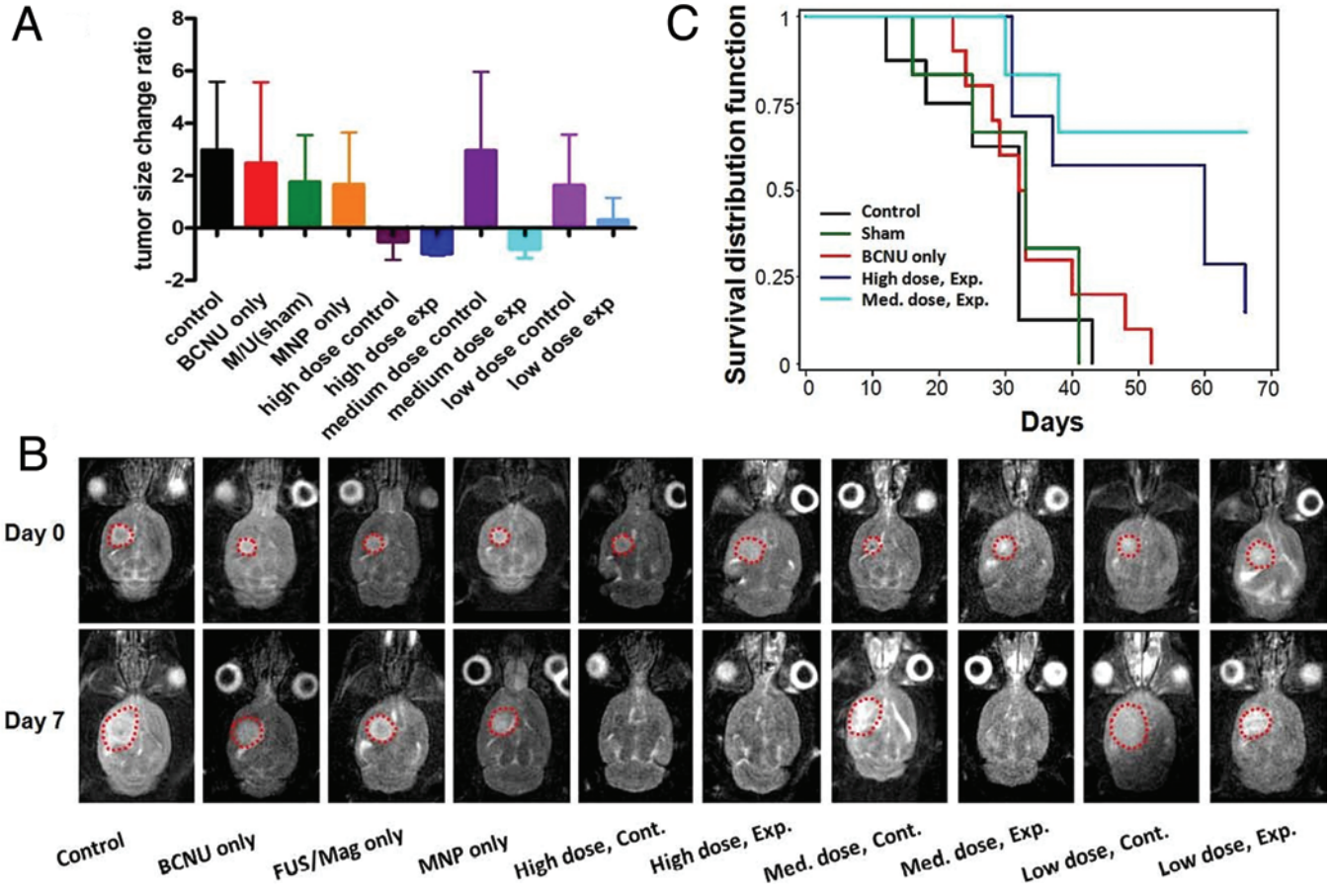

Fig. 6. **A:** Ratios of average tumor volume changes in the 1st week after therapeutic MNP treatment under different conditions. BCNU only = 13.5 mg/kg BCNU; high dose = 5 mg/kg therapeutic MNP; medium dose = 1 mg/kg therapeutic MNP; low dose = 0.5 mg/kg therapeutic MNP. **B:** Representative T2-weighted MR imaging images of the longitudinal glioma follow-up. **C:** Kaplan-Meier survival curves. Survival improvement at high and medium doses is statistically significant. Redrawn and reprinted by permission of Oxford University Press on behalf of the Society for Neuro-Oncology, from Chen et al.: **Neuro Oncol 12:**1050–1060, 2010.

Conclusions and Perspective

When FUS is used to locally enhance BBB disruption and delivery of therapeutic MNPs, it can be integrated with a novel magnetic targeting approach so that drug delivery proceeds not only through passive but also through active diffusion. The magnet is placed externally to provide magnetic targeting after the FUS exposure and does not contribute any additional risk to the procedure, while significantly enhancing the active attraction of the therapeutic MNP by at least an order in concentration. This innovation raises the possibility of improving therapeutic efficacy of chemotherapeutic agents or reducing the total dose to reduce the circulation toxicity in the body. In addition, the intrinsic nature of MNPs render them sensitive to detection by MR imaging so that the distribution of therapeutic MNPs can be monitored or even quantified during image-guided drug delivery for brain tumor treatment.

In conclusion, preclinical research has shown that FUS is a noninvasive method to enhance the targeted delivery of chemotherapeutic agents through the BBB and into brain tumors. This method allows the chemotherapeutic drug dosage to be increased specifically in the tumor regions, thus significantly suppressing tumor growth and prolonging animal survival. BCNU is already a US FDA-approved chemotherapeutic drug for glioma treatment, and doxorubicin has been approved for ovarian cancers. The successful use of these 2 drugs in FUS MNP preclinical experiments suggests that the procedure could be highly clinically relevant. In addition, chemotherapeutic drugs are delivered intravenously rather than intraarterially or by direct cranial injection/implantation, which makes the treatment more practical in a clinical setting. The procedure is noninvasive, reversible, and can be targeted with greater precision to a specific region of interest in the deep brain under the guidance of MR imaging.

Disclosure

This work was supported by the National Science Council (grant nos. NSC-99-2321-B-182-008, NSC-100-2321-B-182-010, and NSC-100-2120-M-182A-001), the National Health Research Institutes (grant no. NHRI-EX100-10004NI), and the Department of Health, Executive Yuan, Taiwan.

Author contributions to the study and manuscript preparation include the following. Conception and design: Wei, Liu. Acquisition of data: Liu. Analysis and interpretation of data: Liu, Yang, Hua. Drafting the article: Liu, Yang, Hua. Critically revising the article: Liu, Yang. Reviewed submitted version of manuscript: Wei, Liu, Hua. Approved the final version of the manuscript on behalf of all authors: Wei. Administrative/technical/material support: Yang, Hua. Study supervision: Wei, Liu.

Acknowledgment

The authors thank the Molecular Imaging Center, Chang-Gung Memorial Hospital, Taoyuan, Taiwan, for supporting the MR imaging of the animals in this study.

References

1. Alam MI, Beg S, Samad A, Baboota S, Kohli K, Ali J, et al: Strategy for effective brain drug delivery. **Eur J Pharm Sci 40:**385–403, 2010
2. Allémann E, Leroux JC, Gurny R, Doelker E: In vitro extended-release properties of drug-loaded poly(DL-lactic acid) nanoparticles produced by a salting-out procedure. **Pharm Res 10:**1732–1737, 1993
3. Banerjee T, Mitra S, Kumar Singh A, Kumar Sharma R, Maitra A: Preparation, characterization and biodistribution of ultrafine chitosan nanoparticles. **Int J Pharm 243:**93–105, 2002
4. Behin A, Hoang-Xuan K, Carpentier AF, Delattre JY: Primary brain tumours in adults. **Lancet 361:**323–331, 2003
5. Bobo RH, Laske DW, Akbasak A, Morrison PF, Dedrick RL, Oldfield EH: Convection-enhanced delivery of macromolecules in the brain. **Proc Natl Acad Sci U S A 91:**2076–2080, 1994
6. Brigger I, Morizet J, Aubert G, Chacun H, Terrier-Lacombe MJ, Couvreur P, et al: Poly(ethylene glycol)-coated hexadecylcyanoacrylate nanospheres display a combined effect for brain tumor targeting. **J Pharmacol Exp Ther 303:**928–936, 2002
7. Burger PC: The anatomy of astrocytomas. **Mayo Clin Proc 62:**527–529, 1987
8. Chen PY, Liu HL, Hua MY, Yang HW, Huang CY, Chu PC, et al: Novel magnetic/ultrasound focusing system enhances nanoparticle drug delivery for glioma treatment. **Neuro Oncol 12:**1050–1060, 2010
9. Chertok B, David AE, Huang Y, Yang VC: Glioma selectivity of magnetically targeted nanoparticles: a role of abnormal tumor hydrodynamics. **J Control Release 122:**315–323, 2007
10. Chertok B, David AE, Yang VC: Polyethyleneimine-modified iron oxide nanoparticles for brain tumor drug delivery using magnetic targeting and intra-carotid administration. **Biomaterials 31:**6317–6324, 2010
11. Chertok B, Moffat BA, David AE, Yu F, Bergemann C, Ross BD, et al: Iron oxide nanoparticles as a drug delivery vehicle for MRI monitored magnetic targeting of brain tumors. **Biomaterials 29:**487–496, 2008
12. Cordon-Cardo C, O'Brien JP, Boccia J, Casals D, Bertino JR, Melamed MR: Expression of the multidrug resistance gene product (P-glycoprotein) in human normal and tumor tissues. **J Histochem Cytochem 38:**1277–1287, 1990
13. Deutsch M, Green SB, Strike TA, Burger PC, Robertson JT, Selker RG, et al: Results of a randomized trial comparing BCNU plus radiotherapy, streptozotocin plus radiotherapy, BCNU plus hyperfractionated radiotherapy, and BCNU following misonidazole plus radiotherapy in the postoperative treatment of malignant glioma. **Int J Radiat Oncol Biol Phys 16:** 1389–1396, 1989
14. Doolittle ND, Miner ME, Hall WA, Siegal T, Jerome E, Osztie E, et al: Safety and efficacy of a multicenter study using intraarterial chemotherapy in conjunction with osmotic opening of the blood-brain barrier for the treatment of patients with malignant brain tumors. **Cancer 88:**637–647, 2000
15. Ewing JR, Brown SL, Lu M, Panda S, Ding G, Knight RA, et al: Model selection in magnetic resonance imaging measurements of vascular permeability: Gadomer in a 9L model of rat cerebral tumor. **J Cereb Blood Flow Metab 26:**310–320, 2006
16. Fine HA, Dear KB, Loeffler JS, Black PM, Canellos GP: Meta-analysis of radiation therapy with and without adjuvant chemotherapy for malignant gliomas in adults. **Cancer 71:** 2585–2597, 1993
17. Foye WO (ed): **Cancer Chemotherapeutic Agents.** Washington: American Chemical Society, 1995
18. Gallego JM, Barcia JA, Barcia-Mariño C: Fatal outcome related to carmustine implants in glioblastoma multiforme. **Acta Neurochir (Wien) 149:**261–265, 2007
19. Gao X, Huang L: Cationic liposome-mediated gene transfer. **Gene Ther 2:**710–722, 1995
20. Groothuis DR, Fischer JM, Lapin G, Bigner DD, Vick NA: Permeability of different experimental brain tumor models to horseradish peroxidase. **J Neuropathol Exp Neurol 41:**164–185, 1982

21. Grossman SA, Batara JF: Current management of glioblastoma multiforme. **Semin Oncol 31:**635–644, 2004
22. Grossman SA, Norris LK: Adjuvant and neoadjuvant treatment for primary brain tumors in adults. **Semin Oncol 22:** 530–539, 1995
23. Grossman SA, O'Neill A, Grunnet M, Mehta M, Pearlman JL, Wagner H, et al: Phase III study comparing three cycles of infusional carmustine and cisplatin followed by radiation therapy with radiation therapy and concurrent carmustine in patients with newly diagnosed supratentorial glioblastoma multiforme: Eastern Cooperative Oncology Group Trial 2394. **J Clin Oncol 21:**1485–1491, 2003
24. Gumerlock MK, Belshe BD, Madsen R, Watts C: Osmotic blood-brain barrier disruption and chemotherapy in the treatment of high grade malignant glioma: patient series and literature review. **J Neurooncol 12:**33–46, 1992
25. Gupta AK, Gupta M: Synthesis and surface engineering of iron oxide nanoparticles for biomedical applications. **Biomaterials 26:**3995–4021, 2005
26. Gupta S, Tsuruo T: **Multidrug Resistance in Cancer Cells: Molecular, Biochemical, Physiological, and Biological Aspects.** Chichester, UK: J. Wiley, 1996
27. Halperin EC, Burger PC, Bullard DE: The fallacy of the localized supratentorial malignant glioma. **Int J Radiat Oncol Biol Phys 15:**505–509, 1988
28. Hua MY, Liu HL, Yang HW, Chen PY, Tsai RY, Huang CY, et al: The effectiveness of a magnetic nanoparticle-based delivery system for BCNU in the treatment of gliomas. **Biomaterials 32:**516–527, 2011
29. Hynynen K, McDannold N, Sheikov NA, Jolesz FA, Vykhodtseva N: Local and reversible blood-brain barrier disruption by noninvasive focused ultrasound at frequencies suitable for trans-skull sonications. **Neuroimage 24:**12–20, 2005
30. Hynynen K, McDannold N, Vykhodtseva N, Jolesz FA: Noninvasive MR imaging-guided focal opening of the blood-brain barrier in rabbits. **Radiology 220:**640–646, 2001
31. Hynynen K, McDannold N, Vykhodtseva N, Jolesz FA: Noninvasive opening of BBB by focused ultrasound. **Acta Neurochir Suppl 86:**555–558, 2003
32. Jemal A, Siegel R, Ward E, Murray T, Xu J, Smigal C, et al: Cancer statistics, 2006. **CA Cancer J Clin 56:**106–130, 2006
33. Judy KD, Olivi A, Buahin KG, Domb A, Epstein JI, Colvin OM, et al: Effectiveness of controlled release of a cyclophosphamide derivative with polymers against rat gliomas. **J Neurosurg 82:**481–486, 1995
34. Kim HS, Oh SY, Joo HJ, Son KR, Song IC, Moon WK: The effects of clinically used MRI contrast agents on the biological properties of human mesenchymal stem cells. **NMR Biomed 23:**514–522, 2010
35. Lemarchand C, Gref R, Passirani C, Garcion E, Petri B, Müller R, et al: Influence of polysaccharide coating on the interactions of nanoparticles with biological systems. **Biomaterials 27:**108–118, 2006
36. Liu HL, Hsu PH, Chu PC, Wai YY, Chen JC, Shen CR, et al: Magnetic resonance imaging enhanced by superparamagnetic iron oxide particles: usefulness for distinguishing between focused ultrasound-induced blood-brain barrier disruption and brain hemorrhage. **J Magn Reson Imaging 29:**31–38, 2009
37. Liu HL, Hua MY, Chen PY, Chu PC, Pan CH, Yang HW, et al: Blood-brain barrier disruption with focused ultrasound enhances delivery of chemotherapeutic drugs for glioblastoma treatment. **Radiology 255:**415–425, 2010
38. Liu HL, Hua MY, Yang HW, Huang CY, Chu PC, Wu JS, et al: Magnetic resonance monitoring of focused ultrasound/magnetic nanoparticle targeting delivery of therapeutic agents to the brain. **Proc Natl Acad Sci U S A 107:**15205–15210, 2010
39. Lu W, Tan YZ, Hu KL, Jiang XG: Cationic albumin conjugated pegylated nanoparticle with its transcytosis ability and little toxicity against blood-brain barrier. **Int J Pharm 295:**247–260, 2005
40. MacKay JA, Deen DF, Szoka FC Jr: Distribution in brain of liposomes after convection enhanced delivery; modulation by particle charge, particle diameter, and presence of steric coating. **Brain Res 1035:**139–153, 2005
41. Natsume A, Mizuno M, Ryuke Y, Yoshida J: Antitumor effect and cellular immunity activation by murine interferon-beta gene transfer against intracerebral glioma in mouse. **Gene Ther 6:**1626–1633, 1999
42. Neuwelt EA, Barnett PA, Bigner DD, Frenkel EP: Effects of adrenal cortical steroids and osmotic blood-brain barrier opening on methotrexate delivery to gliomas in the rodent: the factor of the blood-brain barrier. **Proc Natl Acad Sci U S A 79:**4420–4423, 1982
43. Neuwelt EA, Frenkel EP, D'Agostino AN, Carney DN, Minna JD, Barnett PA, et al: Growth of human lung tumor in the brain of the nude rat as a model to evaluate antitumor agent delivery across the blood-brain barrier. **Cancer Res 45:**2827–2833, 1985
44. Neuwelt EA, Frenkel EP, Gumerlock MK, Braziel R, Dana B, Hill SA: Developments in the diagnosis and treatment of primary CNS lymphoma. A prospective series. **Cancer 58:** 1609–1620, 1986
45. Pardridge WM: Drug and gene delivery to the brain: the vascular route. **Neuron 36:**555–558, 2002
46. Perlstein B, Ram Z, Daniels D, Ocherashvilli A, Roth Y, Margel S, et al: Convection-enhanced delivery of maghemite nanoparticles: increased efficacy and MRI monitoring. **Neuro Oncol 10:**153–161, 2008
47. Rapoport SI: **Blood-Brain Barrier in Physiology and Medicine.** New York: Raven Press, 1976
48. Sawada T, Kato Y, Sakayori N, Takekawa Y, Kobayashi M: Expression of the multidrug-resistance P-glycoprotein (Pgp, MDR-1) by endothelial cells of the neovasculature in central nervous system tumors. **Brain Tumor Pathol 16:**23–27, 1999
49. Schinkel AH, Mayer U, Wagenaar E, Mol CA, van Deemter L, Smit JJ, et al: Normal viability and altered pharmacokinetics in mice lacking mdr1-type (drug-transporting) P-glycoproteins. **Proc Natl Acad Sci U S A 94:**4028–4033, 1997
50. Schinkel AH, Wagenaar E, Mol CA, van Deemter L: P-glycoprotein in the blood-brain barrier of mice influences the brain penetration and pharmacological activity of many drugs. **J Clin Invest 97:**2517–2524, 1996
51. Shapiro WR, Green SB, Burger PC, Selker RG, VanGilder JC, Robertson JT, et al: A randomized comparison of intra-arterial versus intravenous BCNU, with or without intravenous 5-fluorouracil, for newly diagnosed patients with malignant glioma. **J Neurosurg 76:**772–781, 1992
52. Sonavane G, Tomoda K, Makino K: Biodistribution of colloidal gold nanoparticles after intravenous administration: effect of particle size. **Colloids Surf B Biointerfaces 66:**274–280, 2008
53. Staddon JM, Rubin LL: Cell adhesion, cell junctions and the blood-brain barrier. **Curr Opin Neurobiol 6:**622–627, 1996
54. Stupp R, Mason WP, van den Bent MJ, Weller M, Fisher B, Taphoorn MJ, et al: Radiotherapy plus concomitant and adjuvant temozolomide for glioblastoma. **N Engl J Med 352:**987–996, 2005
55. Thorne RG, Nicholson C: In vivo diffusion analysis with quantum dots and dextrans predicts the width of brain extracellular space. **Proc Natl Acad Sci U S A 103:**5567–5572, 2006
56. Tosi G, Costantino L, Rivasi F, Ruozi B, Leo E, Vergoni AV, et al: Targeting the central nervous system: in vivo experiments with peptide-derivatized nanoparticles loaded with Loperamide and Rhodamine-123. **J Control Release 122:**1–9, 2007
57. Tóth K, Vaughan MM, Peress NS, Slocum HK, Rustum YM: MDR1 P-glycoprotein is expressed by endothelial cells of newly formed capillaries in human gliomas but is not expressed in the neovasculature of other primary tumors. **Am J Pathol 149:**853–858, 1996

58. Treat LH, McDannold N, Vykhodtseva N, Zhang Y, Tam K, Hynynen K: Targeted delivery of doxorubicin to the rat brain at therapeutic levels using MRI-guided focused ultrasound. **Int J Cancer 121:**901–907, 2007
59. Treat LH, Zhang Y, McDannold N, Hynynen K: Impact of focused ultrasound-enhanced drug delivery on survival in rats with glioma. **AIP Conf Proc 1113:** 443–447, 2009
60. Walker MD, Green SB, Byar DP, Alexander E Jr, Batzdorf U, Brooks WH, et al: Randomized comparisons of radiotherapy and nitrosoureas for the treatment of malignant glioma after surgery. **N Engl J Med 303:**1323–1329, 1980
61. Wang JX, Sun X, Zhang ZR: Enhanced brain targeting by synthesis of 3′,5′-dioctanoyl-5-fluoro-2′-deoxyuridine and incorporation into solid lipid nanoparticles. **Eur J Pharm Biopharm 54:**285–290, 2002
62. Weissleder R, Elizondo G, Wittenberg J, Lee AS, Josephson L, Brady TJ: Ultrasmall superparamagnetic iron oxide: an intravenous contrast agent for assessing lymph nodes with MR imaging. **Radiology 175:**494–498, 1990
63. Weissleder R, Elizondo G, Wittenberg J, Rabito CA, Bengele HH, Josephson L: Ultrasmall superparamagnetic iron oxide: characterization of a new class of contrast agents for MR imaging. **Radiology 175:**489–493, 1990
64. Westphal M, Hilt DC, Bortey E, Delavault P, Olivares R, Warnke PC, et al: A phase 3 trial of local chemotherapy with biodegradable carmustine (BCNU) wafers (Gliadel wafers) in patients with primary malignant glioma. **Neuro Oncol 5:** 79–88, 2003
65. Wolburg H, Lippoldt A: Tight junctions of the blood-brain barrier: development, composition and regulation. **Vascul Pharmacol 38:**323–337, 2002
66. Yang HW, Hua MY, Liu HL, Huang CY, Tsai RY, Lu YJ, et al: Self-protecting core-shell magnetic nanoparticles for targeted, traceable, long half-life delivery of BCNU to gliomas. **Biomaterials 32:**6523–6532, 2011

Manuscript submitted September 1, 2011.
Accepted October 27, 2011.
Please include this information when citing this paper: DOI: 10.3171/2011.10.FOCUS11238.

Address correspondence to: Kuo-Chen Wei, M.D., Department of Neurosurgery, Chang-Gung University College of Medicine and Memorial Hospital, 5 Fu-Shing Street, Kwei-Shan, Taoyuan 333, Taiwan, R.O.C. email: kuochenwei@cgmh.org.tw.

Neurosurg Focus 32 (1):E5, 2012

Sonothrombolysis for acute ischemic stroke: a systematic review of randomized controlled trials

Edson Bor-Seng-Shu, M.D., Ph.D.,[1] Ricardo De Carvalho Nogueira, M.D.,[2] Eberval G. Figueiredo, M.D., Ph.D.,[1] Eli Faria Evaristo, M.D., Ph.D.,[2] Adriana Bastos Conforto, M.D., Ph.D.,[2,3] and Manoel Jacobsen Teixeira, M.D., Ph.D.[1]

Divisions of [1]Neurological Surgery and [2]Neurology, Hospital das Clinicas, University of Sao Paulo School of Medicine; and [3]Instituto Israelita de Ensino e Pesquisa Albert Einstein, Sao Paulo, Brazil

Object. Sonothrombolysis has recently been considered an emerging modality for the treatment of stroke. The purpose of the present paper was to review randomized clinical studies concerning the effects of sonothrombolysis associated with tissue plasminogen activator (tPA) on acute ischemic stroke.

Methods. Systematic searches for literature published between January 1996 and July 2011 were performed for studies regarding sonothrombolysis combined with tPA for acute ischemic stroke. Only randomized controlled trials were included. Data extraction was based on ultrasound variables, patient characteristics, and outcome variables (rate of intracranial hemorrhages and arterial recanalization).

Results. Four trials were included in this study; 2 trials evaluated the effect of transcranial Doppler (TCD) ultrasonography on sonothrombolysis, and 2 addressed transcranial color-coded duplex (TCCD) ultrasonography. The frequency of ultrasound waves varied from 1.8 to 2 MHz. The duration of thrombus exposure to ultrasound energy ranged from 60 to 120 minutes. Sample sizes were small, recanalization was evaluated at different time points (60 and 120 minutes), and inclusion criteria were heterogeneous. Sonothrombolysis combined with tPA did not lead to an increase in symptomatic intracranial hemorrhagic complications. Two studies demonstrated that patients treated with ultrasound combined with tPA had statistically significant higher rates of recanalization than patients treated with tPA alone.

Conclusions. Despite the heterogeneity and the limitations of the reviewed studies, there is evidence that sonothrombolysis associated with tPA is a safe procedure and results in an increased rate of recanalization in the setting of acute ischemic stroke when wave frequencies and energy intensities of diagnostic ultrasound systems are used.
(http://thejns.org/doi/abs/10.3171/2011.10.FOCUS11251)

Key Words • **sonothrombolysis** • **stroke** • **tissue plasminogen activator** • **transcranial color-coded duplex** • **transcranial Doppler ultrasonography** • **ultrasound-enhanced thrombolysis**

Systemic administration of tPA has been established as an effective therapy for improving neurological outcome after acute ischemic stroke.[25] Considering the "recanalization hypothesis," which states that the reopening of occluded vessels can save threatened ischemic tissues, faster restoration of cerebral tissue blood flow is associated with better neurological recovery.[25] Therefore, therapeutic strategies to increase the rate and speed of arterial recanalization, without increasing the risk of hemorrhagic complications, are the mainstay of patient treatment and future investigations.

Ultrasound energy has been demonstrated to facilitate activity of fibrinolytic agents, a process known as ultrasound-enhanced thrombolysis, contributing to augmentation of fibrinolysis and arterial recanalization.[1,2,16,21] Recently, microbubble sonothrombolysis without tPA has been shown to effectively decrease infarct volumes and occurrence of intracranial hemorrhages in an experimental model of stroke.[11,12]

The objective of the present study is to review randomized clinical studies regarding ultrasound-enhanced thrombolysis in patients with acute ischemic stroke.

Abbreviations used in this paper: NIHSS = National Institutes of Health Stroke Scale; TCCD = transcranial color-coded duplex; TCD = transcranial Doppler; tPA = tissue plasminogen activator; TRUMBI = Transcranial Low-Frequency Ultrasound-Mediated Thrombolysis in Brain Ischemia.

Methods

The PubMed database was searched to identify papers published between January 1996 and July 2011 that addressed studies regarding ultrasound-enhanced thrombolysis for acute ischemic stroke in humans. The following search terms were used: "ultrasound-enhanced thrombolysis," "sonothrombolysis," "ultrasound and thrombolysis," "ultrasound and tissue plasminogen activator," "transcranial Doppler and thrombolytic therapy," "transcranial color-coded duplex and thrombolytic therapy," and "transcranial low-frequency ultrasound and thrombolytic therapy." The reference lists of retrieved articles were also searched. The inclusion criterion was randomized studies on thrombolytic therapy using tPA and ultrasound. Exclusion criteria were as follow: 1) case reports and small case series; 2) nonrandomized studies; 3) investigations using intraarterial tPA, those using intraarterial infusion of microspheres using transforaminal insonation for vertebrobasilar circulation, or those using other thrombolytic agents; 4) abstracts of studies presented at international meetings; 5) randomized studies that included patients who had been previously reported on in other articles from the same institution; and 6) studies comprising experimental animal models.

Data extraction was performed based on ultrasound variables (ultrasound technology, frequency of the ultrasound waves, emitted-power output, ultrasound wave mode, and duration of thrombus exposure to ultrasound energy), patient characteristics (sample size, age, neurological status, affected arterial territory, interval from symptom onset to treatment), and outcome variables (rate of asymptomatic and symptomatic intracranial hemorrhagic complications, and of partial and complete arterial recanalization).

Two reviewers (E.B.S.S. and R.C.N.) independently selected the studies and extracted the data; disagreement between the 2 reviewers was resolved by a third independent reviewer (E.G.F).

Results

There have been 6 randomized controlled trials of sonothrombolysis associated with tPA for acute ischemic stroke.[3,4,15,16,20,23] Two studies were excluded (one consisted of a pilot study with 3 patients in the control arm,[3] and the other was published as an abstract[20]). We did not find any randomized study addressing the effects of low-frequency transcranial ultrasound on thrombolysis. Although opinions can diverge (a recent meta-analysis has considered the TRUMBI study as a randomized controlled trial),[29] we have considered the design of the TRUMBI study as nonrandomized because patients were alternately allocated to standard therapy (tPA alone) and combined therapy (low-frequency ultrasound plus tPA).[13]

Ultrasound Variables Adopted in the Selected Trials

Two studies evaluated the effects of TCD ultrasonography on thrombolysis,[4,22] and the remaining two evaluated the TCCD technology.[15,16] The TCD ultrasonography studies used 2-MHz pulsed ultrasound waves, while TCCD ultrasonography studies used 2-MHz[15] and 1.8-Mhz pulsed waves[16] (1 study each). The duration of thrombus exposure to ultrasound energy varied from 60 to 120 minutes. Ultrasound variable data of the studies are shown in Table 1.

Characteristics of the Included Trials

The TCCD ultrasonography studies were composed of a target group (TCCD ultrasound energy plus tPA) and a control group (only tPA).[15,16] One TCD ultrasonography study consisted of a target group receiving TCD ultrasound energy plus tPA, and a control group receiving only tPA;[2] another TCD ultrasonography study had a target group receiving TCD ultrasound energy plus tPA plus microspheres, and a control group receiving only tPA.[22] Sample sizes, mean ages, median NIHSS scores, affected arterial territories, and the interval between symptom onset and treatment are detailed in Table 2.

Outcome Measures

Symptomatic intracranial hemorrhages were defined as intracranial hemorrhage appearing on CT scans within 72 hours[4,15,16] or within 36 hours[22] from symptom onset associated with neurological deterioration (an increase in NIHSS score of ≥ 4 points). Arterial recanalization was graded by the TIBI (Thrombolysis in Brain Ischemia) flow criteria (Score 2 or 3, partial recanalization; Score 4 or 5, complete recanalization).[4,15,16,22] Safety and efficacy outcomes are summarized in Table 3.

Among the identified studies, the incidence of asymptomatic intracranial hemorrhage ranged from 9% to 21% in the sonothrombolysis group and from 0% to 11% in the control group. In contrast, symptomatic intracranial hemorrhages occurred in 0%–27% of the cases in the sonothrombolysis group, and in 0%–5% of the patients in the control group. All intracranial hemorrhages were associated with thrombolytic therapy. There were no differences in intracranial hemorrhage rates (asymptomatic and symptomatic hemorrhages) between the sonothrombolysis and control groups of the studies, except for 1 study reporting microsphere dose escalation in which a statistically significant increased rate of symptomatic intracranial hemorrhage was noticed in patients who underwent TCD ultrasonography combined with both tPA and 2.8 ml microspheres; in this subgroup 3 patients died (2 deaths were attributed to symptomatic intracranial hemorrhage).[22] Concerning a TCCD ultrasonography study,[16] 3 patients (15.8%) from the sonothrombolysis group and 2 patients (11.8%) from the control group died of space-occupying infarction and symptomatic intracranial hemorrhage. Craniotomy was performed in 1 patient in the sonothrombolysis group due to space-occupying infarction and symptomatic intracranial hemorrhage.

Complete arterial recanalization rates varied from 15% to 67% in the sonothrombolysis group and from 11% to 33% in the control group. Two studies, one using TCD ultrasonography and the other using TCCD ultrasonography,[4,16] demonstrated that patients treated with ultrasound energy in association with tPA had statistically significantly higher rates of both complete recanalization and neurological improvement than those treated with tPA only. In a TCD ultrasonography study,[4] complete recana-

TABLE 1: Ultrasound variables in randomized studies of sonothrombolysis*

Authors & Year	Ultrasound Technology	Frequency (MHz)	Emitted-Power Output (mW/cm^2)	Mode	Duration of Insonation (mins)
Eggers et al., 2003	TCCD	2–4	179	pulsed	60
Alexandrov et al., 2004	TCD	2	<750	pulsed	120
Eggers et al., 2008	TCCD	1.8	179	pulsed	60
Molina et al., 2009	TCD	2	NR	pulsed	90

* NR = not reported.

lization or significant clinical recovery within 2 hours after intravenous tPA bolus occurred in 49% of patients from the sonothrombolysis group, compared with 30% of patients from the control group ($p = 0.03$). In a TCCD ultrasonography study,[16] complete or partial recanalization after 1 hour was found in 57.9% of the sonothrombolysis group and 22.2% of the control group ($p = 0.045$); after 3 months, Barthel Index greater than 95 occurred in 8 patients of the sonothrombolysis group (none from the control group) ($p = 0.003$).

Discussion

Only 4 studies met inclusion criteria of this systematic review.[4,15,16,22] Two studies evaluated the role of TCD ultrasonography on sonothrombolysis[4,22] and 2 evaluated the role of TCCD technology.[15,16] The frequency of ultrasound waves varied from 1.8 to 2 MHz. The duration of thrombus exposure to ultrasound energy ranged from 60 to 120 minutes. Sample sizes were small. Recanalization was evaluated at different time points (60 and 120 minutes). Inclusion criteria were heterogeneous; 2 TCCD studies included only patients with proximal middle cerebral artery occlusion without residual flow, a condition in which recanalization is more difficult;[15,16] 1 TCD study had a target group receiving ultrasound energy, intravenous tPA, and microspheres.[22] Therefore, comparisons among the studies are challenging, and conclusions are difficult to draw. Despite the heterogeneity of the included studies, ultrasound-enhanced thrombolysis seems to be a safe procedure and is associated with a significantly higher rate of arterial recanalization in the acute ischemic stroke setting. It is worth noting that this conclusion was reached considering results of 2 randomized controlled trials (one assessing TCD and the other TCCD).[4,16]

Issues related to instrumentation in ultrasonography are of fundamental importance to interpret the studies regarding sonothrombolysis in acute ischemic stroke. The following 3 different ultrasound modalities were used to increase the thrombolytic activity of tPA: TCD ultrasonography, TCCD ultrasonography, and therapeutic transcranial low-frequency ultrasonography.[27,28] These devices generate ultrasound beams that differ greatly in acoustic properties, such as frequency, mechanical index, and the amount of brain tissue included in the beam (that is, areas of the brain exposed to ultrasound energy). Transcranial Doppler ultrasonography equipped with a 2-MHz transducer has been widely used for evaluating patients with acute ischemic stroke,[27,28] traumatic brain injury,[9,10] and aneurysmal subarachnoid hemorrhage.[7] This nonimaging and hand-held ultrasound examination device provides real-time blood flow velocity from cerebral arteries that can indicate arterial occlusion or recanalization, embolization, functional status of collateral circulatory pathways, and blood steal phenomenon.[27,28] For diagnostic purposes, the emitted-power output is usually set at the maximal achievable level below the allowed limit of 720 mW with selected insonation deaths, and the sample volumes, or gates of insonation, are set at 3–6 mm for power motion Doppler devices and 10–15 mm for other single channel devices.[27,28]

While using TCD ultrasonography to monitor tPA thrombolysis, Alexandrov et al.[2] incidentally suspected the ability of TCD ultrasonography to facilitate arterial recanalization in patients with acute ischemic stroke treated with intravenous tPA, a phenomenon confirmed afterward by the CLOTBUST (Combined Lysis of Thrombus in Brain ischemia using transcranial Ultrasound and Systemic tPA) trial. When signs of arterial occlusion are detected, the TCD ultrasound beam can be continu-

TABLE 2: Characteristics of the patients in randomized clinical trials of sonothrombolysis*

Authors & Year	Target Group†	No. of Cases (target vs control)	Mean Age (yrs)‡	Median NIHSS Score (range)	Occluded Artery	Symptom Onset to Treatment (hrs)
Eggers et al., 2003	TCCD + tPA	11 vs 14	61 ± 9	18 (9–25)	MCA (M_1)	≤3
Alexandrov et al., 2004	TCD + tPA	63 vs 63	69 ± 13	16 (4–34)	MCA	≤3
Eggers et al., 2008	TCCD + tPA	19 vs 18	61 ± 10	17.5 (12–23)	MCA (M_1)	≤3
Molina et al., 2009	TCD + tPA + μS	12 (1.4 ml μS), 11 (2.8 ml μS) vs 12	65 ± 14	12 (4–21)	MCA, PCA	≤3

* μS = microspheres; MCA = middle cerebral artery; PCA = posterior cerebral artery.
† In all studies, the control group received only tPA.
‡ Values are presented as means ± SDs.

TABLE 3: Safety and efficacy in randomized studies on sonothrombolysis*

Authors & Year	Ultrasound Technology	Frequency (MHz)	Target vs Control					
			Group	No. of Cases	aICH	sICH	Complete Recanalization	Partial Recanalization	Recanalization (complete & partial)
Eggers et al., 2003	TCCD	2–4	TCCD + tPA vs tPA	11 vs 14	18 vs 7%	18 vs 0%	27 vs 21% w/in 1 hr	18 vs 0% w/in 1 hr	45 vs 21% w/in 1 hr
Alexandrov et al., 2004	TCD	2	TCD + tPA vs tPA	63 vs 63	NR	5 vs 5%	46 vs 18% w/in 2 hrs†	NR	NR
Eggers et al., 2008	TCCD	1.8	TCCD + tPA vs tPA	19 vs 18	21 vs 11%	15 vs 5%	15 vs 11% w/in 1 hr	42 vs 11% w/in 1 hr	58 vs 22% w/in 1 hr‡
Molina et al., 2009	TCD	2	TCD + tPA + 1.4 ml μS vs tPA	12 vs 12	17 vs 0%	0 vs 0%	67 vs 33% w/in 2 hrs	17 vs 25% w/in 2 hrs	83 vs 58% w/in 2 hrs
			TCD + tPA + 2.8 ml μS vs tPA	11 vs 12	9 vs 0%	27 vs 0%‡	45 vs 33% w/in 2 hrs	0 vs 25% w/in 2 hrs	45 vs 58% w/in 2 hrs

* aICH = asymptomatic intracranial hemorrhage; sICH = symptomatic ICH.
† $p < 0.001$.
‡ $p < 0.005$.

ously focused at the presumed thrombus location, allowing both sonothrombolysis and continuous monitoring of the recanalization process. Unfortunately, this method is highly dependent on the skill of the TCD ultrasonography operator. It is unrealistic to expect that an unskilled TCD ultrasonography clinician can develop skills for a rapid and accurate location of cerebral arterial occlusions.[4,27,28]

Transcranial color-coded duplex is another ultrasound method that, like TCD ultrasonography, provides real-time blood flow dynamics of cerebral arteries. However, unlike TCD technology, TCCD transducers generate multiple small ultrasound beams at dual emitting frequencies, one for gray scale imaging and another for Doppler imaging; hence, besides assessment of cerebral hemodynamics, this technology can also afford both arterial location on color flow imaging and imaging of the brain on B-mode ultrasonography.[5,8,27,28] The TCCD ultrasound beam includes a larger brain area (a greater amount of brain tissue is exposed to ultrasound energy) compared with the more focal TCD ultrasound beam. Among the limitations of TCCD ultrasonography, there are no head frames for transducer fixation (recanalization monitoring is carried out using handheld probes), the mechanical index (an indicator of the likelihood of mechanical biological effects, that is, streaming and cavitation) of the TCCD ultrasonography is higher than that for TCD ultrasonography, and no dose escalation study has been performed to determine the levels of ultrasound intensity needed to enhance thrombolysis without risks.[27,28]

Therapeutic transcranial low-frequency ultrasonography is a nonimaging and nondiagnostic ultrasound technology equipped with a transducer composed of 4 elements arranged in a diamond pattern. This technology uses unfocused, low-frequency ultrasound (300 ± 1.5 kHz to avoid standing waves), a temporal average spatial peak intensity of 700 mW/cm^2, an average temporal pressure less than 1 atmosphere (< 101 kPa for avoiding cavitation), a mechanical index less than 0.2, a thermal index in soft tissue less than 0.5, and a cranial thermal index of approximately 4. The higher cranial thermal index was addressed through the use of a cooling pad and a thermal sensor to detect excessive heating. To decrease the thermal effects, ultrasound is emitted in a pulsed fashion with a 5% duty cycle and a pulse repetition frequency of 100 Hz (cycle/pulse ratio of 225). Despite leading to a higher rate of recanalization, this method sonicates the vessels and brain nonspecifically. The TRUMBI trial was stopped because intracranial hemorrhages were frequently found, even in areas unaffected by ischemia.[13,27,28] The development of high-intensity, focused ultrasound with MR imaging guidance may minimize hemorrhagic complications in the future.

A recent comprehensive review and meta-analysis has assessed the safety and efficacy of ultrasound-enhanced tPA thrombolysis in the treatment of patients with acute ischemic stroke.[29] Taking into account 6 randomized (comprising 224 patients) and 3 nonrandomized (comprising 192 patients) studies, the authors concluded that sonothrombolysis using TCD or TCCD ultrasonography appears to be safe and leads to higher rates of complete recanalization when compared with intravenous tPA thrombolysis.

Sonothrombolysis using TCD or TCCD ultrasonography, with or without microspheres, is associated with a nearly 3-fold increased likelihood of complete recanalization and an approximately 2-fold higher likelihood of functional independence at 3 months. We stressed that this meta-analysis included randomized and nonrandomized studies, as well as abstracts of studies presented at international meetings, and focused on quantitative analysis of them, without taking into consideration ultrasound variables such as type of ultrasound technology, frequency of ultrasound waves, emitted power output, ultrasound wave mode, and duration of thrombus exposure to ultrasound energy, while our manuscript focused on qualitative analysis of Class I evidence studies, classifying them in terms of ultrasound variables, presence of microspheres, sample characteristics, and outcome measures. Although both reviews have provided similar findings (that is, ultrasound-enhanced thrombolysis seems to be a safe procedure and is associated with a significantly higher rate of arterial recanalization in acute ischemic stroke), our study revealed that only 2 randomized controlled studies, one using TCD and the other using TCCD, support these conclusions.

Ultrasound energy has been experimentally demonstrated to improve the thrombolytic effects of tPA.[6] The mechanisms of action are still under debate; however, there is evidence of at least 4 contributing effects as follows: 1) rectified diffusion, which provides a pumping effect to transport drugs into the thrombus; 2) reformation and opening of the fibrin matrix under ultrasound exposure, which enhances drug diffusion; 3) cleaving of fibrin polymers to extend the surface for thrombolytic interaction; and 4) improvement of binding of recombinant tPA to fibrin.[14] Concerning the frequency range used for diagnostic ultrasound examinations, the mechanical pressure wave of the ultrasound energy propagates through the tissues, induces fluid motion, and helps tPA to reach the binding sites.[17] In addition, 2-MHz ultrasound waves enhance tPA-thrombus dissolution by fluid streaming around the clot surface and disaggregation of fibrin fibers, which results in a greater amount of binding sites for tPA without heating or cavitation.[3] In stroke patients treated with tPA, intravenous infusion of microbubbles or microspheres has been proved to accelerate clot lysis during 2-MHz ultrasound monitoring, by transmitting energy momentum from an ultrasound wave to residual flow.[3,11,12,22,23] These mechanisms support the findings of sonothrombolysis in the clinical setting.

Conclusions

Despite the limitations of the included studies, there is evidence that sonothrombolysis associated with tPA with frequencies and energy intensities in a range of diagnostic ultrasound devices is safe and results in an increased rate of arterial recanalization in acute ischemic stroke. Future studies should focus on the development of the following: 1) microspheres associated with ultrasound for augmenting brain perfusion and drug delivery within the penumbra area;[18] 2) an operator-independent ultrasound device that can be used by medical personnel irrespective of experience with TCD or TCCD ultrasonography examinations;[27,28] 3) intraarterial ultrasound devices for thrombolysis;[26] and 4) ultrasound catheters for minimally invasive evacuation of intracranial hematomas as a complication of thrombolytic therapy or other causes.[21,24] In the near future, it is possible that high-intensity focused ultrasound neurosurgery for brain tumors, Parkinson disease, epilepsy, and other conditions may become a reality.[19]

Disclosure

The authors report no conflict of interest concerning the materials or methods used in this study or the findings specified in this paper.

Author contributions to the study and manuscript preparation include the following. Conception and design: Bor-Seng-Shu, Nogueira, Figueiredo. Acquisition of data: Bor-Seng-Shu, Nogueira, Figueiredo. Analysis and interpretation of data: all authors. Drafting the article: Bor-Seng-Shu, Nogueira. Critically revising the article: all authors. Reviewed submitted version of manuscript: all authors. Approved the final version of the manuscript on behalf of all authors: Bor-Seng-Shu. Administrative/technical/material support: Teixeira. Study supervision: Teixeira.

References

1. Alexandrov AV: Ultrasound enhanced thrombolysis for stroke. **Int J Stroke 1:**26–29, 2006
2. Alexandrov AV, Demchuk AM, Felberg RA, Christou I, Barber PA, Burgin WS, et al: High rate of complete recanalization and dramatic clinical recovery during tPA infusion when continuously monitored with 2-MHz transcranial doppler monitoring. **Stroke 31:**610–614, 2000
3. Alexandrov AV, Mikulik R, Ribo M, Sharma VK, Lao AY, Tsivgoulis G, et al: A pilot randomized clinical safety study of sonothrombolysis augmentation with ultrasound-activated perflutren-lipid microspheres for acute ischemic stroke. **Stroke 39:**1464–1469, 2008
4. Alexandrov AV, Molina CA, Grotta JC, Garami Z, Ford SR, Alvarez-Sabin J, et al: Ultrasound-enhanced systemic thrombolysis for acute ischemic stroke. **N Engl J Med 351:**2170–2178, 2004
5. Barsottini OG, Felício AC, de Carvalho Aguiar P, Godeiro-Junior C, Pedroso JL, de Aquino CC, et al: Heterozygous exon 3 deletion in the Parkin gene in a patient with clinical and radiological MSA-C phenotype. **Clin Neurol Neurosurg 113:** 404–406, 2011
6. Blinc A, Francis CW, Trudnowski JL, Carstensen EL: Characterization of ultrasound-potentiated fibrinolysis in vitro. **Blood 81:**2636–2643, 1993
7. Bor-Seng-Shu E, de-Lima-Oliveira M, Teixeira MJ, Panerai RB: Predicting symptomatic cerebral vasospasm after aneurysmal subarachnoid hemorrhage. **Neurosurgery 69:**E501–E502, 2011 (Letter)
8. Bor-Seng-Shu E, Fonoff ET, Barbosa ER, Teixeira MJ: Substantia nigra hyperechogenicity in Parkinson's disease. **Acta Neurochir (Wien) 152:**2085–2087, 2010 (Letter)
9. Bor-Seng-Shu E, Hirsch R, Teixeira MJ, De Andrade AF, Marino R Jr: Cerebral hemodynamic changes gauged by transcranial Doppler ultrasonography in patients with post-traumatic brain swelling treated by surgical decompression. **J Neurosurg 104:**93–100, 2006
10. Bor-Seng-Shu E, Teixeira MJ, Hirsch R, Andrade AF, Marino R Jr: Transcranial doppler sonography in two patients who underwent decompressive craniectomy for traumatic brain swelling: report of two cases. **Arq Neuropsiquiatr 62 (3A):** 715–721, 2004
11. Culp WC, Flores R, Brown AT, Lowery JD, Roberson PK,

Hennings LJ, et al: Successful microbubble sonothrombolysis without tissue-type plasminogen activator in a rabbit model of acute ischemic stroke. **Stroke 42:**2280–2285, 2011
12. Culp WC, Porter TR, Lowery J, Xie F, Roberson PK, Marky L: Intracranial clot lysis with intravenous microbubbles and transcranial ultrasound in swine. **Stroke 35:**2407–2411, 2004
13. Daffertshofer M, Gass A, Ringleb P, Sitzer M, Sliwka U, Els T, et al: Transcranial low-frequency ultrasound-mediated thrombolysis in brain ischemia: increased risk of hemorrhage with combined ultrasound and tissue plasminogen activator: results of a phase II clinical trial. **Stroke 36:**1441–1446, 2005
14. Daffertshofer M, Hennerici M: Ultrasound in the treatment of ischaemic stroke. **Lancet Neurol 2:**283–290, 2003
15. Eggers J, Koch B, Meyer K, König I, Seidel G: Effect of ultrasound on thrombolysis of middle cerebral artery occlusion. **Ann Neurol 53:**797–800, 2003
16. Eggers J, König IR, Koch B, Händler G, Seidel G: Sonothrombolysis with transcranial color-coded sonography and recombinant tissue-type plasminogen activator in acute middle cerebral artery main stem occlusion: results from a randomized study. **Stroke 39:**1470–1475, 2008
17. Francis CW, Blinc A, Lee S, Cox C: Ultrasound accelerates transport of recombinant tissue plasminogen activator into clots. **Ultrasound Med Biol 21:**419–424, 1995
18. Holland CK, McPherson DD: Echogenic lipsomes for targeted drug delivery. **Proc IEEE Int Symp Biomed Imaging 2009:**755–758, 2009
19. Jagannathan J, Sanghvi NT, Crum LA, Yen CP, Medel R, Dumont AS, et al: High-intensity focused ultrasound surgery of the brain: part 1—A historical perspective with modern applications. **Neurosurgery 64:**201–211, 2009
20. Larrue V, Viguier A, Arnaud C, Cognard C, Petit R, Rigal M, et al: Transcranial ultrasound combined with intravenous microbubbles and tissue plasminogen activator for acute ischemic stroke: a randomized controlled study. **Stroke 38:**472, 2007
21. Medel R, Crowley RW, McKisic MS, Dumont AS, Kassell NF: Sonothrombolysis: an emerging modality for the management of stroke. **Neurosurgery 65:**979–993, 2009
22. Molina CA, Barreto AD, Tsivgoulis G, Sierzenski P, Malkoff MD, Rubiera M, et al: Transcranial ultrasound in clinical sonothrombolysis (TUCSON) trial. **Ann Neurol 66:**28–38, 2009
23. Molina CA, Ribo M, Rubiera M, Montaner J, Santamarina E, Delgado-Mederos R, et al: Microbubble administration accelerates clot lysis during continuous 2-MHz ultrasound monitoring in stroke patients treated with intravenous tissue plasminogen activator. **Stroke 37:**425–429, 2006
24. Newell DW, Shah MM, Wilcox R, Hansmann DR, Melnychuk E, Muschelli J, et al: Minimally invasive evacuation of spontaneous intracerebral hemorrhage using sonothrombolysis. Clinical article. **J Neurosurg 115:**592–601, 2011
25. Rha JH, Saver JL: The impact of recanalization on ischemic stroke outcome: a meta-analysis. **Stroke 38:**967–973, 2007
26. Soltani A, Singhal R, Obtera M, Roy RA, Clark WM, Hansmann DR: Potentiating intra-arterial sonothrombolysis for acute ischemic stroke by the addition of the ultrasound contrast agents (Optison™ & SonoVue®). **J Thromb Thrombolysis 31:**71–84, 2011
27. Tsivgoulis G, Alexandrov AV: Ultrasound-enhanced thrombolysis in acute ischemic stroke: potential, failures, and safety. **Neurotherapeutics 4:**420–427, 2007
28. Tsivgoulis G, Culp WC, Alexandrov AV: Ultrasound enhanced thrombolysis in acute arterial ischemia. **Ultrasonics 48:**303–311, 2008
29. Tsivgoulis G, Eggers J, Ribo M, Perren F, Saqqur M, Rubiera M, et al: Safety and efficacy of ultrasound-enhanced thrombolysis: a comprehensive review and meta-analysis of randomized and nonrandomized studies. **Stroke 41:**280–287, 2010

Manuscript submitted September 15, 2011.
Accepted October 31, 2011.
Please include this information when citing this paper: DOI: 10.3171/2011.10.FOCUS11251.

Address correspondence to: Edson Bor-Seng-Shu, M.D., Ph.D., Rua Loefgreen, 1272, CEP 04040-001, Sao Paulo, SP, Brazil. email: edsonshu@hotmail.com.

Neurosurg Focus 32 (1):E6, 2012

Utility of intravascular ultrasound in intracranial and extracranial neurointerventions: experience at University at Buffalo Neurosurgery–Millard Fillmore Gates Circle Hospital

Peter Kan, M.D., M.P.H.,[1,5] Maxim Mokin, M.D., Ph.D.,[2,6] Adib A. Abla, M.D.,[1,5] Jorge L. Eller, M.D.,[1,5] Travis M. Dumont, M.D.,[1,5] Elad I. Levy, M.D.,[1,3–5] and Adnan H. Siddiqui, M.D., Ph.D.[1,3–5]

Departments of [1]Neurosurgery, [2]Neurology, and [3]Radiology, and [4]Toshiba Stroke Research Center, School of Medicine and Biomedical Sciences, University at Buffalo, State University of New York; and Departments of [5]Neurosurgery and [6]Neurology, Millard Fillmore Gates Circle Hospital, Kaleida Health, Buffalo, New York

Intravascular ultrasound (IVUS) generates high-resolution cross-sectional images and sagittal reconstructions of the vessel wall and lumen. As a result, this imaging modality can provide accurate measurements of the degree of vessel stenosis, allow the detection of intraluminal thrombus, and analyze the plaque composition. The IVUS modality is widely used in interventional cardiology, and its use in neurointerventions has gradually increased. With case examples, the authors illustrate the utility of IVUS as an adjunct to conventional angiography for a wide range of intracranial and extracranial neurointerventions.
(http://thejns.org/doi/abs/10.3171/2011.10.FOCUS11242)

Key Words • **intravascular ultrasound** • **neurointervention** • **virtual histology**

Intravascular ultrasound is widely used in interventional cardiology. It is routinely used to assess proper stent apposition after coronary stent placement and to determine the most appropriate treatment for indeterminate lesions on the basis of conventional coronary angiography.[2] Recently, IVUS assessment of coronary atherosclerotic plaque progression was used as a surrogate primary end point in large statin trials.[10] Few reports have been published regarding the use of IVUS in neuroendovascular interventions. In this review, we discuss IVUS technology and our clinical experience with this modality over a wide range of extra- and intracranial neurointerventions, and we also present illustrative cases.

The IVUS Modality for Neurointerventions: Equipment, Technique, and Background

At Millard Fillmore Gates Circle Hospital, we use the 3.5 F 20-MHz Eagle Eye IVUS probe (Volcano Therapeutics) as an adjunct to conventional angiography for select neurointerventions. This cylindrical transducer sends ultrasound signals into the adjacent tissue and detects the reflected echoes. The reflected signals allow the generation of a cross-sectional image of the vessel wall and lumen at high resolution as a conventional gray-scale intravascular sonogram. Due to differences in reflected signals from different tissues, conventional gray-scale IVUS can distinguish normal vessel lumen and vessel wall from atherosclerotic plaque, intraluminal thrombus, and intimal dissection with high sensitivity.[1] Within the atherosclerotic plaque, it can further identify the deposition of lipid (hypoechoic signal) and calcium (hyperechoic signal with distal shadowing). The probe is mounted near the tip of a monorail catheter that tracks over a 0.014-in guidewire (Fig. 1). All IVUS images are displayed and recorded using an IVUS workstation (Invision Imaging System, Volcano Therapeutics). Once the radiopaque probe is placed distal to the lesion of interest under direct fluoroscopic guidance, intravascular sonograms are generated by a continuous slow withdrawal of the catheter at approximately 1 mm per second. These live cross-sectional images are simultaneously converted into a continuous sagittal reconstruction of the vessel un-

Abbreviations used in this paper: AP = anteroposterior; CA = carotid artery; CAS = CA angioplasty and stent placement; CCA = common CA; ICA = internal CA; IVUS = intravascular ultrasound; VH = virtual histology.

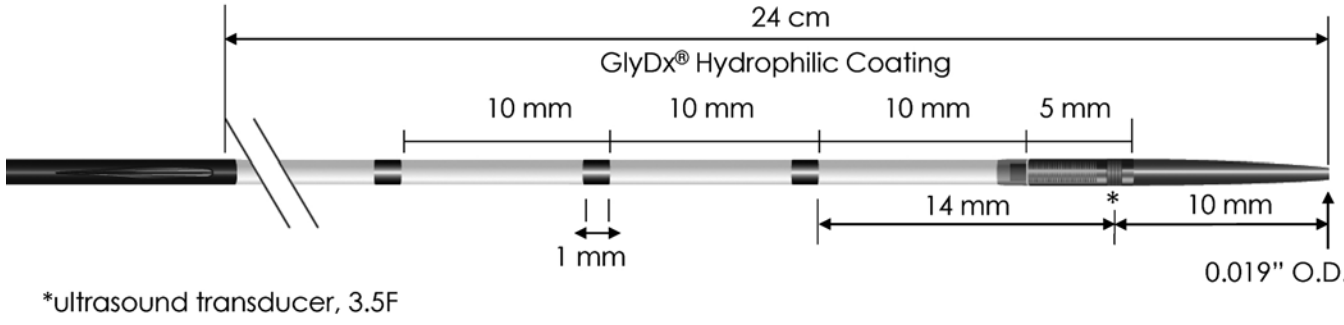

Fig. 1. The Eagle Eye IVUS imaging transducer and catheter (Volcano Therapeutics). Reproduced with permission from Volcano Corporation. O.D. = outer diameter.

der study, allowing a direct comparison of the images to conventional angiography studies, because they are in the same plane. The patient typically undergoes heparinization during the procedure to reduce the risk of thromboembolic complications.

The recent advancement of IVUS technology has resulted in more sophisticated features, such as color flow and VH. Color-flow IVUS was designed for better visualization of intraluminal blood flow (red in color-flow IVUS) and to optimize the transition zone between intraluminal blood flow and the vessel wall.[4] The main advantage of color-flow IVUS is its ability to differentiate intraluminal blood from atherosclerotic plaque along the vessel wall,[6] because both blood flow and the plaque (if it is rich in lipid) are hypoechoic on conventional gray-scale IVUS. With color-flow IVUS, at the area of maximal stenosis the color changes from red to orange as a result of velocity increase of intraluminal blood flow.[4]

The IVUS-VH modality is based on the principle that different parts of the vessel wall reflect the ultrasound signal at different frequencies and intensities, allowing the generation of a real-time VH map to assess plaque morphology and composition.[11] By defining plaque composition, IVUS-VH allows risk stratification of individual plaque depending on the fibrous, fibrofatty, lipid, and calcium content of the lesion.[5] Overall, plaques that are heavily calcified are more stable compared with plaques with a heavy lipid core. In the Carotid Artery Plaque Virtual Histology Evaluation study, Diethrich et al.[5] reported a high concordance between VH generated from IVUS-VH and true histology obtained from carotid endarterectomy. In this study, the diagnostic accuracy of IVUS-VH compared with true histology was 99.4% for thin-cap fibroatheroma, 96.1% for calcified thin-cap fibroatheroma, 85.9% for fibroatheroma, 85.5% for fibrocalcific atheroma, 83.4% for pathological intimal thickening, and 72.4% for calcified fibroatheroma.

Use of IVUS in CA Interventions

The use of IVUS as an adjunct to CA interventions was first reported by Wilson et al.[17] In that report, IVUS was used to evaluate the results of CAS quantitatively by measuring real-time luminal diameter. Several subsequent reports have supported the diagnostic utility of IVUS in CA disease. Tresukosol et al.[14] reported on a patient who was found to have a 50% stenosis of the left CCA on conventional angiography, whereas IVUS subsequently revealed a 90% stenosis with complex superficial calcification. This patient subsequently underwent left CAS as a result. In an early CA study, Miskolczi et al.[9] reported that IVUS may have a higher sensitivity than conventional angiography for detecting intimal thickening, concentric plaques, plaque surface ulceration, and calcifications. A recent case from our institution in which IVUS determined the degree of a stenosis on an ICA lesion that was indeterminate on conventional angiography is illustrated in Fig. 2.

Increasing experience with IVUS during CA intervention led to its use as a tool for evaluation of plaque morphology and intramural lesions in addition to luminal diameters, often resulting in a change in the endovascular strategy and potentially reducing the risk of embolic strokes associated with CAS. In another case from our institution, IVUS accurately identified intraluminal thrombus after CA angioplasty (Fig. 3). The identification of intraluminal lesions allowed the alteration of the treatment strategy and guided the placement of an additional stent to trap the extruded thrombus prior to the removal of distal embolic protection. In fact, we have found the greatest utility with IVUS in assessing the extrusion of constrained plaque debris through the tines of the stent following CAS. Conventional angiography often will not allow detailed visualization of the small "cheese grated" material, which may flow downstream and cause an embolic stroke postprocedure. The IVUS modality reliably detects these excrescences, allowing for remedial measures prior to the removal of distal embolic filters. Perhaps this is of even greater value during procedures in which proximal occlusion with flow arrest or flow reversal during CAS is used. In these cases, the whole procedure is completed while avoiding anterograde angiography, which may push embolic debris intracranially. Use of IVUS allows assessment of the stent without a need for the injection of contrast material, such that flow reversal can be maintained until stent patency is confirmed by IVUS, and angiography is performed only after the flow reversal is withdrawn.

The IVUS modality can also optimize and direct the intervention by identifying residual stenosis, suboptimal plaque coverage, dissection, and poor wall apposition. In a series of 107 CAS procedures, Clark et al.[3] reported that after a satisfactory result was determined by angiography,

Fig. 2. Case 1. This 78-year-old man with a history of right carotid endarterectomy and bilateral CAS with subsequent angioplasties for in-stent stenosis underwent routine transcranial Doppler studies that revealed right ICA velocities in the range of 500 cm/second. The patient subsequently underwent diagnostic angiography, and the result was equivocal (**left**, CCA injection, lateral cervical view). In-stent stenosis could not be excluded, and the apparent jet flow *(arrow)* suggested the presence of a high-grade stenosis. An IVUS study was then performed during the same procedure and revealed no significant in-stent stenosis **(right)**, despite the high Doppler velocities. The patient was discharged without intervention. Repeat Doppler studies obtained at a different laboratory revealed right ICA velocities in the range of 140 cm/second.

subsequent IVUS findings resulted in additional treatment in 9% of patients: 4 patients required poststent angioplasty, 3 required additional stents to achieve complete plaque coverage, and 3 were found to have malapposition of the stent.

Finally, IVUS can be very useful for the special circumstance of CCA origin stent insertion.[12] Accurate stent placement at the CCA origin from the aortic arch is very challenging due to poor visualization of the CCA origin on conventional catheter-based angiography. With color-flow IVUS, the probe can detect an abrupt change in the size of the color flow once the transducer is moved from the stenosis into the aorta, enabling precise identification of the CCA origin and accurate stent placement.

Use of IVUS in Intracranial Interventions

The utility of IVUS can extend to intracranial le-

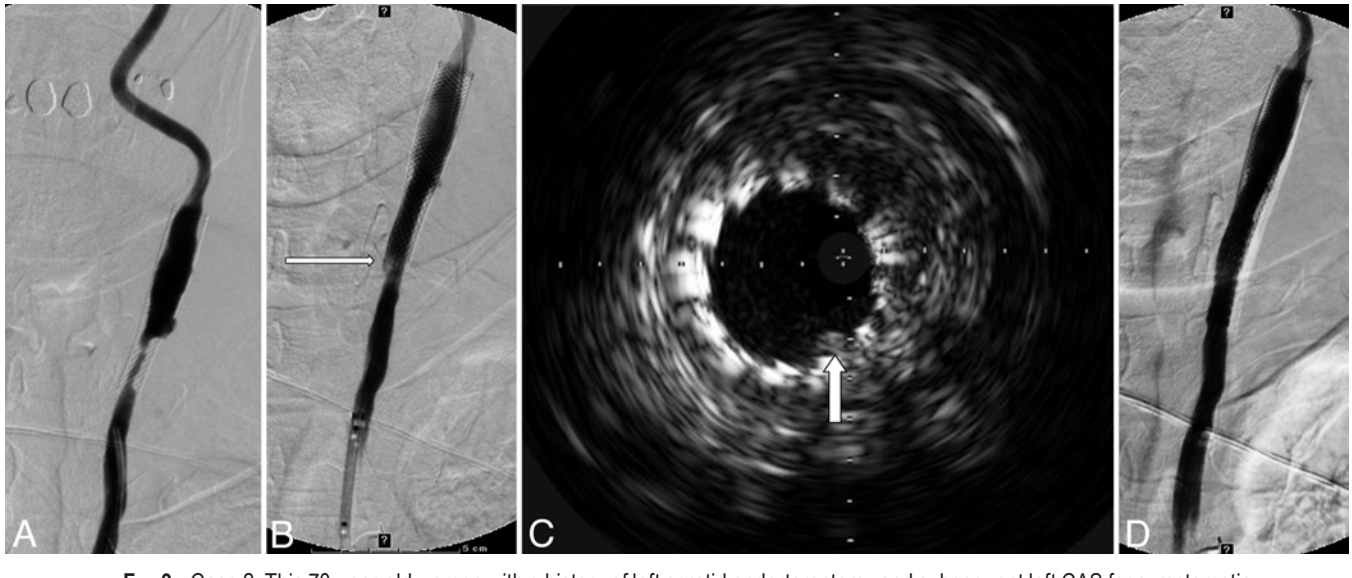

Fig. 3. Case 2. This 70-year-old woman with a history of left carotid endarterectomy and subsequent left CAS for symptomatic restenosis presented with a left hemispheric transient ischemic attack 8 months after stent placement. Doppler imaging studies demonstrated velocities of 700 cm/second within the stent, suggestive of high-grade in-stent stenosis. Conventional angiography (**A**, AP view, left CCA injection) revealed 75% in-stent stenosis, and the patient underwent balloon angioplasty with no difficulties. However, the final angiographic run (**B**, AP view, left CCA injection) revealed a subtle lucency starting just proximal to the stent tines *(arrow)*. An IVUS study was then performed **(C)**, and the findings were consistent with an intraluminal thrombus within the proximal stent at the 5:30 o'clock position *(arrow)*. An additional stent was then placed proximal to the existing stent, with some overlap. The final angiographic run showed good revascularization with no abnormalities (**D**, AP view, left CCA injection).

sions. Most importantly, it is the only imaging modality that details both the arterial wall and plaque composition of the intracranial circulation. We reported the first 2 successful applications of IVUS in intracranial interventions.[16] One patient underwent intracranial stent insertion to treat an occlusive dissection of the left ICA (from the petrous segment to the cavernous segment) that occurred during arteriovenous malformation embolization. The other patient underwent stent placement for high-grade restenosis of the basilar artery. In the first patient, IVUS accurately identified the entire length of the dissection and prevented suboptimal stent coverage, which could potentially lead to recurrence. In addition, the color-flow feature of the IVUS equipment allowed the assessment of proper stent apposition by confirming the cessation of flow in the pseudolumen. In the second patient, IVUS gave insight into the composition and morphological features of the restenosis. The identification of a fibrous lesion after previous angioplasty suggested that the lesion was safe for stent placement.[7] Moreover, IVUS provided us with a confirmatory set of measurements that allowed us to better choose our devices. Since our initial report, there have been other papers supporting the use of IVUS for intracranial lesions. Meyers et al.[8] reported the use of IVUS to characterize both the degree of stenosis and plaque composition in a petrous ICA atherosclerotic lesion. The patient subsequently underwent successful stent placement.

Use of IVUS in Venous Interventions

Compared with arterial neurointerventions, the clinical application of IVUS in the management of cerebral venous circulation disease is less well established. In the venous system, IVUS offers similar advantages of high-resolution cross-sectional images and accurate measurements of the degree of stenosis, detection of intraluminal thrombus, and venous wall thickness. However, compared with the arterial circulation, the venous system consists predominantly of vessels with a large diameter and less resistance, thus enabling navigation through a significant portion of the intracranial venous vasculature, including the transverse, sigmoid, and superior sagittal sinuses.

At Millard Fillmore Gates Circle Hospital, IVUS is routinely used in conjunction with angiography to evaluate diseases of cerebral venous outflow obstruction, including dural sinus thrombosis and pseudotumor cerebri. In both cases, IVUS can provide critical confirmatory information, such as the presence of intraluminal thrombus in dural sinus thrombosis and the accurate assessment of the degree of stenosis and its response to angioplasty or stent insertion in the transverse sinus in patients with pseudotumor cerebri. For patients with pseudotumor cerebri who undergo angioplasty or stent insertion in the transverse sinus, follow-up information regarding the location, degree, and morphological features of the restenosis or any in-stent stenosis can also be readily identified by IVUS. In Fig. 4, a case from our institution is illustrated in which IVUS confirmed the persistent right-sided transverse sinus stenosis following balloon angioplasty, which led us to perform the subsequent stent placement procedure.

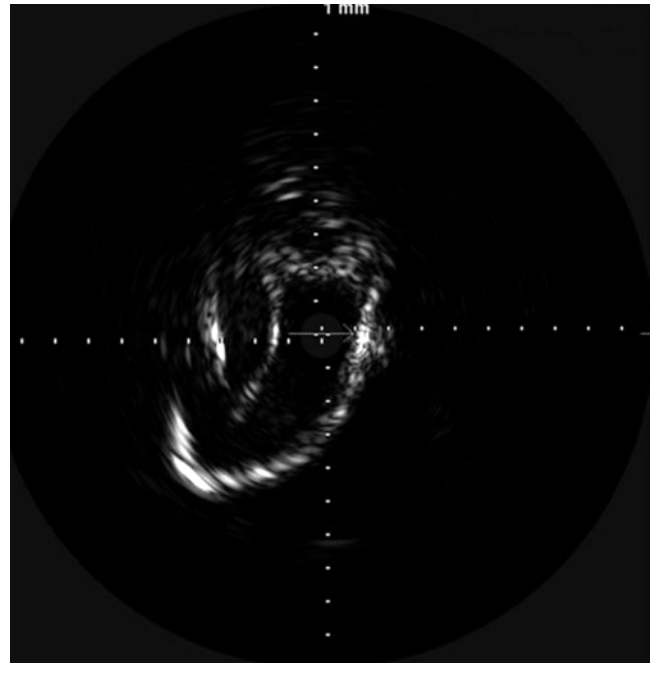

Fig. 4. Case 3. This 27-year-old woman with a history of benign intracranial hypertension presented with worsening headache and blurry vision. Despite long-term medical treatment with acetazolamide and topiramate, as well as serial lumbar punctures, her headache continued to worsen, and neurological examination revealed severe papilledema. Computed tomography venography showed bilateral transverse sinus stenosis, and the patient underwent angiography for further evaluation of the degree of stenosis and possible stent placement. Diagnostic angiography confirmed severe transverse sinus stenosis bilaterally. The patient underwent multiple balloon angioplasty attempts in the right and left transverse sinuses, without any significant improvement on the right. A postangioplasty IVUS recording confirmed persistent severe stenosis of the transverse sinus on the right (see *arrow* in cross-sectional IVUS image). The patient subsequently underwent successful stent treatment of the right transverse and sigmoid sinus. Postoperatively, her headaches and vision improved significantly.

Apart from cerebral venous occlusive disease, successful application of IVUS has also been reported in other venous interventions. Shindo et al.[13] reported the use of IVUS-assisted transvenous embolization of a dural arteriovenous fistula. In that case, IVUS was used to map the exact fistulous sites formed to guide the transvenous embolization.

Future IVUS Applications in Neurointerventions

The main restriction of IVUS for neurointerventional applications at present is its use in the intracranial circulation. This is related to limited navigability because of the tortuosity and small luminal diameter of the distal intracranial circulation as well as the limited flexibility and relatively large diameter of the IVUS catheter. With smaller and softer catheters to improve navigability, the use of IVUS could extend beyond the conditions discussed in this review. For example, in acute ischemic stroke, IVUS can delineate the composition of the culprit lesion (calcific vs soft), which in turn would help to guide the intervention (angioplasty or stent insertion for calcific/atherosclerotic lesion and thrombolysis, thrombectomy,

or clot retrieval for soft embolus). With respect to aneurysms, IVUS could be used to define the neck better and to understand aneurysm wall composition and intraaneurysmal contents, such as thrombus.[15]

Conclusions

The IVUS modality is a valuable adjunct to conventional angiography in the treatment of extra- and intracranial arterial and venous diseases. Through technical advances in different IVUS modalities and availability of smaller and softer catheters, its use could extend to diseases that involve more distal arterial and venous vasculatures. Continued application of this underutilized diagnostic tool is important to accumulate a larger experience of IVUS in the clinical setting of neurointervention.

Disclosure

Drs. Abla, Dumont, Eller, Kan, and Mokin report no financial relationships. Dr. Levy receives research grant support (principal investigator: Stent-Assisted Recanalization in acute Ischemic Stroke [SARIS]), other research support (devices), and honoraria from Boston Scientific (this company's neurovascular business has been acquired by Stryker), and research support from Codman & Shurtleff, Inc. and ev3/Covidien Vascular Therapies; has ownership interests in Intratech Medical Ltd. and Mynx/Access Closure; serves as a consultant on the board of Scientific Advisors to Codman & Shurtleff, Inc.; serves as a consultant per project and/or per hour for Codman & Shurtleff, Inc., ev3/Covidien Vascular Therapies, and TheraSyn Sensors, Inc.; and receives fees for carotid stent training from Abbott Vascular and ev3/Covidien Vascular Therapies. Dr. Levy receives no consulting salary arrangements. All consulting is per project and/or per hour.

Dr. Siddiqui has received research grants from the National Institutes of Health (co-investigator: NINDS 1R01NS064592-01A1, Hemodynamic induction of pathologic remodeling leading to intracranial aneurysms; not related to present manuscript) and the University at Buffalo (Research Development Award); holds financial interests in Hotspur, Intratech Medical, StimSox, and Valor Medical; serves as a consultant to Codman & Shurtleff, Inc., Concentric Medical, ev3/Covidien Vascular Therapies, GuidePoint Global Consulting, and Penumbra; belongs to the speakers' bureaus of Codman & Shurtleff, Inc. and Genentech; serves on an advisory board for Codman & Shurtleff; and has received honoraria from Abbott Vascular, American Association of Neurological Surgeons' courses, Genentech, Neocure Group LLC, an Emergency Medicine Conference, and from Abbott Vascular and Codman & Shurtleff, Inc. for training other neurointerventionists in CA stent placement and for training physicians in endovascular stent insertion for aneurysms. Dr. Siddiqui receives no consulting salary arrangements. All consulting is per project and/or per hour.

Author contributions to the study and manuscript preparation include the following. Conception and design: Siddiqui, Kan. Acquisition of data: all authors. Analysis and interpretation of data: all authors. Drafting the article: Kan. Critically revising the article: all authors. Reviewed submitted version of manuscript: all authors.

Acknowledgments

The authors thank Paul H. Dressel, B.F.A., for assistance with preparation of the illustrations and Debra J. Zimmer, A.A.S., C.M.A.-A., for editorial assistance.

References

1. Blessing E, Hausmann D, Sturm M, Wolpers HG, Amende I, Mügge A: Intravascular ultrasound and stent implantation: intraobserver and interobserver variability. **Am Heart J 137:** 368–371, 1999
2. Böse D, von Birgelen C, Erbel R: Intravascular ultrasound for the evaluation of therapies targeting coronary atherosclerosis. **J Am Coll Cardiol 49:**925–932, 2007
3. Clark DJ, Lessio S, O'Donoghue M, Schainfeld R, Rosenfield K: Safety and utility of intravascular ultrasound-guided carotid artery stenting. **Catheter Cardiovasc Interv 63:**355–362, 2004
4. Diethrich EB, Irshad K, Reid DB: Virtual histology and color flow intravascular ultrasound in peripheral interventions. **Semin Vasc Surg 19:**155–162, 2006
5. Diethrich EB, Pauliina Margolis M, Reid DB, Burke A, Ramaiah V, Rodriguez-Lopez JA, et al: Virtual histology intravascular ultrasound assessment of carotid artery disease: the Carotid Artery Plaque Virtual Histology Evaluation (CAPITAL) study. **J Endovasc Ther 14:**676–686, 2007
6. Irshad K, Reid DB, Miller PH, Velu R, Kopchok GE, White RA: Early clinical experience with color three-dimensional intravascular ultrasound in peripheral interventions. **J Endovasc Ther 8:**329–338, 2001
7. Levy EI, Hanel RA, Bendok BR, Boulos AS, Hartney ML, Guterman LR, et al: Staged stent-assisted angioplasty for symptomatic intracranial vertebrobasilar artery stenosis. **J Neurosurg 97:**1294–1301, 2002
8. Meyers PM, Schumacher HC, Gray WA, Fifi J, Gaudet JG, Heyer EJ, et al: Intravascular ultrasound of symptomatic intracranial stenosis demonstrates atherosclerotic plaque with intraplaque hemorrhage: a case report. **J Neuroimaging 19:** 266–270, 2009
9. Miskolczi L, Guterman LR, Flaherty JD, Hopkins LN: Depiction of carotid plaque ulceration and other plaque-related disorders by intravascular sonography: a flow chamber study. **AJNR Am J Neuroradiol 17:**1881–1890, 1996
10. Nissen SE, Tuzcu EM, Schoenhagen P, Brown BG, Ganz P, Vogel RA, et al: Effect of intensive compared with moderate lipid-lowering therapy on progression of coronary atherosclerosis: a randomized controlled trial. **JAMA 291:**1071–1080, 2004
11. Okubo M, Kawasaki M, Ishihara Y, Takeyama U, Yasuda S, Kubota T, et al: Tissue characterization of coronary plaques: comparison of integrated backscatter intravascular ultrasound with virtual histology intravascular ultrasound. **Circ J 72:** 1631–1639, 2008
12. Reid DB, Irshad K, Diethrich EB: Intravascular ultrasound applications, in AbuRahma AF, Bergan JJ (eds): **Noninvasive Vascular Diagnosis: A Practical Guide to Therapy, ed 2.** London: Springer-Verlag, 2007, pp 506–516
13. Shindo A, Kawanishi M, Masada T, Kawai N, Tamiya T, Nagao S: [Usefulness of intravascular ultrasound in embolization of dural arteriovenous fistula: a case report.] **No Shinkei Geka 31:**1323–1329, 2003 (Jpn)
14. Tresukosol D, Wongpraparut N, Lirdvilai T: The value of intravascular ultrasound-facilitated internal carotid artery stenting in a patient with heavily calcified and ambiguous common carotid artery stenosis. **J Invasive Cardiol 19:**E203–E206, 2007
15. Waller BF, Pinkerton CA, Slack JD: Intravascular ultrasound: a histological study of vessels during life. The new 'gold standard' for vascular imaging. **Circulation 85:**2305–2310, 1992
16. Wehman JC, Holmes DR Jr, Hanel RA, Levy EI, Hopkins LN: Intravascular ultrasound for intracranial angioplasty and stent placement: technical case report. **Neurosurgery 59 (4 Suppl 2):**ONSE481–ONSE483, 2006
17. Wilson EP, White RA, Kopchok GE: Utility of intravascular ultrasound in carotid stenting. **J Endovasc Surg 3:**63–68, 1996

Manuscript submitted September 12, 2011.
Accepted October 18, 2011.
Please include this information when citing this paper: DOI: 10.3171/2011.10.FOCUS11242.

Address correspondence to: Adnan H. Siddiqui, M.D., Ph.D., University at Buffalo Neurosurgery, 3 Gates Circle, Buffalo, New York 14209. email: asiddiqui@ubns.com.